Predicting velocities and turbulent exchange in isolated street canyons and at a neighborhood scale

by

Terianne Catherine Hall

S.B. Mechanical Engineering, 2008
B.S.A.D. Architecture, 2008
Massachusetts Institute of Technology

Submitted to the Department of Mechanical Engineering
in partial fulfillment of the requirements for the degree of

Master of Science in Mechanical Engineering

at the

MASSACHUSETTS INSTITUTE OF TECHNOLOGY

June 2010

Author .....
Department of Mechanical Engineering
May 28, 2010

Certified by .....
Leslie K. Norford
Professor of Building Technology
Thesis Supervisor

Certified by .....
Leon R. Glicksman
Professor of Mechanical Engineering and Building Technology
Reader in Department

Accepted by .....
David E. Hardt
Chairman, Department Committee on Graduate Theses

Predicting velocities and turbulent exchange in isolated street canyons and at a neighborhood scale

by

Terianne Catherine Hall

Submitted to the Department of Mechanical Engineering
on May 28, 2010, in partial fulfillment of the
requirements for the degree of
Master of Science in Mechanical Engineering

Abstract

Urban planners need a fast, simple model to assess the impact of early design phase iterations of neighborhood layout on the microclimate. Specifically, this model should be able to predict the expected urban heat island intensity and the locations in neighborhood layouts that are prone to pollutant retention. Current models are inadequate for this purpose because they use computationally intensive techniques to solve for flow through a neighborhood and often require a strong technical background for effective use of the models.

In this thesis, we use analytical equations and empirical relationships to calculate the expected wind speeds in isolated, idealized street canyons. We demonstrate that flow in street canyons is driven by momentum exchange with the air above. We discuss the importance of flow separation and turbulent exchange between the urban canopy layer and the urban boundary layer for removing heat and pollutants from street canyons. Next, we introduce a method to parameterize this exchange and extend this work to more realistic street canyons and idealized neighborhoods. We evaluate this work using computational fluid dynamics and comparison to experimental results and models from the literature. We examine cases where the flow is influenced by buoyancy effects and assess the applicability of our work in these situations. Finally, we address how this work could be further developed into generalized planning guidelines and incorporated into a comprehensive model for urban planners.

Thesis Supervisor: Leslie K. Norford
Title: Professor of Building Technology

Reader in Department: Leon R. Glicksman
Title: Professor of Mechanical Engineering and Building Technology

Acknowledgments

I am exceedingly thankful to my advisor, Professor Leslie K. Norford, for his guidance, support and sense of humor throughout this process. Les is extemely hard-working and continues to push me to find answers to difficult problems without waving my hands. I like to think that as I spend more time with him, here and in Singapore, his rigorous approach to reseach is slowly rubbing off on me. I convince myself of this by remembering that this is much more likely to rub off on me than his bravery in the hawker centre. He was very patient and encouraging during the exasperating "ENVI-met year," and I will never forget that. I look forward to continuing to work with and learn from Les in the coming years for my PhD.

The work in this thesis would not have been possible without our collaboration with Dr. Rex Britter. The previous statement is true for more reasons than his daily or twice-daily contribution to my caffeine intake. Rex is really good at fluid mechanics; he is also really good at explaining fluid mechanics. The previous statements are ironic understatements, and are not meant to be sarcasm. I use this difficult literary device because even with a thesaurus I couldn't find a grand enough word to replace"good." He doesn't give up on explaining difficult concepts to me, he doesn't get mad when I disagree with him, he doesn't gloat when I eventually realize that he's correct and he is always ready with a something positive to say about this work. I also look forward to working with him for my PhD.

I am also very grateful to Professor Leon Glicksman. He acted as my reader from the Mechanical Engineering department, and he provided valuable insight that added more than a little substance to this document. I hope that he will continue to talk with me about this work during my PhD, especially as I prepare to extend these ideas to heat transfer processes.

I would also like to thank my labmates in the Building Technology department for their diverse perspective on and valuable input to this work.

Finally, I would like thank my friends and family who have listened to me talk about various aspects of this project ad nauseam. Without their support, my outlook on my continuing MIT experience would not be the same.

The research described in this project was funded by the Singapore National Research Foundation (NRF) through the Singapore-MIT Alliance for Research and Technology (SMART) Center for Environmental Sensing and Modeling (CENSAM).

Contents

List of Figures

List of Tables

Chapter 1

Introduction

This work focuses on the island nation of Singapore. Singapore has undergone rapid urban development in the past 50 years. This development has led to changes in the island microclimate, specifically there have been measurable differences in the nighttime air temperature, which can be attributed to the urban heat island (UHI) phenomenon. As the island continues to become more populated, there will be an increase in pollutants, for example vehicle emissions, released into the heavily populated urban canopy layer, that will be retained there unless removed into the urban boundary layer. [43] Insufficient removal of pollutants is a result of weak turbulent exchange between the urban canopy layer and the urban boundary layer, and this can be directly attributed to building geometry, neighborhood layout and atmospheric conditions. [7] It follows that urban form contributing to insufficient removal of pollutants will also put Singaporeans at risk in the event of an accidental or intentional release of toxic chemicals.

Singapore's government has declared that its population will increase by 50% to 6.5 million people in the next 40-50 years. [29, 37, 36] This expected population increase is due in part to the provision of economic incentive to families for reproducing as well as the encouragement of the immigration of skilled foreigners. [40, 29, 52] This growth will lead to an increase in housing demand and a need for new housing and infrastructure construction. Understanding how building geometry and urban form contribute to the removal of pollutants and the temperature of the microclimate

would be particularly useful during this time of expansion because if the urban heat island of Singapore is exacerbated, it could potentially limit population growth.

The purpose of this work is to better understand and predict how air carries pollutants, sensible and latent heat, and toxic chemicals arising from accidental or intentional releases through a neighborhood. Where will the plume of released pollutant go and how can we mitigate the urban heat island effect by changing the form of the neighborhood? The results of this research will be relevant to Singapore and other developing tropical and subtropical neighborhoods.

In the rest of Chapter 1, we provide background information about the urban heat island effect and pollutant retention and we discuss the importance of these topics in greater detail. The ability to have an influence on these problems by modifying building form is contingent on first understanding: How does air move through a neighborhood? In Chapter 2, we address this question with a complicated fluid mechanical model, and assess the benefits and drawbacks of these types of models. We assert that the results of this work would be most valuable in the form of a simple model intended for use by urban planners and others who are involved in the design and renovation of new and existing neighborhoods in Singapore. In Chapter 3, we study the fluid mechanics responsible for flow in a single, idealized and infinitely long street canyon. This study shows that the fluid flow in the urban canopy layer is driven by a momentum exchange with the air in the urban boundary layer. The exchange of fluid between the two air masses is then modelled using concepts and relationships that draw on plume entrainment theory. Chapter 4 focuses on the differences between the idealized canyon and a real street canyon. We also compare the relationships found in Chapters 3 and 4 to simulated and experimental results. Chapter 5 extends this work to the study of idealized neighborhoods. In Chapter 6 we discuss when it is appropriate to apply this work to a neighborhood, and when it may be less applicable. Chapter 7 discusses the significant outcomes of this work, and relevant future work.

1.1 UHI background

Modification of the microclimate has the greatest impact on pedestrian comfort when the changes occur in the urban canopy layer, defined as the space in a neighborhood that is lower than roof level. [43] Poorly planned urban development can lead to significantly higher temperatures in the urban canopy layer particularly at night, which in many climates results in decreased thermal comfort for pedestrians and residents and increased building energy consumption. This temperature difference is known as the urban heat island (UHI) intensity, and it is shown schematically in Figure 1-1.

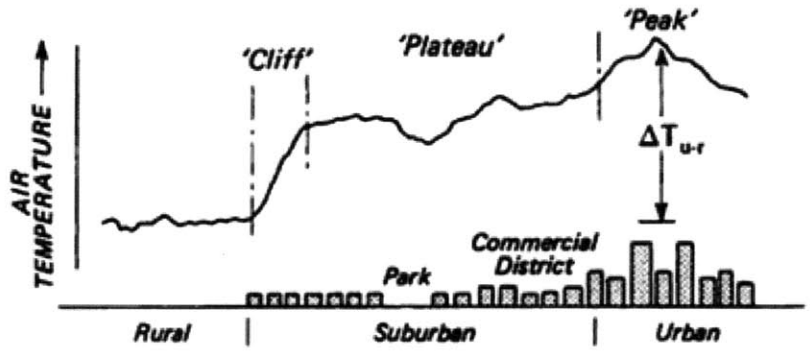

Figure 1-1: Generalized cross-section of a typical urban heat island [43]

When air flows over a city from an undeveloped area, it encounters increased roughness due to urban construction and often increased temperatures due to the UHI effect. This causes a boundary layer to form above the city, known as the urban boundary layer, which is defined as the area whose temperature and wind speeds are affected by the processes in the urban canopy layer. The urban canopy layer and a growing urban boundary layer are depicted schematically over an urban area in Figure 1-2. Boundary layer meteorologists consider the fluxes between these two layers when comparing the surface-energy balance of cities to rural and suburban areas. [43]

Urbanization modifies the atmosphere and surface characteristics of a region. Because man-made materials have different thermal properties and geometries than natural materials, the microclimate of the urban area is different from that of neighboring

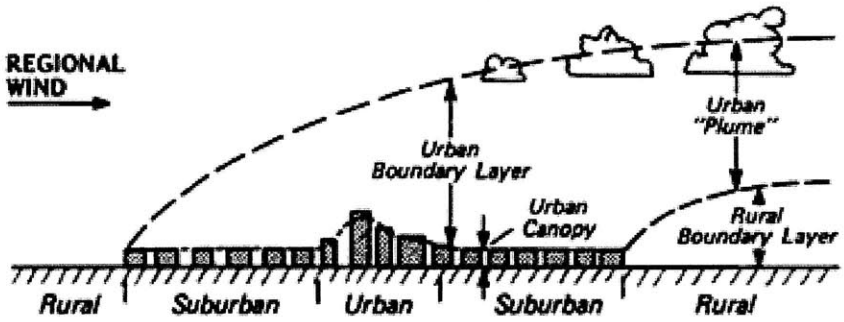

Figure 1-2: Schematic representation of the urban atmosphere illustrating a two-layer classification of urban modification [43]

rural areas. With urbanization, the heat storage capacity of the city is increased due to the increased surface area (from buildings) that is available to absorb and reflect short wave radiation. Buildings and ground surfaces in a street canyon absorb short wave radiation during daylight hours, and would normally reradiate it through long wave radiation to the cooler sky, however building geometry decreases the surface view factor associated with radiative cooling. [43] The surface view factor is based on how much of the sky is seen from the surface in question. Consider a flat plane, analogous to a rural landscape; a large extent of the sky can be seen from anywhere on the plane, and in turn all of the plane can be seen by a large extent of the sky. In contrast, consider a dense urban area; a much smaller extent of the sky can be seen from a street surface than from the flat plane, and the same argument can be made for a building façade in a dense urban area. The greatest temperature difference between the rural and urban area is usually found at night. In rural scenarios this is when a majority of radiative cooling occurs via long wave radiative heat transfer between the building surfaces and the cool night sky. Because the city canyons have lower sky view factors than the rural area, the amount of long wave radiation loss from surfaces is decreased in the city. [43]

Building geometry further contributes to the UHI phenomenon by reducing the momentum in the air which results in lower wind speeds. This causes a reduction in the advective cooling of building surfaces. Because of the increased shear stress felt by the air due to canyon geometry, wind speeds are typically lower in an urban

canyon than in the upper atmosphere or in a neighboring rural area. This leads to a decrease in mixing between the urban canopy layer and the urban boundary layer, and thus there is a decrease in turbulent heat transport out of the urban canyon. [43]

Another cause of the UHI is increased waste heat contributed to the urban microclimate by anthropogenic activities and industry. This includes waste heat expelled by automobiles and by building air conditioning units – which is particularly relevant in tropical cities like Singapore that have a cooling climate throughout the year. As neighborhoods become more crowded, this effect of anthropogenic activities becomes even more prevalent. [43] In warm climates this problem is compounded because the increased outdoor temperature leads to an increase in the amount of energy needed to keep buildings at a constant temperature. This increase in energy consumption leads to an increase in the waste heat emitted into the city, which can further increase the outdoor temperature. The magnitude of this temperature increase is dependent on where the heat is released into canyon, and how it travels through the city. [10, 11] Additionally, increased air temperatures at street level in hot and humid climates like Singapore are uncomfortable for pedestrians.

Measurements taken continuously over the course of a year in different parts of Singapore show that the maximum UHI effect experienced each day, and averaged over the month is up to five degrees Celsius, and consistently greater than three degrees Celsius, as shown in Figure 1-3. [15] The lines in Figure 1-3 are representative of types of land use in Singapore: COM - commercial area, CBD - Central Business District, HDB - high-rise residential flats and RES - low-rise residential estate. The temperatures measured are compared with a nearby undeveloped secondary rainforest.

The focus of this research is the microclimate near the HDB flats, represented by triangles in Figure 1-3. These flats are designed by Singapore's Housing Development Board (HDB), and are government owned buildings. In 2010, Singapore's Research and Planning Department estimated that more than 80% of Singapore residents live in HDB flats. [14] Additionally, HDB communities are where many Singaporeans spend their evening hours. There is often a centralized outdoor dining area located in each

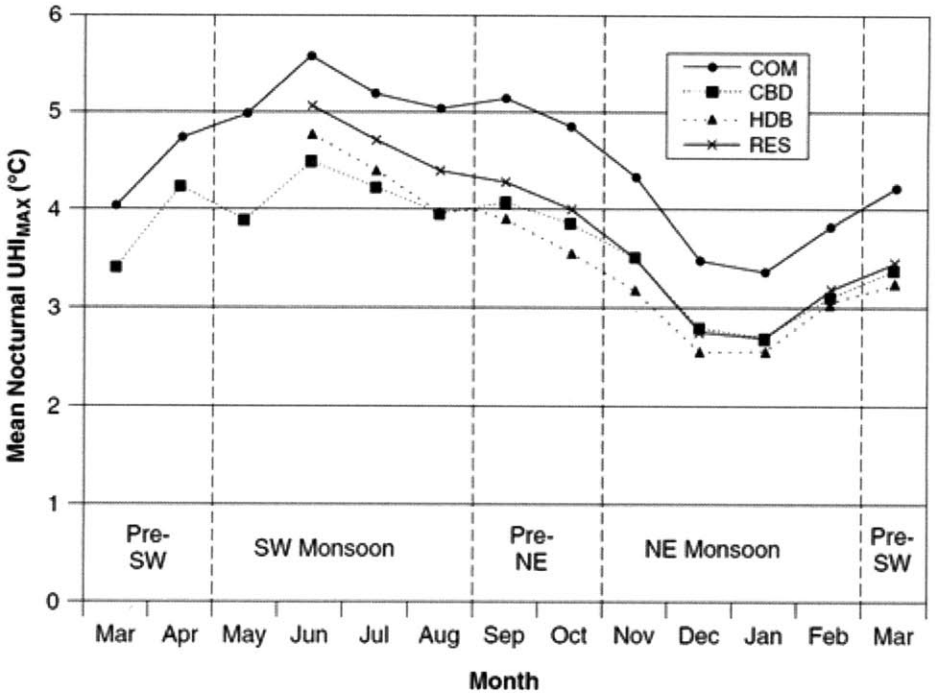

Figure 1-3: Monthly mean urban heat island intensity under all weather conditions from four urban stations, 2003-2004 [15]

HDB neighborhood which is where many residents eat dinner and interact with their neighbors. Because the UHI effect occurs in the evening, HDB flats are worthwhile to research as these areas affect the quality of life of many Singaporeans. The ability to predict how sensible and latent heat travels and is stored in the city, both spatially and temporally, will result in informed decision making by urban planners who are responsible for the design of future Singaporean neighborhoods.

1.2 Pollution background

Pollutants, such as vehicle emissions, released into the heavily populated urban canopy layer remain there unless they are removed into the urban boundary layer. [43] This pollutant retention leads to a reduction in urban air quality surrounding pedestrians. The insufficient removal of pollutants is a result of weak turbulent exchange between the urban canopy layer and the urban boundary layer. [7] This can be directly attributed to building geometry and the neighborhood layout.

Prediction of pollutant transport from a source is exceedingly important; when large amounts of hazardous materials are accidentally or intentionally released into urban areas, it is essential to predict the temporal and spatial concentration of the contaminant in the affected neighborhood. The ability to predict areas that are prone to high pollutant concentrations in the urban canopy layer will lead to better decision making by urban planners and architects about the placement of sidewalks and building air intakes. Understanding the flow and mixing processes could lead to the development of guidelines for urban planners to design neighborhoods with cleaner air. [7]

Chapter 2

Methodology and motivation

One must study both heat transfer and airflow processes to understand the UHI phenomenon. A common way of studying these complex processes is through experiment. Many research groups set up sensors inside the urban canopy to better understand microclimate processes. The same is true of studying pollutant transport. Large-scale experimental chemical releases have been organized to study pollutant transport through real neighborhoods. [2, 17] This type of work is invaluable because real data is needed to evaluate any computer model; however it is time intensive, and in the case of Singapore requires special permission from the government. We are working with a group of climatologists in Singapore including Roth, whose data was used in Figure 1-3, to get relevant temperature and wind data for the entire island of Singapore. We are also working with them to gather airflow and temperature data with a dense network of sensors for a single developing neighborhood in Singapore.

The other method used for studying the UHI effect and pollutant transport is with modelling and computer simulation. There are many environmental models available, each with advantages and drawbacks. Section 2.1 discusses the results of a neighborhood scale simulation using ENVI-met. This model is particularly relevant because it is designed to be used by planners and architects as a tool to analyze the interactions between urban design and the microclimate. [9] In Section 2.2 we address the shortcomings of ENVI-met, discuss alternative models and methodologies and assert that a simple analytical model evaluated with computational fluid dynamics

would be most appropriate for use by urban planners.

2.1 A neighborhood-scale simulation with "everything"

A German group, led by Professor Michael Bruse, has attempted to create a microclimate model specifically for the urban environment. This tool is called ENVI-met and it is a three-dimensional model designed to simulate surface-plant-air interactions with a typical resolution of 0.5 to 10 meters in space and 10 seconds in time. ENVI-met includes soil, water, vegetation and building models. These models are all relevant to studying the processes that contribute to the UHI effect at a neighborhood scale. The air flow model in ENVI-met is based on a finite difference discretization of the incompressible Navier-Stokes equations, using the Boussinesq-approximation. The turbulence model is a form of the $k-\epsilon$ model; this type of model will be discussed in Section 2.2. [9, 8] An upwind scheme is used in combination with an Alternating Directions Implicit (ADI) scheme to solve these equations. [8] The ADI scheme is numerically efficient because it often results in a system of equations with a tridiagonal matrix, which can be solved with low computational expense. [12] The order of these schemes is not specified in space or time, however we assume that they are first order because Bruse admits that they are highly numerically diffusive. [8, 20]

Using ENVI-met, we built an idealized neighborhood, entitled Grid City. Grid City consists of 49 buildings, each 50 meters wide, 50 meters long and 40 meters high, arranged in a 7 x 7 grid. The streets separating adjacent buildings are 25 meters wide. This is depicted schematically in Figure 2-1. The domain was meshed with hexahedral elements that were 5 meters wide, 5 meters long with a vertical height that varied. Specifically, five layers of finite volumes were concentrated near the street surface, with a height of 1 meter to ensure a fine mesh in the area of interest for pedestrian comfort, and above these volumes, beginning at a height of 5 meters, the volumes had a uniform height of 5 meters. The extents of the domain was 150 x 150 x 29 volumes, which is equivalent to 750 x 750 x 125 meters. A schematic of the domain is shown in Figure 2-1.

In the Grid City simulation, the wind speed was uniform horizontally at the inlet

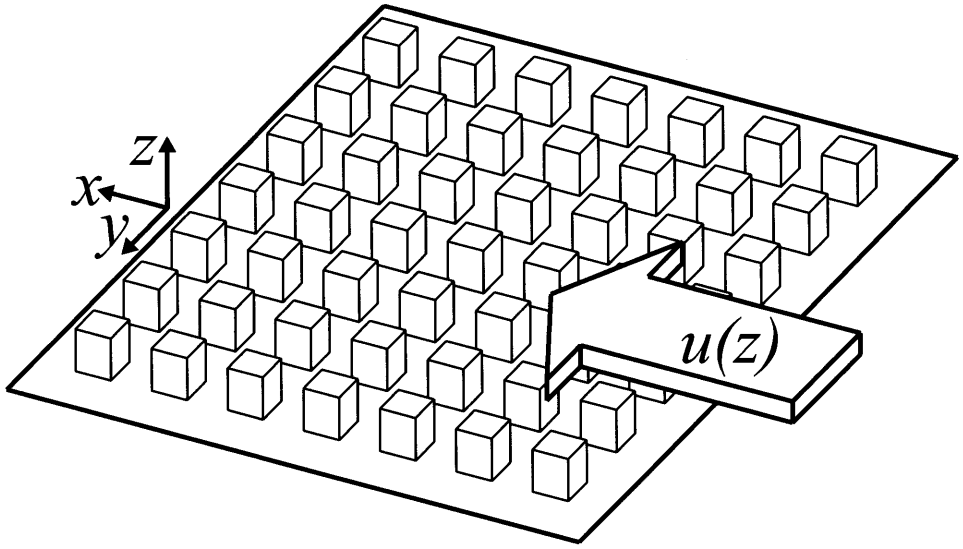

Figure 2-1: Schematic of Grid City

of the domain, and it varied logarithmically in the vertical direction as

$$u(z) = \left(\frac{u_*}{\kappa}\right) \ln\left(\frac{z}{z_0}\right), \tag{2.1}$$

where $u(z)$ is the horizontal wind speed, κ is the von Karman constant, taken as 0.40, u_* is the friction velocity, z is the height above the bottom of the domain and z_0 is the aerodynamic roughness length. [49] For the simulation, the wind speed at 10 meters from the ground was set to 5 m/s, and the aerodynamic roughness height was set to 0.03 meters, which is equivalent to flow over grassland. [49] The domain was set to Singapore's longitude and latitude, and was initialized for August 1, with an initial air temperature of 305 Kelvin, typical of Singapore in August. The simulation start time was midnight, and it ran until the simulation time reached 8:00 am on August 1. This simulation ran three to four times slower than real time. The wind data for the 8:00 am results were analyzed to study the flow through the neighborhood of Grid City. The results in Figure 2-2 are taken from a slice of data that is 10 meters above the ground surface, where the wind is coming from the south.

The contours and vectors in Figure 2-2, depicting wind speed and wind direction respectively, provide some insight about flow through a neighborhood. As expected, the flow in the canyons that were perpendicular to the wind, known as recirculating

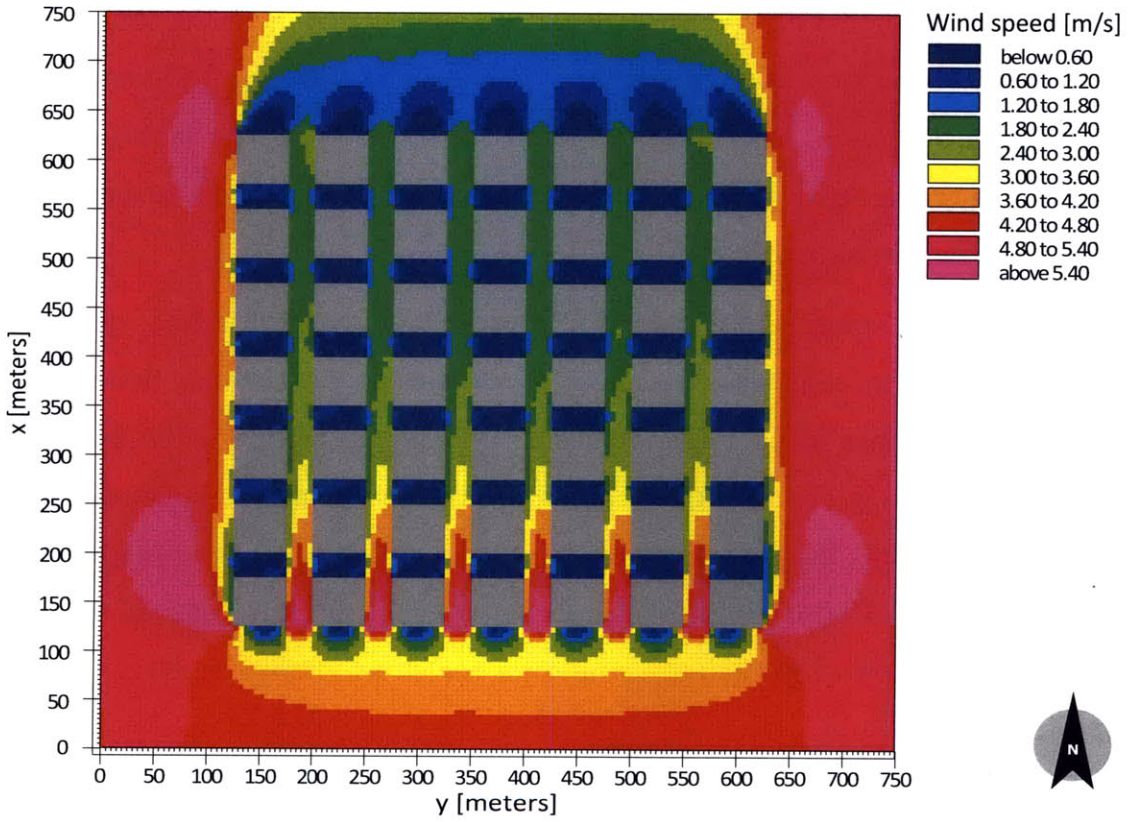

Figure 2-2: ENVI-met wind speed data for Grid City on August 1, at 08:00 am at $z = 10$ meters

flow, had much lower wind speeds than the flow in the canyons with longitudinal axes aligned with the wind. Recirculating flow is more often studied than longitudinal flow because it is considered the worst case scenario for pollutant and heat retention due to the characteristic low wind speeds. This misconception has been addressed by Soulhac et al in 2008, and Britter and Hanna in 2003 to some degree, however a comprehensive and simple model to predict wind speeds in street canyons and turbulent exchange between the urban canopy layer and the urban boundary layer has not been developed. [7, 47] Their work suggests that mixing is inherent in recirculating flow because of the large vortices that arise in the flow structure. Additionally, the large difference between the canyon velocity and free stream velocity in recirculating flow causes more vertical exchange across the rooftop boundary because of the velocity difference between the two air masses.

We consider a street canyon that is aligned with the wind direction, defined as the volume that encompasses the length of the street, the distance between two neighboring buildings along the street, and the building heights. The façades of interest when talking about a street canyon are the street and the building façades that flank the road. [18] The aspect ratio, defined as the ratio of the height of the flanking buildings divided by the width of the street, of the street canyon will have an effect on the flow. [18] The aspect ratio for the street canyons in Grid City was approximately 1.5.

While the meshing of the areas between buildings is not very fine in the Grid City simulation, the contours in Figure 2-2 are suggestive of the fluid mechanics that we expect in this scenario. As the flow approaches the bluff buildings and enters the street canyons in Grid City, the contours in Figure 2-2 suggest that there is a contraction effect at the first row of buildings – initially there is an increase in the velocity along the street canyon. After the contraction, the velocity decreases with distance along the street canyon. This decrease in velocity is due to a reduction in momentum induced by a drag force on the flow from the street and the building façades. Because the horizontal mass flow rate along this part of the canyon is decreasing, we assert that fluid must be expelled vertically from the street canyon to the atmosphere

for mass to be conserved. The flow between the next rows of buildings exhibits little change in velocity along the canyon, which raises the questions – can the flow through a neighborhood be fully developed? For what areas of a neighborhood is this approximation valid? We will address this question more thoroughly in Chapter 5, however the Grid City data gives us an estimate of how the flow develops in a street canyon that is aligned with the wind.

To study the characteristic flow down a street canyon aligned with the wind, we extract the magnitude of the velocity in all of the finite volumes that fall in the volume defined by the width of the street canyon aligned with the wind that is just left of the center of Grid City, the height of the buildings, and the entire length of the domain in the x-direction. Next we process this data as a function of the distance along the domain in the x-direction. To do this, we consider the longitudinal bulk velocity, spatially averaged over the canyon which is defined as,

$$u_{cl}(x) = \frac{\int_0^H \int_0^W u(y,z)\ dy\, dz}{A_c}, \tag{2.2}$$

where $u_{cl}(x)$ is the longitudinal bulk velocity at some distance down the domain in the x-direction, H is the building height, W is the street canyon width, $u(y,z)$ is the velocity in the x-direction within a particular finite volume in the cross-section of the canyon, dy is the width of the street canyon volume, dz is the height of the street canyon volume and A_c is the cross-sectional area of the canyon, in this case the height of the buildings times the width of the street. This longitudinal bulk velocity is plotted against distance along the Grid City domain in the x-direction in Figure 2-3. The grey boxes on the graph represent the locations of the buildings that flank the street canyon.

The longitudinal bulk velocity of the flow along the canyon appears to be approaching a constant value. While the flow is not yet fully developed, the trend in Figure 2-3 suggests that the flow would reach a fully developed state in a larger neighborhood. The scalloped shape of the bulk velocity profile suggests that at cross-streets, where a longitudinal canyon intersects a perpendicular canyon, there is some

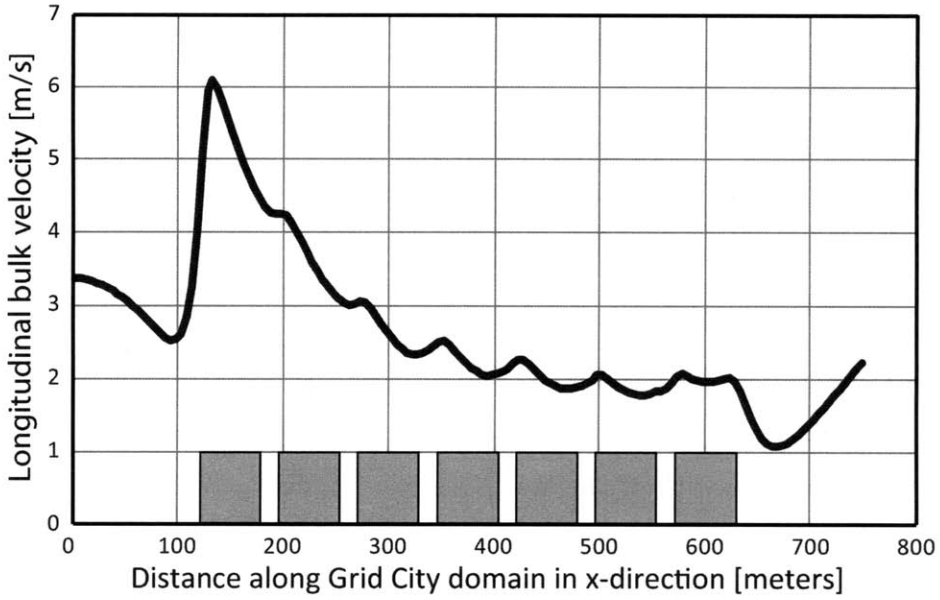

Figure 2-3: Longitudinal bulk velocity down a typical canyon in Grid City

additional fluid entering the longitudinal canyon, either from above or from the perpendicular canyons. This leads to the small increases in bulk velocity, which is likely a sign of increased turbulent mixing in that area of the neighborhood.

Flow through urban canyons in a real neighborhood is a combination of longitudinal and recirculating flow, resulting in helicoidal flow. [47] Therefore relevant neighborhood scale question are - What is the relationship between the canyon velocity and the atmospheric velocity for longitudinal flow? For what angles of flow to a canyon is a longitudinal flow model relevant? These questions will be addressed in Chapters 3 and 4.

2.2 Need for a simple model; an urban planning tool

It would be beneficial to assess the UHI potential of neighborhoods in the early design phase, before making major design decisions such as layout and street orientation; these early decisions have the greatest impact on a neighborhood's microclimate. This also applies to the influence of a particular urban form on pollutant retention. Currently, UHI studies are performed by engineers and meteorologists in existing neighborhoods as in Chow and Roth, 2006. [15] In these studies there is little that can be done in the way of mitigation because the buildings and roads have already been constructed – the building sites and materials cannot be modified. Because early design work for neighborhood layout is principally conducted by urban planners, there is a need for a neighborhood scale microclimate model to assess neighborhoods that caters to the skill set of urban planners. The inputs and outputs of such a conceptual model should be practical and meaningful to an urban planner, and the model should be robust enough that it can be run with confidence by someone without an engineering or urban climatology background.

ENVI-met has advantages and drawbacks in this context. One advantage is that it is very easy to use. The user needs only limited site information to initialize the model including aerodynamic roughness, specific humidity at a height of 2500 meters, wind speed at 10 meters – and the number of outputs generated by the model is enormous. Three-dimensional datasets are created at each time step for more than 50 variables including wind speed, surface heat flux and potential temperature. This information can be visualized spatially with the Leonardo tool, or transiently using a more brute force approach. The ease of use of this model can also be viewed as a disadvantage, uninformed users are able to run the model for a test-case day with default initialization parameters, and will end up with meaningless results for many climates.

An important strength of ENVI-met is that it is a meteorological model – it includes many processes that are not found in computational fluid dynamic codes,

such as models for soil and vegetation. These models are useful to urban planners who are designing neighborhoods with parks and green areas. ENVI-met also allows the user to place the model anywhere in the world and specify a simulation date with which it calculates the sun path and incident radiation on the site.

Aside from considerations for urban planners, it is important to address issues with ENVI-met as a general tool. The model has not been formally evaluated and is not a universally accepted code. The most thorough examination of ENVI-met in English is the doctoral dissertation of Fazia Ali Toudert of Berichte des Meteorologischen Institutes der Universität Freiburg. [1] This document is not a validation of the model, however it provides an explanation of many of the underlying equations and concepts that Bruse used to create ENVI-met, and it discusses the applicability of the model to neighborhood scale studies of outdoor thermal comfort in hot, dry climates.

Aside from the lack of evaluation of ENVI-met, there are also shortcomings built into the model. The most frequently cited shortcoming is the software's treatment of buildings. The building materials in ENVI-met, including roofs and walls, cannot store heat. This is a major argument against using the program for UHI studies because the cause of the UHI phenomenon is often attributed to the increase of impervious, heat storing surfaces in the urban canopy. [1] Further limitations in the building model include an inability to change the schedules of the HVAC systems in the buildings, as well as constant thermal resistance and capacitance properties for all building façades in a given domain, as well as all roofs in the domain.

Another shortcoming of ENVI-met is that users may not vary the boundary conditions for airflow. ENVI-met is initialized by a 1D model which calculates a vertical wind profile based on the logarithmic law in Equation 2.1 using the roughness length and the wind speed at 10 meters. The only type of inlet boundary condition is an open boundary condition, meaning the profile in Equation 2.1 is applied along the domain inlet, and then the wind speed is calculated at each grid point using the finite difference method. After each time step, the wind speed at the grid point just downwind of the inlet boundary is transferred back to the inlet boundary, and the results are calculated with this updated boundary condition. While it may not describe envi-

ronmental airflow perfectly, for the purposes of model evaluation, a more appropriate inlet boundary condition would be a forced condition where the wind profile at the inlet is held constant.

One example of an UHI study using ENVI-met is the work of Hedquist et al from the Center for Environmental Fluid Dynamics at Arizona State University. This group used ENVI-met to simulate the air temperature in Phoenix, Arizona, and subsequently this data was compared to field-measurements taken over a diurnal period. Their ENVI-met simulation under-predicted maximum afternoon temperatures and over-predicted the minimum nighttime temperatures for each of their Phoenix sites, however surface temperature results were generally within 0.5 Kelvin of experimental results. The group was satisfied with the small inconsistencies in air and surface temperature results, and are going to move forward with simulating other design days. Ground surface temperature results were not so promising, with results as high as 30 Kelvin above measured results during midday. Nighttime surface temperature results were within 5 Kelvin of the experimental data. [26] This study did not assess how well ENVI-met wind data compared to the experimental data. This study is typical of the work done with ENVI-met. It yields results that seem acceptable, but because the model has not been evaluated, and the calculations are based on so many models with so few inputs, the results of these studies are not reliable.

Additionally, because the model calculates so many things, it takes a very long time to run even a single case. Domains with buildings often run slower than real time. Increasing computing power does not help, as the model imposes maximum memory limitations and does not run on parallel processors. This is unacceptable for use by urban planners who wish to use a model in the early design phase of a project to quickly assess different design iterations.

This computational time is also unacceptable for a model that has a largest possible spatial grid of 250 x 250 x 30 cells as in ENVI-met 3.1. The size of this simulation is trivial for most commercial computational fluid dynamics software, and the vertical resolution is not fine enough to resolve the street canyon and five building heights above the urban canopy layer, which is stated as best practice by the COST Ac-

tion 732 guidelines. [21]

Overall, ENVI-met in not an acceptable tool for use by urban planners in the early design phase of a project. The building model does not allow for heat storage in the building envelope, which is cited as a major contributor to changes in urban microclimates. It takes hours or days to run simple domains, and because the model had not been evaluated and is not an industry standard, the results are untrustworthy. Aside from being slow and unevaluated, the model was also unacceptable for numerical reasons including the limit on the number of grid points, the limited boundary conditions options and lack of user control. Case studies have been conducted to compare ENVI-met results to experimental measurements, but the results are not convincing and point out further shortcomings of ENVI-met. [16, 19, 26] For example, Chow et al stated that the model has reasonable accuracy, however they find the simulation under predicted temperature on average, and systematically under predicted the temperature in the urban areas of study. They also found that asphalt surfaces cooled more than other urban surfaces after sunset, which they attribute to a lack of regional-scale turbulent exchange, thermal mass of building surfaces and building scheduling. [16] These errors are significant because heat storage in urban surfaces is cited as a major contributor to the UHI effect, and the systematic errors occur in the urban areas, which are the areas of interest. The simulation in this study was run for only a 24-hour period, from 6:00 am to 6:00 am the following day, which means that their results may be confounded because the model may not be fully initialized.

The other models currently available to assess urban microclimate are ill-fitted to be used as an early design phase tool for urban planners. For example, the Weather Research and Forecasting (WRF) model is a mesoscale weather model that is used in atmospheric research. Efforts have been made to use WRF to study the UHI by including an urban plug-in to the model. Because the resolution of WRF is on the order of 0.5 km, individual streets are not modelled and the effect of neighborhood layout on the UHI cannot be studied. Computational fluid dynamics (CFD) models at the scale of a street canyon or neighborhood require a strong background in numerical methods to set up input files, create an appropriate mesh for calculations, and input

the processing instructions that govern the solution of the momentum equations. Such programs are too slow to be useful in preliminary design, often demand significant post-processing to extract useful information and usually do not consider vegetation, building construction and building energy systems. A model made for urban planners would sacrifice some accuracy to allow for faster calculation of results – on the order of one hour.

The work in the following chapters is intended to address the airflow portion of a model for urban planners. Evaluation of this model will be based on comparison with experiment, as well as a more in-depth study with CFD. The method used evaluate this model will be chosen based on computational time and accuracy. Types of airflow models are described below in order of descending computational time:

- Direct numerical simulation (DNS) - a type of CFD that solves the Navier-Stokes equations without a turbulence model; the mesh must resolve the smallest turbulence scale.
- Large Eddy Simulation (LES) - a type of CFD that solves approximate Navier-Stokes equations on a coarser grid than DNS. Sub-grid scale eddies are considered stress terms that act on the explicitly solved large eddies.
- Reynolds-averaged Navier Stokes (RANS) - a type of CFD that solves approximate Navier-Stokes equations with additional Reynolds stress terms to approximate fluctuating velocities (i.e. turbulence). Simulations using the k - ϵ turbulence model, fall into this category. These yield time averaged results. Unsteady flow can be considered with this approach as well.
- Semi-empirical model - a model that relies on experimental relationships rather than theoretical formulas. An example of this is using surface roughness parameterizations to calculate wind profiles.
- Mass-consistent model - a model that fulfills continuity but does not solve the Navier-Stokes equations to calculate the wind field.
- Analytical model - a model that solves theoretical formulas explicitly. Analytical models are not practical for problems with complex geometries or flow conditions.

Ideally, the evaluation model would be a robust industry standard, that can be used with parallel processing. Both DNS and LES are too computationally intensive for evaluation of a model for urban planners. Because we are willing to sacrifice some accuracy to allow for quick results, the evaluation model need not be cutting-edge CFD. A steady RANS model would be appropriate for model evaluation, because these models still discretize the Navier-Stokes equations and solve them on a mesh. Though this model solves the momentum equations throughout the computational domain, the computation of turbulent eddies is simplified to save on computational time. Many commercial CFD codes include RANS models, and we have elected to use Fluent 6.3. [20] This model is widely accepted, can be run on parallel processors, and gives the user the ability to define functions to override parts of the code if more accuracy or specific types of inputs are needed. Within Fluent, we will use the k-ϵ turbulence model. Though this steady turbulence model fail to capture changes in the flow in the time domain, it is appropriate for comparing to wind tunnel results, as the time averaged flow at the inlet does not change with time in a wind tunnel. [21] While real experimental data is the most valuable for evaluating a model, a first step would be to evaluate a model with idealized wind tunnel data or a CFD software package, such as Fluent, that has the option of using the k - ϵ turbulence model.

The type of model we will develop for urban planners will be a combination of a semi-empirical model and an analytical model. A single street canyon will be studied analytically in Chapter 3. In Chapter 4 the street canyon will be made more realistic by introducing parameterizations based on semi-empirical data and relationships. In Chapter 5, this analysis will be extended to idealized neighborhoods by varying values of parameters based on CFD and experimental results.

There is no comprehensive methodology for use by urban planners in the early design phase to determine the impact of their development on the microclimate. The conceptual model that we develop will be able to compare the airflow and turbulent exchange of design iterations, and will enable the user to spatially assess his design for areas that may be prone to the UHI effect or high pollutant retention. This model could be coupled with a similarly intensive model that includes temperature to

act as a starting point for answering design questions such as, for what parts of the year would it be reasonable to cool the buildings in this neighborhood with natural ventilation, and how would this decrease in building energy consumption affect the expected impact of the building on the microclimate?

Chapter 3

Isolated, idealized urban street canyon

Idealized cities are often considered as a series of blocks that act as roughness elements to the atmospheric flow above. [13] Using this approach, we simulated the airflow around a grid of evenly spaced, cube-like buildings with a logarithmic wind profile at the inlet using ENVI-met as discussed in Section 2.1. After some distance along the canyon, the flow exhibited little change in longitudinal bulk velocity, and the net vertical velocity out of the street canyon was nearly zero – in this section of the canyon, the flow was almost fully developed. This is in agreement with Dobre et al; they make observations about the flow in a real intersection in London based on the idealization of an infinitely long street with the assumption that there is no net vertical mass flux associated with the longitudinal canyon flow. [17]

Assuming that fully developed flow occurs in real neighborhoods, which are made up of series of intersecting street canyons, we first consider an idealized version of this fundamental neighborhood element, an infinitely long street canyon approximated by a plane with a notched channel. [46] The urban boundary layer flow can be approximated as boundary layer flow over a rough plate. This raises the question: what drives the flow in the urban canopy layer? Specifically, what overcomes the decrease in momentum from the shear stress on the fluid imposed by the no slip boundary condition at the canyon walls? If the street canyons were four-sided ducts the flow would

have to be pressure driven, but is there a pressure drop along a street canyon, what about across the entire neighborhood? What is the bulk velocity in the canyon? We address the pressure drop question for an isolated, ideal canyon in Section 3.1 using Fluent 6.3 by studying a domain made of a three-sided channel with a large volume of fluid above it meant to approximate the large mass of air in the urban boundary layer. The pressure drop down the domain is found to be small in comparison to the pressure drop required to drive the flow in a canyon-sized three-sided channel. In the case with the large volume of fluid above the channel, the air above the channel is driven by this small pressure drop, and momentum exchange with this large air mass in drives the flow in the street canyon. The fully developed, momentum driven case where the atmospheric flow is parallel to the canyon is studied analytically with control volume arguments in Section 3.2. An exchange coefficient is defined in Section 3.3 for the interaction of the in-canyon and above-canyon flow based on plume entrainment theory. [41] This approach is extended to street canyons oriented perpendicular and at any angle to the atmospheric flow direction in Sections 3.4 and 3.5.

3.1 What drives the flow down an idealized street canyon?

If the simplest idealization of a neighborhood domain is a plane with a series of notched channels, one of these channels may be isolated to consider the simplest idealization of a street canyon. Before building and simulating this domain in Fluent, we modelled a square duct of street canyon scale to test the ability of the software to accurately simulate fully developed flow over rough surfaces. The square duct has a length of 50 meters, a height and width of 20 meters and is shown in Figure 3-1.

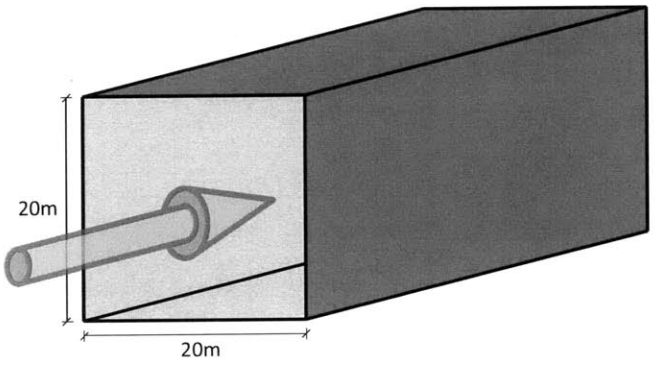

Figure 3-1: Square, four-sided duct domain

The duct was uniformly meshed with 0.5 meter hexahedral finite volumes, and the $k - \epsilon$ model with default initial values was selected as the Reynold-Averaged Navier-Stokes (RANS) turbulence model. The inlet and outlet surfaces were set to streamwise-periodic boundary conditions to approximate an infinitely long duct. The periodic boundary conditions were run with a fixed mass flow rate, and the initial pressure drop was set to zero, however streamwise-periodic boundary conditions allow a pressure drop across periodic boundaries that are separated by a translation. [20] Periodic boundary conditions are explained qualitatively below, and are shown schematically in Figure 3-2:

- Mass enters the domain at the inlet with a uniform velocity profile.
- Mass flows through the domain and the flow parameters begin to develop.
- Velocity and turbulence profiles calculated at the outlet are set to the inlet.

- Previous two steps are repeated until inlet and outlet profiles are equal.

The mass flow rate of air through the domain was set to 4900 kg/s at a density of 1.225 kg/m^3, which is equivalent to a uniform velocity profile of 10 m/s for air flowing normal to the inlet plane. The four walls of the duct were set to zero velocity and the Nikuradse sand grain roughness was increased for each successive simulation in increments of 0.05 meters, from 0.05-0.25 meters. This sand grain roughness is defined as the average depth of the projections of roughness elements on the duct walls into the duct. Nikuradse used sifted sand for his experiments to ensure the materials producing the roughness were of similar heights. [42] The limit on the maximum turbulent viscosity ratio was increased from $1 \cdot 10^5$ to $5 \cdot 10^6$. This ratio is defined as

$$TVR = \frac{\mu_t}{\mu} = \frac{u' L}{\mu} \tag{3.1}$$

where TVR is the turbulent viscosity ratio, μ_t is the eddy viscosity, μ is the dynamic viscosity, u' is the velocity fluctuation, and L is the turbulence length scale. A low turbulent viscosity ratio limit prevents large-scale mixing of the fluid. While the turbulent viscosity ratio may not reach $1 \cdot 10^5$ for this square duct, it was increased to a value that is much larger than typical values for street canyons or neighborhood scale simulations. Because increasing the limit will not affect the smaller scale simulations, the increase should ensure that the limit does not become a confounding variable in later simulations. The default first order upwind scheme was used for discretizing the

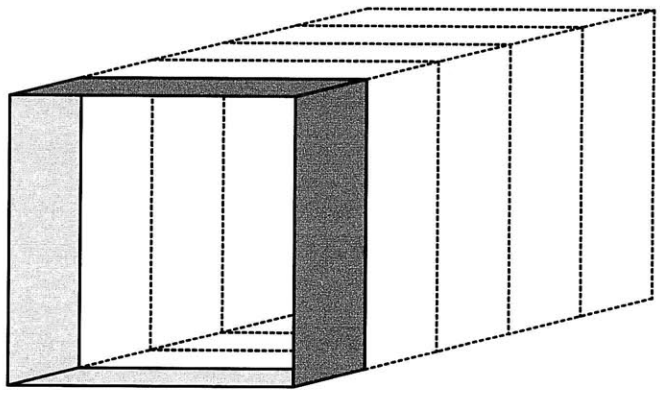

Figure 3-2: Schematic of periodic boundary condition

governing equations about each finite control volume because it is less computationally intensive and converges more quickly than second order schemes. [20] Simulation results are compared to empirical results in this section to ensure that the accuracy of this scheme is appropriate for the idealized street canyon problem. Finally, the cell-based Green-Gauss solver is used because it is less computationally intensive than the node-based solver. [20] Because the meshes in this work are structured and often uniform, this scheme and solver combination will be less prone to numerical diffusion and errors due to interpolations of gradients onto cell-faces. [20]

The Reynolds number, which is defined as

$$Re = \frac{\rho\, u\, D_h}{\mu}, \tag{3.2}$$

is $1.37 \cdot 10^7$ for this domain where ρ is the density of air, μ is the dynamic viscosity of air, $1.7894 \cdot 10^{-5}$ kg/(m·s) at 300 K, and D_h is the hydraulic diameter of a rectangular duct:

$$D_h = \frac{4\, area}{wetted\, perimeter} = \frac{2\, H\, W}{H + W}, \tag{3.3}$$

where H and W are the height and the width of the duct, respectively. The relative roughness of the walls in this domain can be calculated as

$$relative\, roughness = \frac{k_s}{D_h} \tag{3.4}$$

where k_s is the Nikuradse sand grain roughness applied to the no-slip wall boundary conditions on the duct walls.

The rough wall functions used in Fluent have the form of standard smooth wall functions, with additional empirically derived constants to account for the presence of Nikuradse sand grain roughness. [20] These additional constants have been correlated to non-dimensional roughness height for cases of uniform roughness. This relationship is displayed in Equation 3.5:

$$k_s^+ = \frac{\rho\, k_s\, u_*}{\mu}, \tag{3.5}$$

where u_* is the friction velocity, which we approximate as 1/10 of the mean flow. Fluent considers three flow regimes when using the rough wall function – the hydrodynamically smooth regime: $k_s^+ \leq 2.25$, the transitional regime: $2.25 < k_s^+ \leq 90$ and the fully rough regime: $k_s^+ > 90$. For the smallest Nikuradse sand grain roughness considered, 0.05 meters, we find that k_s^+ is equal to the more than 3000 times the friction velocity. This means that at the roughnesses we are considering, Fluent always uses the fully rough version of the rough wall function. [20] Smooth wall functions have parameters that define a range of distances appropriate for the distance between the wall and the nearest calculation node. In the case of the rough wall function, however, it is not meaningful to have a mesh with the center of the finite volume cell closer to the wall than the value of the Nikuradse sand grain roughness. [20] This means that for the Nikuradse sand grain roughnesses considered in Chapters 3, 4 and 5, ranging from 0.05-0.8 meter mesh sizes on the order of 1-2 meters are appropriate. The effect of the coarseness of the mesh on simulation results will be discussed in a mesh sensitivity analysis in Section 4.5. Blocken et al address issues with Fluent's rough wall function and its ability to generate the boundary layer flow characteristic of flow over building-like roughness. [5] We avoid this problem by using periodic inlet and outlet conditions which approximate fully developed flow, or by building domains that are long enough to allow the flow to become fully developed in the urban canopy layer.

Using Equation 3.4 we find our range of k_s/D_h is 0.0025-0.0125, and using the Moody diagram for pipe flow displayed in Figure 3-3, we conclude that all of our simulations are all in the fully rough regime.

This means that the Darcy-Weisbach friction factor can be calculated using the asymptotic solution of Nikuradse's equation as

$$f = \left(1.74 + 2\ \log_{10}\left(\frac{D_h}{2\,k_s}\right)\right)^{-2}. \text{ [39, 42]} \tag{3.6}$$

The friction factor values calculated with Equation 3.6 were compared to the simulated friction factor calculated using pressure drop results simulated in Fluent and

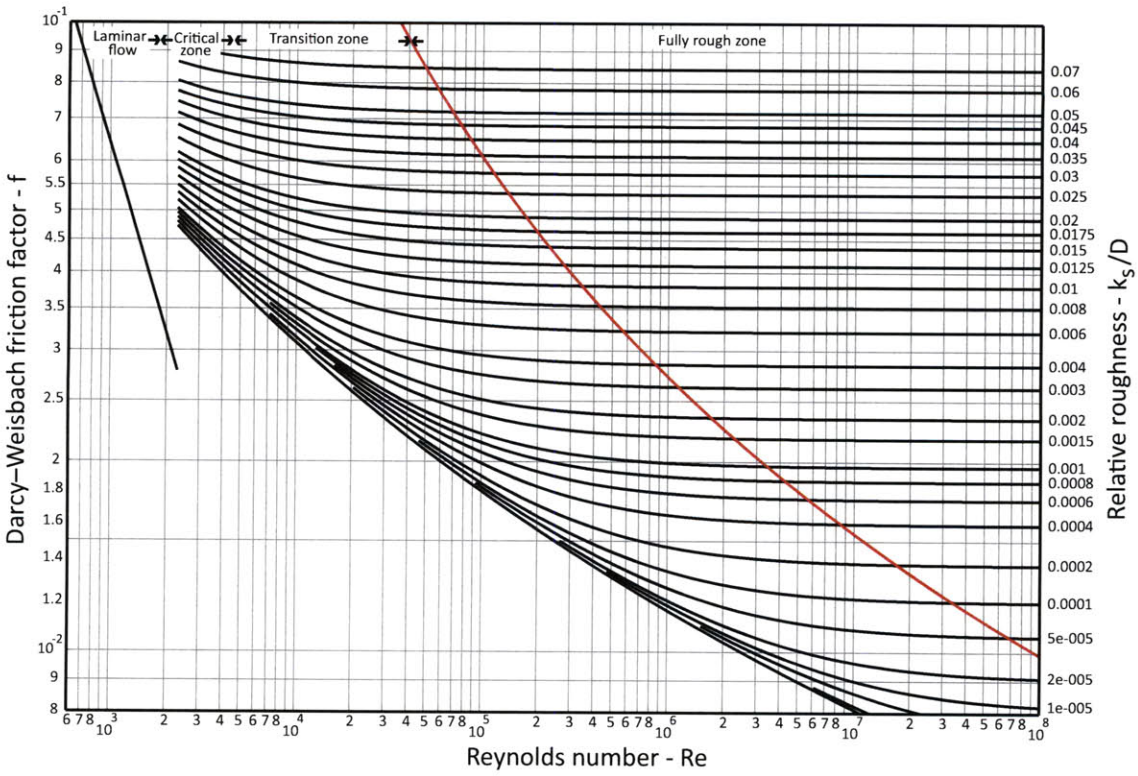

Figure 3-3: Moody diagram for pipe flow [39]

the Darcy-Weisbach equation,

$$f = \frac{\Delta P}{\frac{L}{D_h}\frac{\rho u_\infty^2}{2}}. \tag{3.7}$$

In this equation, $\Delta P/L$ is pressure drop per unit length calculated by Fluent, and u_∞ is the free stream velocity of the flow, which is the mean velocity in the case of a duct and is the velocity outside of the boundary layer in the case of boundary layer flow. Because the inlet and outlet boundary conditions for these simulations are periodic, the flow in the duct becomes fully developed. This means that the velocity profiles are unchanged along the longitudinal axis of the duct, therefore the drag force imposed on the fluid by the walls is constant, so it follows with the application of the steady flow momentum equation, that the pressure drop per unit length is constant along the length of the duct to overcome this force. The friction factor results are plotted in Figure 3-4. The dashed line is a linear least-squares regression fit for the data with a fixed y-intercept at zero. The slope of the line is 0.997 and the coefficient of

determination is 0.986. Because these values are nearly unity, we assert that Fluent is an appropriate tool for modelling a rough rectangular duct, and the accuracy of the tool will be acceptable for future work with idealized, and therefore inherently somewhat unrealistic, street canyons and neighborhoods.

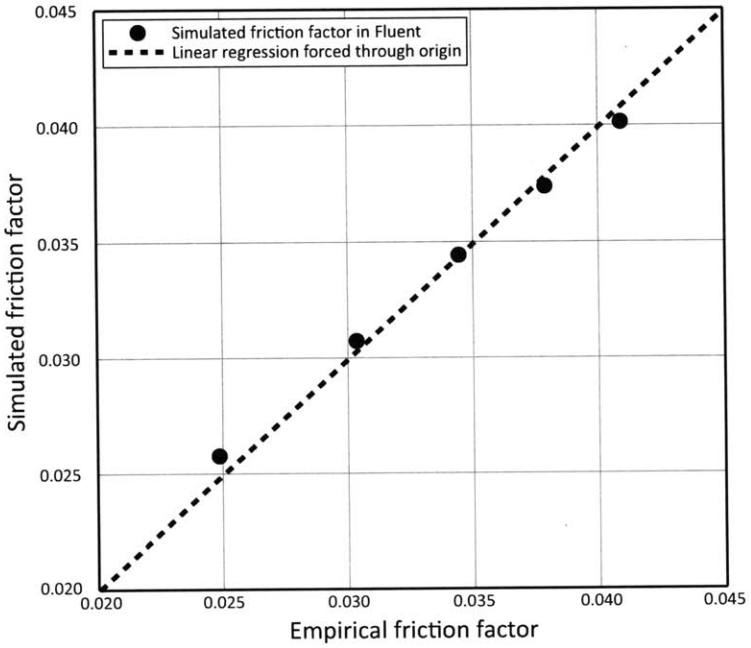

Figure 3-4: Simulated friction factor vs. Empirical friction factor: study of a square duct

The next step towards understanding the idealized, isolated street canyon is to confirm that the flow in the three-sided channel is pressure driven, and that the pressure drop can be predicted by Equations 3.6 and 3.7. This scenario was tested in Fluent using the computational domain in Figure 3-5. This domain is the same as the four-sided duct domain in Figure 3-1, except that the no-slip boundary condition on the upper wall is replaced with a slip boundary condition. A surface with a slip boundary condition applies no shear stress to the fluid to the fluid. Substituting the friction factor calculated with Equation 3.6 into Equation 3.7 and solving for $\Delta P/L$ for the four-sided duct domain, we may compare this calculated pressure drop per unit length for the four-sided duct to the simulated linear pressure drop for the three-sided channel. We expect the friction factor associated with the walls to be the same for the domains in Figures 3-1 and 3-5. Because the wetted perimeter in Equation 3.3

is 75% that of the three-sided channel, we expect the pressure drop per unit length for fully developed flow in the three-sided channel to be about 75% of that found for the four-sided duct for a given Nikuradse sand grain roughness, mean velocity and fluid density as per Equation 3.7.

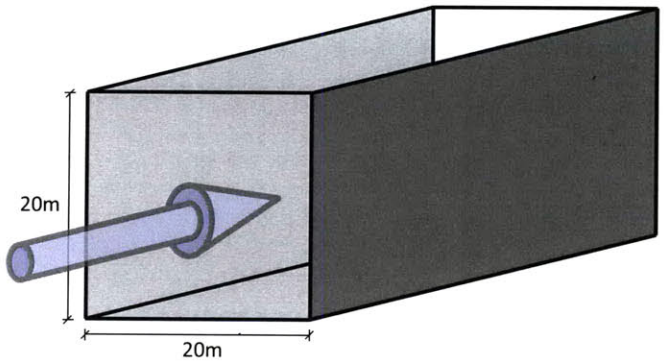

Figure 3-5: Three-sided channel domain

The domain in Figure 3-5 was simulated for the same roughnesses as those simulated for the four-sided duct. Aside from the slip boundary condition on the top wall, all of the settings in Fluent were kept constant. The pressure drop per unit length results were normalized by those calculated for the four-sided duct using Equations 3.6 and 3.7, and are plotted against the sand grain roughness for the five simulations in Figure 3-6.

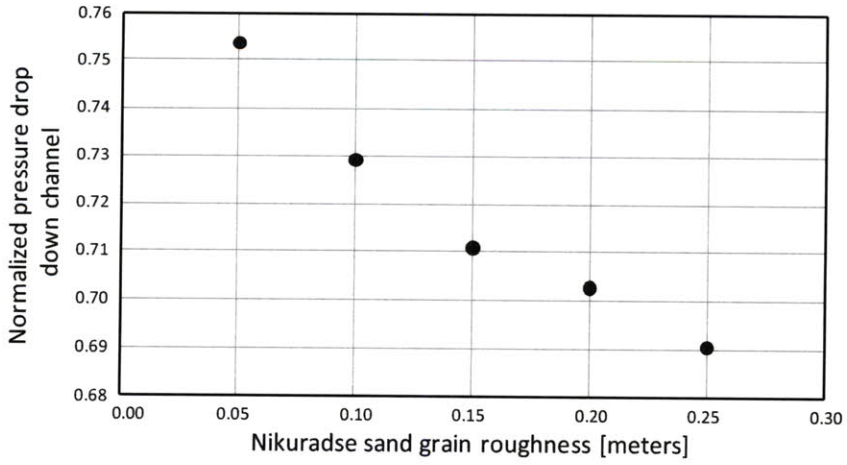

Figure 3-6: Fluent results for normalized pressure drop down the three-sided channel vs. Nikuradse sand grain roughness, k_s [meters]

Figure 3-6 shows that for small roughnesses, the pressure drop per unit length down the three-sided channel is about 75% that of the four-sided duct. However as the roughness increases, the pressure drop required to overcome the shear stress on the rough walls decreases. This phenomenon can be explained qualitatively by comparing the velocity contours of the most rough and least rough simulations performed for the three-sided channel and the four-sided duct. These contours are displayed in Table 3.1. The contours for both four-sided duct cases behave as expected – the velocity gradients are approximately the same for each of the four walls in a given simulation. The velocity gradients are larger for the case with a larger Nikuradse sand grain roughness, as evidenced by the maximum velocity being higher in the case with the larger roughness. The velocity gradients near the no-slip wall conditions for the three-sided and the four-sided cases are fairly similar for a given roughness. The three-sided case, however, clearly has less cross-sectional area affected by areas with steep velocity gradients. There is a higher mass flow rate near the wall with the slip boundary condition than near that wall when it has a no-slip condition in the four-sided duct case. This means that the maximum velocity must be greater in the four-sided case than in the three-sided case to conserve mass for a particular roughness. Therefore, the velocity gradients will be smaller in the three-sided case which in turn means the shear stress on the three walls will be lower than the shear stress on the walls in the four-sided case. Thus, the pressure drop required to overcome this shear stress will be less than 75% of the pressure drop required for the four-sided case. This effect becomes more pronounced as the wall roughness increases because the change in the area of the pipe that does not experience steep velocity gradients increases. Therefore, when comparing the duct domain to the channel domain, the change in pipe area that has larger flow velocities is increased by a bigger percentage for the ducts with larger Nikuradse sand grain roughnesses. This means that the maximum velocity decreases by a bigger percentage between the two domains in the cases with larger Nikuradse sand grain roughness. There is a larger change in velocity gradients between the duct and the channel cases as the roughness of the walls increase, resulting in lower shear stresses on the walls in these cases, and thus

there is a lower pressure drop down the domain normalized to the four-sided case of the same roughness.

The results from the three-sided duct are consistent with our intuition, thus Fluent proved to be an appropriate simulation tool for this type of domain. Additionally, the friction factor and hydraulic diameter arguments held for predicting the pressure drop down an infinitely long channel with a low relative roughness. Knowing that the expected pressure drop down the three-sided channel is approximately 75% of the pressure drop down the duct, we can simulate an idealized street canyon, as in Figure 3-7, and compare the pressure drop results of the three-sided channel to better understand what drives the flow down a long street canyon in the real world. In this domain the three-sided channel is allowed to interact with a large volume of air above. The simulation was run for two scenarios, first the lateral boundary conditions on all surfaces except the channel walls were set to slip boundary conditions. This domain was meshed uniformly with 2 meter hexahedral elements. Mesh size decisions will be discussed in Section 4.5. The length of this domain was increased to 1000 meters. Next the horizontal surfaces above the building façades were changed to no-slip wall boundary conditions and were assigned Nikuradse sand grain roughnesses equal to those inside the channel. These surfaces are equivalent to building roofs and are labeled in Figure 3-7. In this domain, the channel was meshed uniformly with 2 meter hexahedral elements. The large volume above was meshed with hexahedral elements that started as 2 meter cubes; the vertical dimension of these elements was set to grow as distance from the channel increased at a constant rate of 1.065. This does not exceed maximum cell expansion ratio of 1.2 for a high quality mesh. [21] The reasoning behind these changes in mesh structure is discussed in Section 4.5. Each scenario was run for the five roughness values used for the duct and the channel. For all 10 cases the mass flow rate was increased to 127,400 kg/s to maintain an initial uniform inlet of 10 m/s. All other Fluent parameters were the same as the previous simulations.

The pressure drop per unit length, normalized to 75% of the pressure drop per unit length of the four-sided duct with canyon dimensions, is plotted against sand

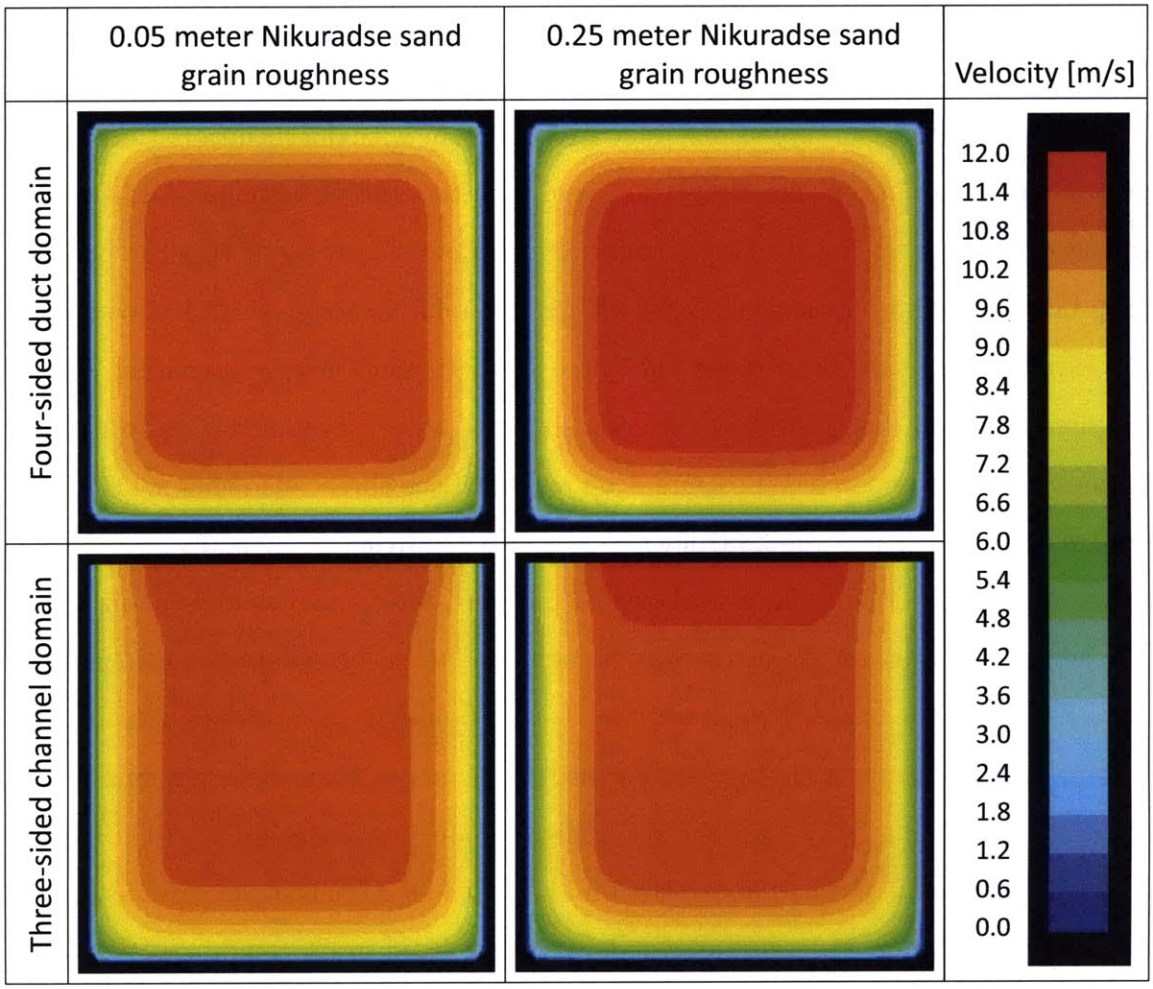

Table 3.1: Comparison of simulated velocity contours for four-sided duct and three-sided channel domains

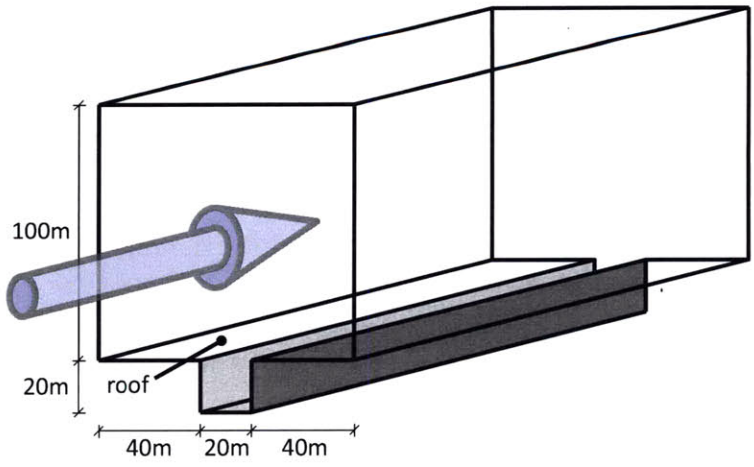

Figure 3-7: Three-sided channel domain with large volume above

grain roughness in Figure 3-8. We consider this to be analagous to normalizing to the expected pressure drop of the three-sided channel. The pressure drop per unit length for the three-sided channel domain with slip boundary conditions on the roof was approximately 1.5% of the expected value, and the pressure drop per unit length for the three-sided channel with no-slip wall boundary conditions on the roof was approximately 3.0% of the expected value. The mass flow rate through the street canyon in this domain was approximately 50% that of the three-sided channel domain for these simulations.

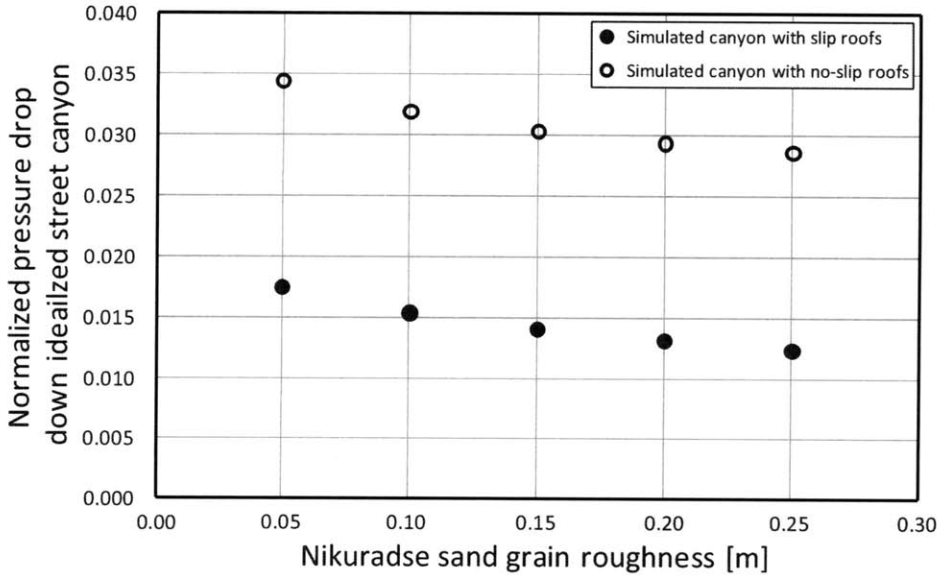

Figure 3-8: Fluent results for normalized pressure drop down the idealized street canyon vs. Nikuradse sand grain roughness, k_s [meters]

Based on Equation 3.7, we conclude that if the flow in the street canyon in Figure 3-7 were pressure driven, the normalized pressure drops in Figure 3-8 should be 25% for the case where the velocity, and therefore mass flow rate in the street canyon is reduced by 50%. Because the values in Figure 3-8 are much less than 25%, we conclude that the large airmass above the canyon was driven by the small pressure drop down the street canyon domain, and momentum exchange with this large air mass drove the flow in the canyon. If the size of the large volume above the channel was increased, the required pressure drop to drive this large air mass would continue to approach zero. The shape of the curves suggested by the results in Figure 3-8

can be explained by the same arguments used to justifiy the results in Figure 3-6. This effect is less extreme than in street canyon domains because much of the fluid leaves the canyon before reaching the fully developed solution. The boundary layer in the street canyon domain can grow without being bounded by the top surface of the channel, so the velocity gradient normal to the no-slip surfaces be will approximately uniform, much like the four-sided duct domain in Figure 3-1. The longitudinal bulk velocity data for the simulations displayed in Figure 3-8 is discussed in Section 4.4.

The physics behind momentum exchange in a turbulent flow can be explained by considering simplified versions of the Navier-Stokes equations. Though turbulent flow satisfies the Navier-Stokes equations at any instant in time, there are fluctuations in velocity and pressure at small scales that cannot be quickly realistically resolved computationally. [31, 45] For our work, we are not interested in exact magnitude or location of these small fluctuations, so we consider the time-averaged Navier-Stokes equations. These consider each velocity and pressure term in the full equations to be the sum of an averaged term plus a fluctuating term. These equations simplify to a set of equations that describe the mean motion of the flow, and the effect of the fluctuations on the mean flow. The effect of the fluctuations of the mean flow are known as the Reynolds stress terms, and are displayed for Cartesian coordinates in the Reynolds stress tensor:

$$\tau_{x,y} = \begin{bmatrix} -\rho\,\overline{u'^2} & -\rho\,\overline{u'\,v'} & -\rho\,\overline{u'\,w'} \\ -\rho\,\overline{u'\,v'} & -\rho\,\overline{v'^2} & -\rho\,\overline{v'\,w'} \\ -\rho\,\overline{u'\,w'} & -\rho\,\overline{v'\,w'} & -\rho\,\overline{w'^2} \end{bmatrix}, \tag{3.8}$$

where $\tau_{x,y}$ is the Reynolds stress tensor and $\overline{u'}$, $\overline{v'}$ and $\overline{z'}$ are the velocity fluctuations in the x, y and z-directions respectively. [31, 45] These terms represent the stress in the fluid due to the turbulent velocity components. The off-diagonal terms are of particular importance to our work because they are the turbulent shear stresses in the fluid.

If we consider two-dimensional turbulent flow over a rough horizontal flat plate with a no-slip boundary condition, the derivative of the velocity profile, du/dy, will

be non-zero. This means that fluid particles at greater distances from the plate will have greater velocities than those at the same horizontal position that are closer to the plate. The turbulence in this flow is due to momentum exchange caused by the Reynolds shear stress in the flow.

A common qualitative explanation for this phenomenon involves two infinitely long trains filled with rocks that are moving on nearby tracks at different speeds. The faster train is like the fluid particle that is at a greater distance from the horizontal plate, and the slower train is like the fluid particle nearer to the plate. These trains want to travel at the same speed, so the people in the fast train throw some of their rocks into the slow train, and vice versa. For rocks of the same mass, the rocks from the slow train have less momentum than the rocks from the fast train because the rocks from the fast train have a greater horizontal velocity. This vertical exchange of rocks, will result in a loss of momentum and therefore a decrease of velocity of the fast train, and a gain of momentum and increase in velocity of the slow train. The vertical exchange between the trains is analogous to a vertical fluctuation; the transfer of particles (and momentum) vertically results in changes in the horizontal velocity (and momentum) of the particles.

Solving the time-averaged Navier-Stokes equations with these fluctuations for a street canyon domain would require computational fluid dynamics. To avoid this, we consider a simplification of this idea based on the assumption that the flow in the street canyon is approximately uniform and the flow above the street canyon is also approximately uniform, and moves at a different speed than the street canyon flow. [4] This is expressed schematically in Figure 3-9.

The above canyon and in canyon flows on the right hand side of Figure 3-9 are like the two trains, except that rather than slowing each other there is some non zero turbulent exchange at the interface of the flows. This is equivalent to saying that the Reynolds shear stress in two flows is negligible in comparison to the Reynolds shear stress at the interface of the two flows. The magnitude of this shear stress will be directly related to the velocity difference of the two uniform flows. [4, 23] Typical contours for turbulent kinetic energy (TKE) and longitudinal velocity are

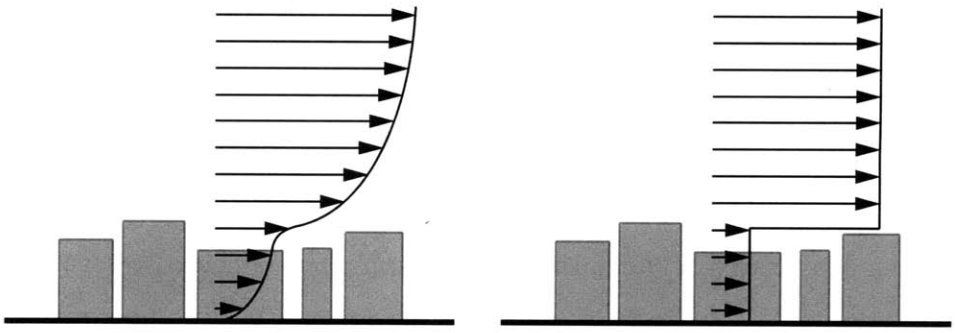

Figure 3-9: Schematic of boundary layer flow through building array (left) and simplified flow through building array (right)

shown in Table 3.2 for the cases where the roof surface in Table 3-7 is assigned a slip boundary condition and a no-slip boundary condition. Based on the TKE contours, we conclude that much of the mixing between the urban canopy layer and the urban boundary layer occurs at roof level. Similar assumptions are made by Morton et al for the parameterization of plume entrainment as discussed in Section 3.3. [41] This assumption becomes less appropriate as the aspect ratio of the considered street canyon increases because the velocity in narrow street canyons will be less uniform than in wide street canyons. The momentum flux due to the Reynolds shear stress at this interface will be used in a control volume approach to this problem in Section 3.2.

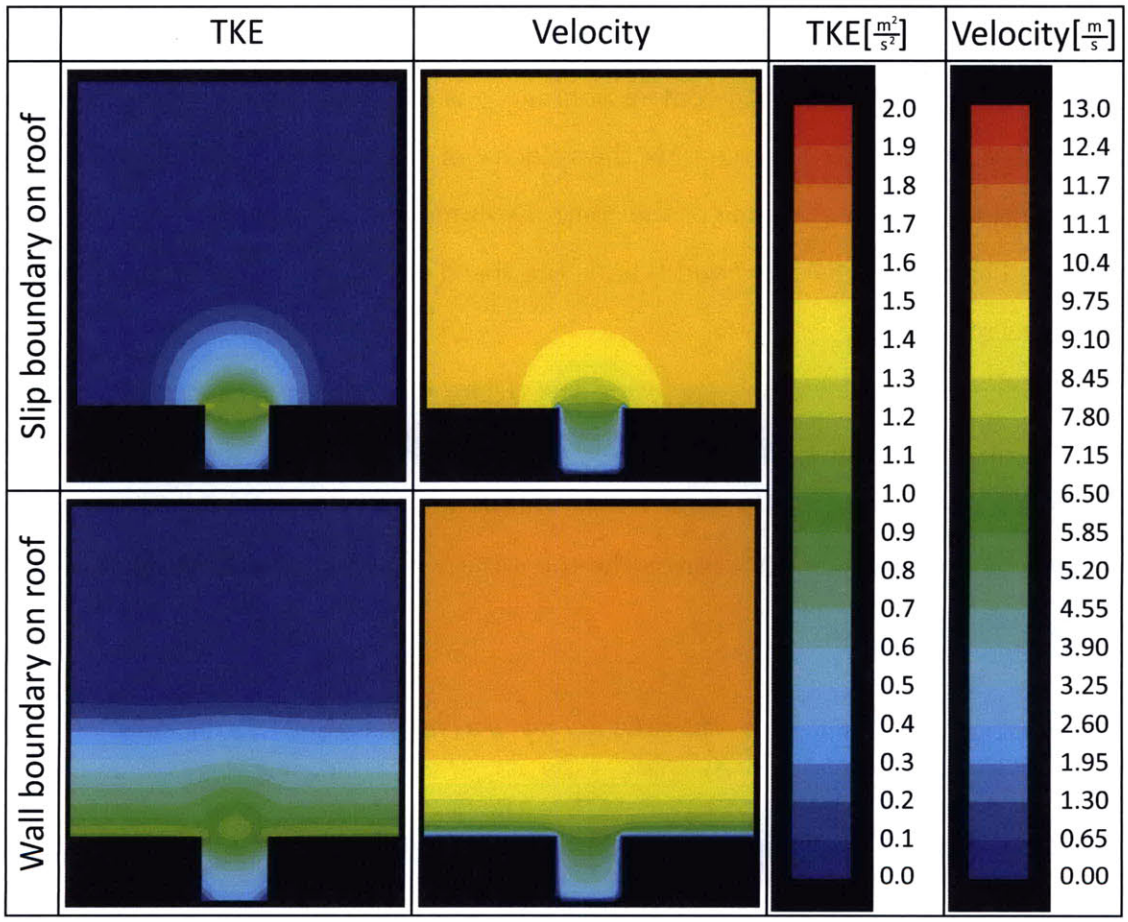

Table 3.2: Typical velocity and TKE contours for the three-sided channel with large volume above domain

3.2 Control volume arguments

The case where the atmospheric wind is aligned with the canyon axis can be studied analytically for the momentum driven case that was simulated in Section 3.1. Recall the equation for linear momentum for a control volume:

$$\sum \vec{F}_{CV} = \frac{d}{dt} \int_{CV} \rho\, v\, dV + \oint_{CS} \rho\, v\, (\vec{v} \cdot \vec{n})\, dA \tag{3.9}$$

where F_{CV} is any force on the control volume, ρ is the density of the fluid, v is the speed of the fluid in the volume, $\vec{v}$ is the velocity of the fluid, $\vec{n}$ is the normal to the control surface, V is the volume of the control volume and A is the area of the control surfaces. The dot product of $\vec{v}$ and $\vec{n}$ finds the speed of the fluid that is perpendicular to the control surface.

Consider a control volume enclosing the urban canopy layer in a street canyon parallel to the atmospheric wind. For the fully developed and steady state case where the shear stress applied to the fluid by the building façades and the ground must be balanced by a momentum flux across the top surface of the canyon, Equation 3.9 can be rewritten as

$$-\oint_{CS-ground} \tau\, dA \; - \oint_{CS-leftwall} \tau\, dA \; - \oint_{CS-rightwall} \tau\, dA = \oint_{CS-top} \rho\, u_e\, u_{cl}\, dA \; - \oint_{CS-top} \rho\, u_e\, u_a\, dA. \tag{3.10}$$

In this equation, τ is the shear stress applied to the fluid by the building façades and the ground, u_a is the characteristic atmospheric velocity, u_{cl} is the spatially averaged longitudinal bulk velocity in the canyon for the fully developed case, and u_e is the spatially averaged exchange velocity between the street canyon and the atmospheric flow as defined by Bentham and Britter. [4] The exchange velocity is in the vertical direction, and is responsible for the turbulent mixing between the urban canopy layer and the urban boundary layer. In the fully developed flow case, the net vertical velocity is zero, to conserve mass. The exchange velocity, u_e is non-zero in the fully developed case. It is a fluctuating velocity that can be combined with the relative velocity between the two fluid masses to approximate the momentum flux at

the interface of the above canyon and in canyon flow due to the Reynolds stresses, defined in Equation 3.8:

$$\rho \overline{u' v'} \sim \rho (u_a - u_c)\ u_e \tag{3.11}$$

The exchange velocity transfers mass, momentum, pollutants and heat into and out of the canyon, and is responsible for driving the flow in the canyon. This situation is depicted schematically in Figure 3-10 for the idealized street canyon domain, introduced in Section 3.1, as it pertains to a gridded city.

The average shear stress on the walls surrounding the canyon is often written as

$$\tau = \rho\, u_*^2 \tag{3.12}$$

where u_* is the friction velocity. Substituting Equation 3.12 into Equation 3.10 and introducing the appropriate control surface areas we find

$$\rho\, u_*^2\, (L\,W + L\,H + L\,H) = \rho\, u_e\, (u_a - u_{cl})\, L\,W. \tag{3.13}$$

A roughness parameter, the skin friction coefficient: C_f, is the non-dimensional surface shear stress which is defined as

$$C_f = \frac{\tau}{\frac{1}{2}\,\rho\, u_\infty^2}, \tag{3.14}$$

where u_∞ is the characteristic free stream velocity of the fluid flowing over a surface. For the street canyon, we assume $u_\infty = u_{cl}$. Combining Equations 3.12, 3.13 and 3.14, we can express the exchange velocity between the street canyon and the atmosphere in non dimensional form as:

$$\left(\frac{u_e}{u_a - u_{cl}}\right) = C_f \left(\frac{u_{cl}}{u_a - u_{cl}}\right)^2 \left(\frac{H}{W} + \frac{1}{2}\right), \tag{3.15}$$

where the expression has been non-dimensionalized with respect to the relative velocity between the atmospheric wind velocity and the bulk longitudinal velocity in a street canyon.

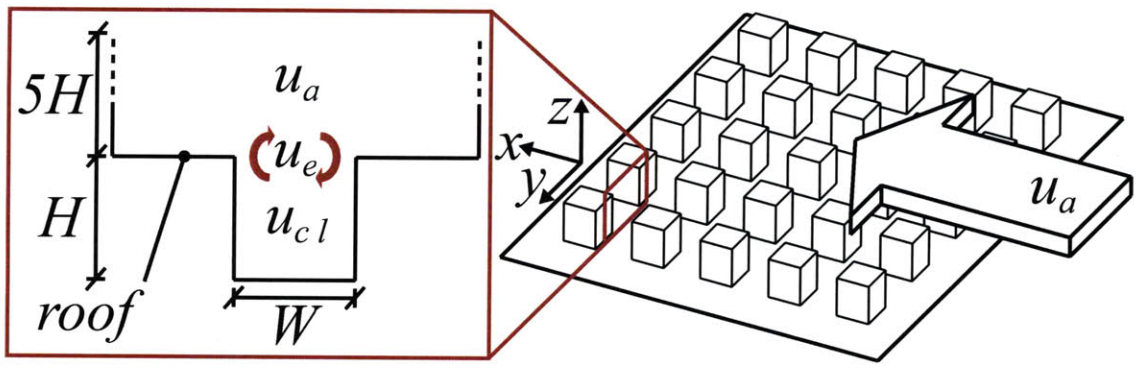

Figure 3-10: Cross sectional view of a street canyon that is parallel to atmospheric flow, idealized as three-sided channel with a large volume above

3.3 Exchange coefficient for longitudinal flow

We define the left hand side of Equation 3.15 to be an exchange coefficient,

$$\alpha = \frac{u_e}{u_a - u_{cl}}. \tag{3.16}$$

This exchange coefficient is our way of parameterizing the exchange process between two uniform flows with different velocities. The idea of parameterizing the mixing process with a constant coefficient was introduced in plume entrainment theory. [41] Morton et al approximates the shape of the profile across a buoyant plume in a stationary fluid as a top hat. They tested this idea experimentally and found that their entrainment velocity was related to the velocity of the plume. Specifically, they discovered that the ratio of these values was a constant. Our exchange coefficient is based on the velocity difference between the flow in the street canyon and the flow above, and the turbulent exchange between these regions, which is quantified by the exchange velocity, u_e as in Equation 3.11. In the case of a street canyon that is parallel to the flow, u_{cl} and u_a are in the same direction, and the relative velocity in the denominator of Equation 3.16 generates a shear stress in the fluid and turbulent mixing between the urban canopy layer and the urban boundary layer above. The flow in a neighborhood is equivalent to flow around and over many bluff bodies. [44] At Reynolds numbers that are large, meaning greater than $Re = 10,000$, there is separation in the flow over bluff bodies regardless of the nature of the boundary layer. [50] Because the flow in street canyons meets this Reynolds number threshold, the flow structure and turbulent mixing in neighborhoods will largely be based on the separation off of and reattachment onto building surfaces, and will be insensitive to Reynolds number. Therefore, like the entrainment coefficient for a plume, we assert that the exchange coefficient is constant for a given neighborhood geometry, and we conclude that for street canyon flows, it is insensitive to Reynolds number. [41] This means that knowing the atmospheric wind velocity, geometry of the canyon, and the skin friction coefficient of the canyon surfaces, we can analytically determine an approximation of the bulk longitudinal velocity in the canyon. This

information could be of considerable use to urban planners, and is expressed by combining Equations 3.15 and 3.16 as

$$\frac{u_{cl}}{u_a} = \left(\sqrt{\frac{C_f \left(\frac{H}{W} + \frac{1}{2} \right)}{\alpha}} + 1 \right)^{-1} . \tag{3.17}$$

The left hand side of Equation 3.17 shows that for a given canyon aligned with the wind, the bulk velocity in the street canyon scales linearly with the atmospheric velocity. Typical values for the skin friction of a façade in a real street canyon will be discussed in Section 4.1. The exchange coefficient varies with neighborhood geometry, and the effect of varying the exchange coefficient on the flow in a single, infinitely long canyon will be discussed in Sections 4.2 and 4.4. The relationship between the exchange coefficient and neighborhood parameters will be discussed in Section 5.3.

3.4 Exchange coefficient for perpendicular flow

The most commonly studied canyon flow is the case where the atmospheric flow is perpendicular to the axis of the street canyon. These flows are characterized by one or more recirculating vortices in the canyon, and the number of vortices is partially dependent on the aspect ratio of the canyon (H/W). [27, 7] Figure 3-11 shows this situation schematically as it pertains to a gridded city. Like the longitudinal case, the perpendicular case has an exchange velocity which is responsible for ventilating the canyon. We define an exchange coefficient for the recirculating case as

$$\alpha = \frac{u_e}{u_a - u_{crh}} \longrightarrow \frac{u_e}{u_a} \tag{3.18}$$

where u_{crh} is defined here as the component of the rotational velocity that is horizontal as in the right hand side of Figure 3-11, spatially averaged over the cross section of the canyon. This component of the canyon flow is perpendicular to both the longitudinal bulk velocity and the vertical velocity associated with the vortex, however at the top of the canyon it is parallel to the atmospheric flow. This means that the relative velocity in the denominator of Equation 3.18 is a measure of the shear stress in the fluid across the top of the canyon, which is responsible for the turbulent mixing. The exchange coefficient is constant for a given geometry, and in the case of a street canyon that is perpendicular to the flow, u_{crh} and u_a are in the same direction. In the ideal perpendicular case, both u_{crh} and u_{cl} are zero.

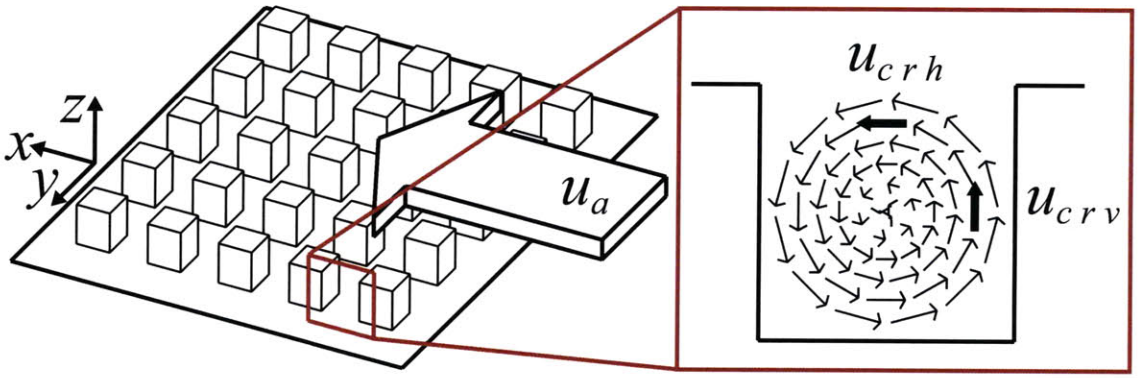

Figure 3-11: Cross sectional view of a street canyon that is perpendicular to atmospheric flow

3.5 Exchange coefficient for angle flow

When the canyon is at an angle to the free stream atmospheric flow, the flow in the canyon is a combination of recirculating flow and longitudinal flow. This scenario is the most realistic, yet it is less studied than the cases where the wind is aligned with or perpendicular to the street canyon. [47] Dobre et al looked at experimental results from the DAPPLE project in London for a canyon at an angle to the atmospheric flow. [17] They found that both the longitudinal and recirculating flow velocities varied linearly with the component of the atmospheric velocity along the parallel and perpendicular axes of the canyon respectively. This is in agreement with the relationship derived in Equation 3.17; the right hand side of the equation is a constant for a particular canyon. Soulhac et al compare an analytical model based on flow regime to numerical simulation for various wind directions and canyon aspect ratios. Their results agree with Dobre et al and Equation 3.17 for most canyon orientations. [17, 47] An interesting result is their finding that for many canyon angles, the bulk longitudinal velocity in the canyon divided by the component of the atmospheric velocity that is parallel to the canyon is independent of canyon orientation. This means that Equation 3.17 can be extended to street canyons that are at an angle to the atmospheric flow. Specifically, they found that this relationship holds for street canyons that are up to 60 degrees from being parallel to the atmospheric flow.

Both Dobre et al and Soulhac et al worked in rotated coordinate systems; however for the purposes of the exchange coefficient we chose a coordinate system that is aligned with the atmospheric flow and x, y, and z are defined as in Figures 3-10 and 3-11. The angle between the canyon and the atmospheric flow, θ, is defined as a positive rotation from the x-axis about the vertical z-axis. Coordinate transformations are displayed for clarity below:

$$u_{cl} = u_{cx} \cos\theta + u_{cy} \sin\theta; \tag{3.19}$$

$$u_{crh} = u_{cx} \sin\theta - u_{cy} \cos\theta; \tag{3.20}$$

$$u_{crv} = u_z. \tag{3.21}$$

In these transformations, the rotational and longitudinal canyon velocities are defined such that the transformed velocity component is positive in the atmospheric direction.

The exchange of air between the urban boundary layer and the urban canopy layer varies with the relative velocity between the atmospheric flow and the flow in the canyon that is parallel to the atmospheric flow. We define the exchange coefficient in both coordinate systems as

$$\alpha = \frac{u_e}{u_a - (u_{cl}\ \cos\theta + u_{crh}\ \sin\theta)} = \frac{u_e}{u_a - u_{cx}}. \tag{3.22}$$

u_{cx} is aligned with the flow, making the denominator of this exchange coefficient a measure of the shear stress in the fluid between the urban canopy layer and the urban boundary layer, as in Sections 3.3 and 3.4. u_{cx} is the relevant velocity for this expression because it is in the same direction as the atmospheric flow. This means that the relative velocity, $u_a - u_{cx}$, is a measure of the shear stress in the fluid responsible for the turbulent mixing across the top of the canyon, as in the denominator of Equations 3.16, 3.18 and 3.22.

The exchange coefficients defined in this chapter will be useful for assessing the momentum exchange across the boundary between the urban canopy layer and the urban boundary layer. This will give us a non-dimensional way to compare the expected turbulence in different types of neighborhoods. Increased turbulence is of interest to urban planners because it follows that areas with high turbulence will have lower pollutant retention times and greater heat transfer out of the neighborhood. Future work to quantify these relationships is discussed in Chapter 7.

Chapter 4

Isolated, realistic street canyon

Through the derivation of Equation 3.17 and the introduction of the exchange coefficient, we have begun to answer the question of canyon velocity raised at the beginning of Chapter 3. The analysis is still idealized and different from a real street canyon. To understand the fluid mechanics in an isolated, more realistic street canyon other questions must be answered: What is the skin friction coefficient of a real urban street canyon? How does varying the exchange coefficient affect the bulk velocity in the street canyon at any orientation? What is the exchange velocity between a particular street canyon and the atmosphere?

Real street canyons in Singapore have balconies attached to nearly every apartment. It is not obvious how this sort of large-scale roughness can be translated into the Nikuradse sand grain roughness parameter used for rough walls in Fluent. This will be addressed in Section 4.1 Additionally, many apartments have air-conditioner units attached to the building façades and the streets are often filled with cars – these roughness elements act as momentum sinks and also as pollutant and heat sources within the canyon. As stated in Section 1.2, it would be interesting to determine how long these pollutant and heat sources remain in a rough-walled street canyon for a given geometry and flow condition. The first step towards an answer is determining the exchange coefficient and the exchange velocity for a particular canyon; these parameters will be discussed in Sections 4.2 and 4.3 respectively. Additionally, the longitudinal bulk velocity in a single street canyon calculated with our model will be

compared with experimental results in Section 4.4. The sensitivity of the simulated results to mesh size and mesh gradient will be discussed in Section 4.5.

4.1 Roughness

Real street canyons are often covered with balconies and air-conditioner units as in Figure 4-1, and in densely populated areas the streets are filled with cars and buses. This surface roughness will lead to increased shear stress on the surfaces and decreased longitudinal velocities in the canyon. Additionally, these obstructions could lead to increased turbulence in the canyon flow, and may lead to an increase in the turbulent exchange between the above-canyon and in-canyon flows. The skin friction coefficient, as defined in Equation 3.14, is a non-dimensional measure of the surface shear stress and is a function of the surface roughness.

Physical roughness elements can be related to an equivalent skin friction coefficient using empirical relationships and control volume arguments. First, the skin friction coefficient is directly related to the Darcy-Weisbach friction factor by solving the equation for linear momentum, Equation 3.9, for steady, fully developed flow in the square duct in Figure 3-1. Rewriting Equation 3.9 for the pressure driven flow in the duct we find,

$$P_{inlet}\,A_{inlet} - P_{outlet}\,A_{outlet} - \underset{CS-top}{\oint \tau\,dA} - \underset{CS-bottom}{\oint \tau\,dA} - \underset{CS-leftwall}{\oint \tau\,dA} - \underset{CS-rightwall}{\oint \tau\,dA} = 0, \quad (4.1)$$

where P_{inlet} is the pressure on the inlet control surface and P_{outlet} is the pressure on the outlet control surface. Combining Equation 4.1 with the definition of the skin friction coefficient in Equation 3.14 and substituting duct values for the control surface areas, the expression arising from linear momentum in a duct is reduced to:

$$\Delta P\,H\,W = \rho\,C_f\,u_\infty^2\,(H\,L + W\,L)\,, \quad (4.2)$$

where ΔP is the pressure drop over the length of duct considered. Combining Equation 4.2 with the definition of the Darcy-Weisbach friction factor in Equation 3.7 and the definition of the hydraulic diameter in Equation 3.3 we find that the skin friction

Figure 4-1: Building façades in Singapore with roughness elements

coefficient can be directly related to the friction factor as:

$$C_f = \frac{f}{4}. \tag{4.3}$$

Equation 4.3 can be combined with Equation 3.6 to relate the skin friction coefficient to the Nikuradse sand grain roughness. This must be related to the realistic situation for building façades, which consist of regular arrays of roughness elements of simple geometry. [51] An example of this is the cube-like elements on the tropical façades in Figure 4-1. This can be done using the empirical relationships devised by Koloseus and Davidian. They combined a wealth of experimental data to relate element heights, sizes and patterns to the Nikuradse sand grain roughness for a variety of obstruction types. [30, 51] These relationships are displayed in Figure 4-2. The geometric parameter used to quantify the roughness is known as the roughness concentration, λ_f, defined as:

$$\lambda_f = \frac{frontal\ area\ per\ element}{specific\ area}, \tag{4.4}$$

where the *frontal area per element* is the projected surface area of the roughness elements that is normal to the wind and in the windward direction, and the *specific area* is the total plan area of the rough surface. The roughness concentration is also known as the frontal area index, and colloquially quantifies the elements seen by the wind. [22] This parameter will be used to quantify multiple roughness elements, such as balconies on a façade, as well as to quantify the geometry of many buildings in a neighborhood. In both cases, the calculation of λ_f is performed by summing the *frontal area per element* of all of the elements on a particular surface, and dividing by the *specificarea*, which is considered the area of that surface. In Figure 4-2, k_s is the equivalent Nikuradse sand grain roughness, and k is the roughness element height and m is a "coalescing factor" which has been adjusted empirically to give unit slope in the straight-line range of the data. [30, 51] When comparing roughness elements or buildings with this parameter, the size and shape of the *specificarea* considered should remain constant for the elements or buildings considered, and if

possible should be include only roughness elements, k, of similar size or buildings of similar height. The shape of the curves in Figure 4-2 suggest that at low roughness concentrations, the flow is affected by each roughness element, meaning the flow regime is either isolated roughness flow or wake interference flow. [43] At high roughness concentrations the effect of each roughness element on the flow becomes less important, and the flow transitions to a skimming flow regime as evidenced by the decay in the equivalent Nikuradse sand grain roughness in Figure 4-2. [30, 43, 51] This methodology to parameterize roughness elements as sand grain roughness has applicability in CFD modelling. Fully modelling building façades with balconies is time consuming to build and mesh, and adds a significant number of finite volumes to a three-dimensional airflow simulation. The increase in the number of finite volumes will lead to an increase in the computational time required to simulate the domain. Future work to assess these ideas is discussed in Chapter 7.

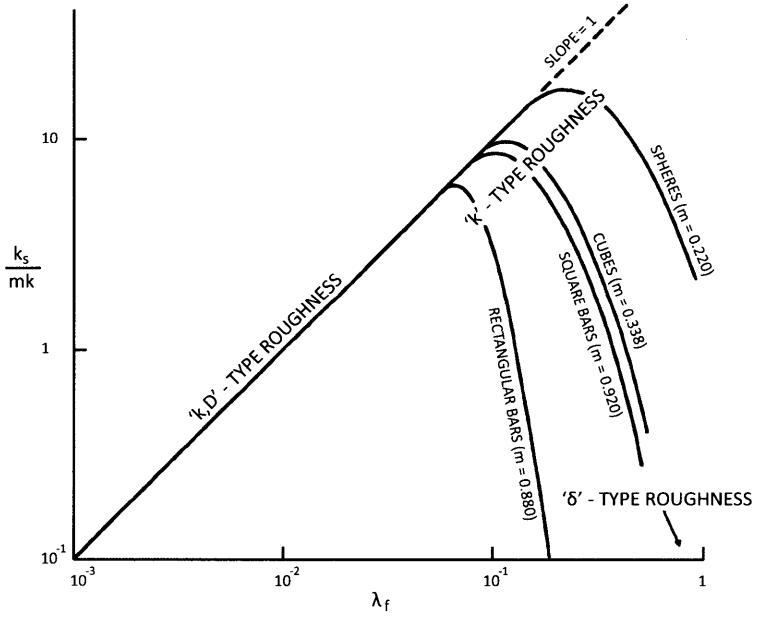

Figure 4-2: Variation of equivalent roughness height, $k_s/(m\,k)$ vs. Roughness concentration, λ_f [30, 51]

The gray box drawn on the Moody Diagram in Figure 4-3 depicts the region relevant to flow in street canyons. The range of Reynolds numbers is based on typical canyon geometry and wind speeds. The range of relative roughness is based on the

work by Koloseus and Davidian and typical roughness elements on canyon façades scaled by the canyon width. [30]

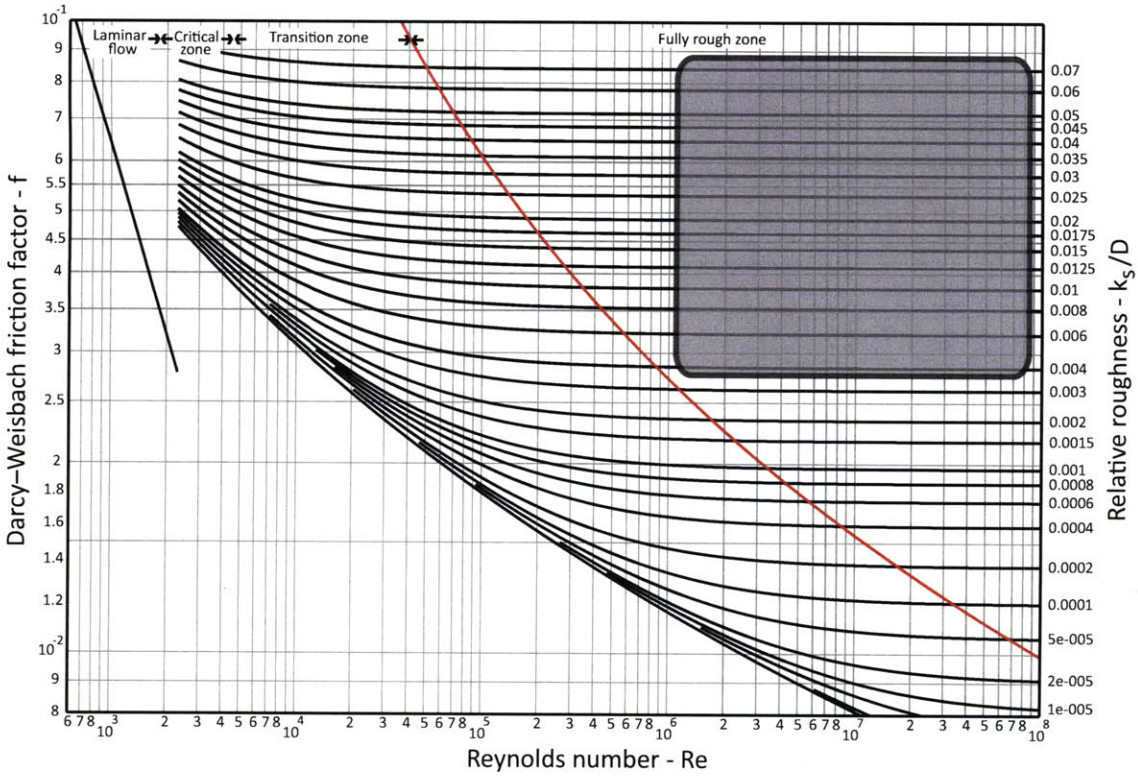

Figure 4-3: Moody diagram for pipe flow with relevant area highlighted [39]

The skin friction coefficient is plotted against the relative roughness in Figure 4-4. Assuming that flow around a rectangular cuboid-shaped balcony is almost the same as flow around a cube, the relationships displayed in Figure 4-2 define an equivalent sand grain roughness for a canyon wall. This requires that we approximate the roughness concentration associated with the roughness elements on the canyon surface as per Equation 4.4. If we allow that many canyon roughness elements can be approximated by cubes, then we can use the empirical relationships displayed in Figures 4-2 and 4-3 to translate the roughness of real building façades and streets into an equivalent Nikuradse sand grain roughness, and a predicted skin friction coefficient. An example of this is presented in Section 4.2. We find the range for typical skin friction coefficients for street canyons is small: 0.007 to 0.020, roughly a factor of three. This means that the effect of roughness, which is translated to an equivalent skin friction

coefficient, on the bulk longitudinal velocity in the canyon may be less important than other parameters in Equation 3.17. For example, the geometric parameter, H/W, can vary by a factor of 10.

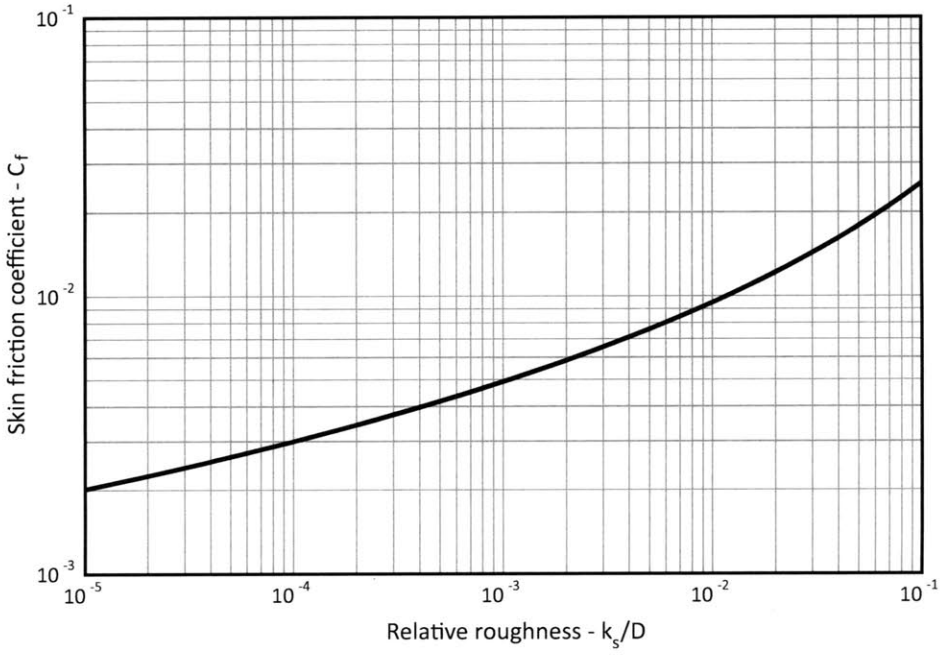

Figure 4-4: Skin friction coefficient, C_f vs. Relative roughness, k_s/D

4.2 How does the exchange coefficient vary with parameters of the street canyon?

The typical range for the exchange coefficient in a neighborhood is 0.01 to 0.10, and the exact value is a function of neighborhood geometry. [4, 35] Using this range we can produce graphical representations of Equation 3.17. First, we consider a building façade with 3 x 1 x 1 meter balconies spaced every 10.5 meters horizontally and every 4 meters vertically. The geometry of these roughness elements is equivalent to a λ_f of 1/42 because there is one square meter of balcony surface area normal to the flow for every 42 square meters of façade surface area. The height of the roughness elements in the direction normal to the building façade is one meter. Using Figure 4-2, we find an equivalent sand grain roughness of 0.8 meters by approximating the balconies as cubic elements. This is equivalent to a skin friction coefficient of 0.016 as per Equations 3.6 and 4.3.

Figure 4-5 shows Equation 3.17 with the skin friction coefficient held constant at 0.016 for the typical range of exchange coefficients. This plot is for the case where the axis of the canyon is aligned with the wind direction. The exact value of the exchange coefficient will be determined by the geometry of the neighborhood surrounding the canyon. This will be discussed in Section 4.4 and Chapter 5.

Figure 4-6 shows Equation 3.17 for a street canyon with an aspect ratio of unity for the appropriate range of skin friction coefficients and exchange coefficients and for the case where the street canyon is aligned with the wind direction.

Comparing the shapes of the curves in Figures 4-5 and 4-6, we see trends that may be applicable to the creation of urban design guidelines. It is intuitive that increasing the skin friction coefficient or the street canyon aspect ratio will result in a lower normalized bulk velocity in the street canyons because both changes cause a relative increase in the drag force imposed on the fluid by the walls per unit volume of fluid in the street canyon. This is reflected in the curves. Less obvious, however, is the idea that a street canyon with an aspect ratio of unity in a neighborhood with a low exchange coefficient, say 0.01, may have the same longitudinal bulk velocity as a

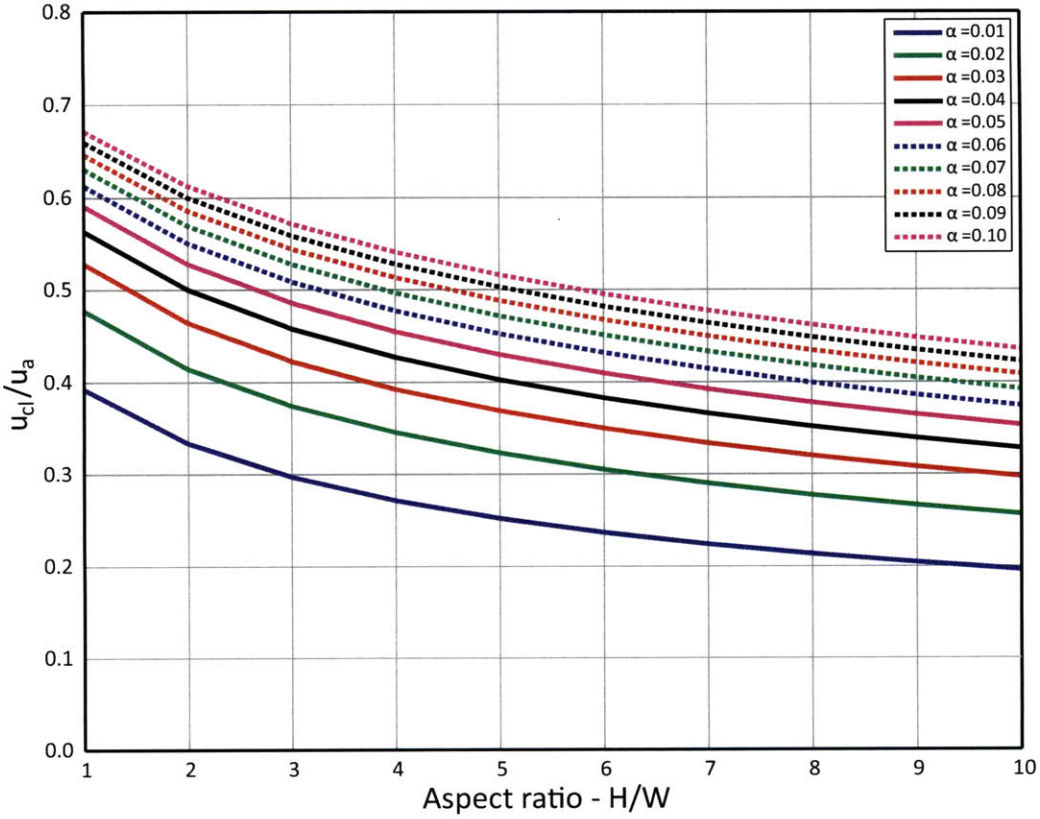

Figure 4-5: u_{cl}/u_a vs. Aspect ratio, H/W: based on a street canyon aligned with the atmospheric flow with a skin friction coefficient of 0.016 for various exchange coefficients

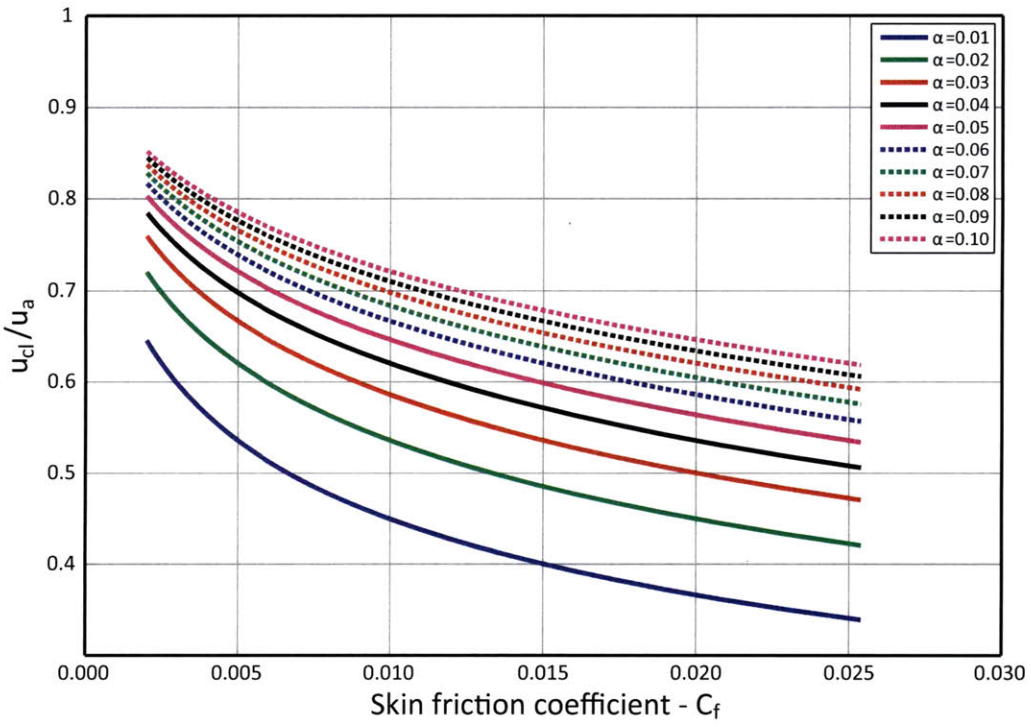

Figure 4-6: u_{cl}/u_a vs. Skin friction coefficient, C_f: based on a street canyon aligned with the atmospheric flow with an aspect ratio of unity for various exchange coefficients

street canyon with a height to width ratio of 10 in a neighborhood with an exchange coefficient of 0.08. In a real neighborhood, an increase in street canyon aspect ratios will likely lead to a decreased exchange coefficient because it will affect some geometric parameters that govern the exchange coefficient, as discussed in Section 5.4. Therefore, this scenario is highly unlikely in a real street canyon. It is important to realize, however, that at a neighborhood scale there are more complex geometries and processes at work, such as the introduction of street intersections, abrupt changes in street orientation and building height variability that will affect the value of the exchange coefficient. These neighborhood elements cause increases in turbulent mixing from flow separation off of the bluff building surfaces. These processes will be discussed in Chapter 5. Understanding how these factors affect the exchange coefficient will help urban planners achieve design goals like the need to plan a densely populated city that retains a large exchange coefficient, and therefore has lower pollutant concentrations and a smaller urban heat island effect than similarly dense cities.

A more subtle conclusion may be drawn from the spacing of the curves for various exchange coefficients. The spacing remains constant for the range of street canyon aspect ratios in Figure 4-5. According to the graph, increasing the average exchange coefficient of a neighborhood from 0.02 to 0.1 would result in an increase of u_{cl} by about 20% of the total value of u_a regardless of street canyon aspect ratio. This is in contrast to Figure 4-6 where we see that the effect of changing the exchange coefficient of a neighborhood has a visibly smaller effect on the normalized longitudinal bulk velocity for small skin friction coefficients than for large skin friction coefficients. This effect is more apparent in street canyons with small aspect ratios.

4.3 Longitudinal bulk velocity and exchange velocity for canyons in any orientation

In Section 3.5 we briefly discussed a profound result found by Soulhac et al. [47] Through simulation of angled canyons, they found that

$$\frac{u_{cl}}{u_a \cos\theta} = \beta \tag{4.5}$$

where β is a constant. They found this relationship held for canyons with an orientation of up to 60 degrees from the atmospheric wind direction. We postulate that this relationship is true for the spatially averaged rotational velocity as well, as

$$\frac{u_{crh}}{u_a \sin\theta} = \gamma \tag{4.6}$$

where γ is a constant. The relationships in Equations 4.5 and 4.6 can be combined with Equations 3.19 and 3.20 to find an expression for u_{cx}, the velocity necessary to calculate of the exchange coefficient for angled canyons. This relationship is

$$\frac{u_{cx}}{u_a} = \beta \cos^2\theta + \gamma \sin^2\theta. \tag{4.7}$$

For an ideal street canyon, γ is zero because there will be no net flow in the wind direction in the ideal recirculating case. We can calculate β for a particular canyon – it is simply the right hand side of Equation 3.17. We tested the relationship in Equation 4.7 in Fluent for canyons at various angles to the atmospheric flow. The domain used for these simulations is displayed schematically in Figure 4-7. The simulations were performed with periodic boundary conditions on the inlet and outlet to approximate fully developed flow. The change of angle in the domain makes the geometry of the inlet surface the same as the outlet surface, which is a requirement for using periodic conditions. The two building façades and the street surface were modelled with a Nikuradse sand grain roughness of 0.5 meters, and all other sides of the domain were assigned slip boundary conditions. The canyon was meshed

with 2 meter hexahedral volumes, and the expansive volume above was meshed with 2 meter hexahedral volumes that grew vertically at a rate of 1.065. These mesh decisions are based on the mesh sensitivity analysis, which is discussed in Section 4.5. The mass flow rate varied with the particular domain because the area of the inlet varied with the angle of the canyon – but was equivalent to 10 m/s multiplied by the density of air and the area of the inlet boundary.

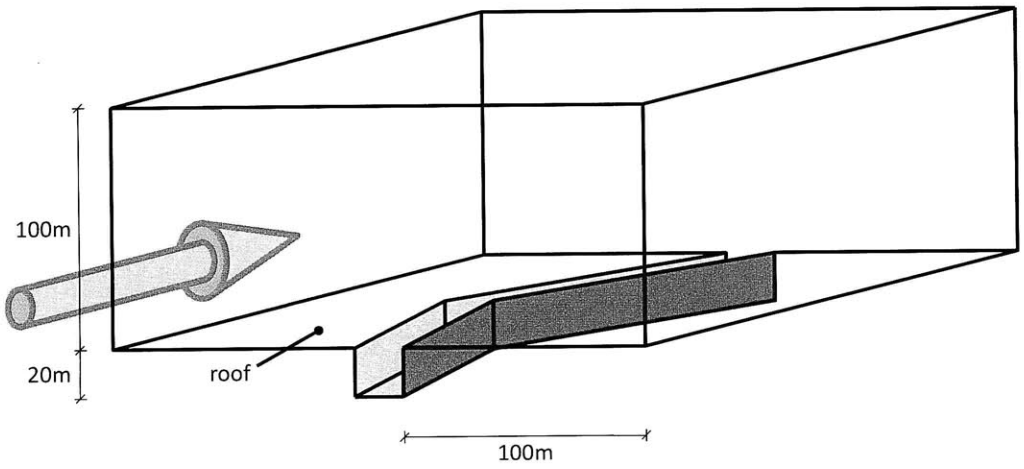

Figure 4-7: Three-sided channel domain at an angle to the atmospheric wind with a large volume above

The results of these simulations are plotted in Figures 4-8 and 4-9. The curve drawn on Figure 4-8 was found with Equation 4.7 for an ideal canyon, that is $\gamma = 0$, and the curve drawn on Figure 4-9 was found with using Soulhac's relationship in Equation 4.5. The values for u_{cx} were averaged over a plane that was 75% of the way down the second canyon in the domain in Figure 4-7 because by this time the net vertical velocity out of the canyon was approximately zero, and the flow can be considered fully developed. The values for u_{cl} were calculated from the simulation outputs at the same plane using Equation 3.19. The calculated values follow the trends predicted by combining our model with Soulhac et al. Based on the y-intercepts of the fitted curves, and Equation 3.17, we find that the exchange coefficient is 0.004 for this geometry. This value is low, and this can be attributed to the lack of intersections and height variations in this domain. These neighborhood characteristics are responsible for much of the turbulent mixing in neighborhoods.

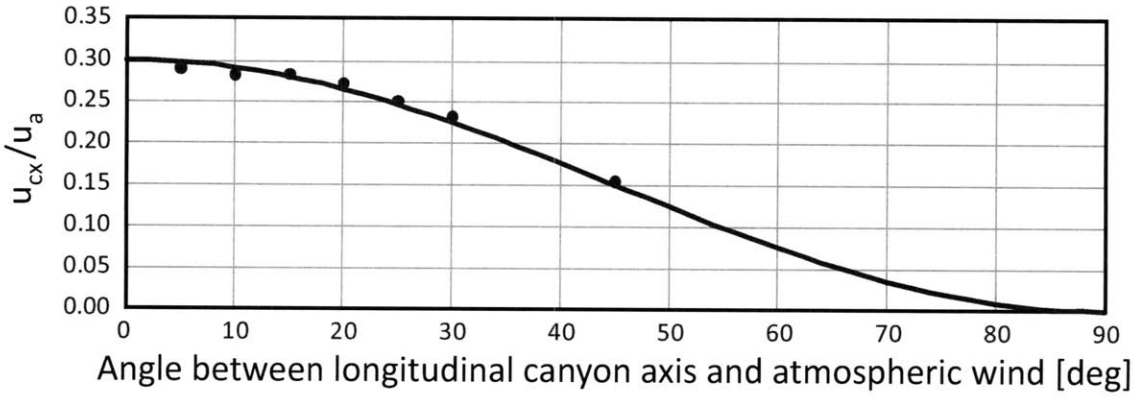

Figure 4-8: u_{cx}/u_a vs. Angle between longitudinal canyon axis and atmospheric wind [deg]

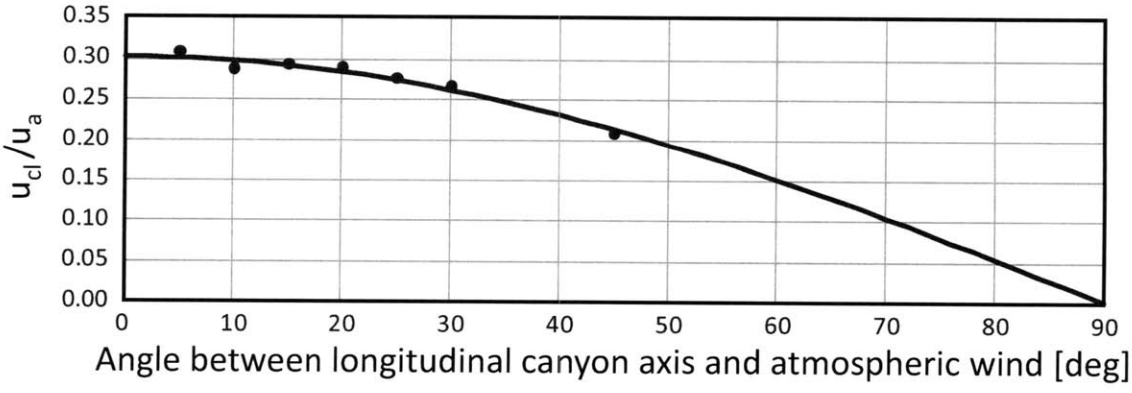

Figure 4-9: u_{cl}/u_a vs. Angle between longitudinal canyon axis and atmospheric wind [deg]

Combining Equations 3.22 and 4.7, we create an explicit expression for the exchange velocity normalized to the atmospheric velocity as

$$\frac{u_e}{u_a} = \alpha \left(1 - \beta \cos^2 \theta\right). \tag{4.8}$$

This relationship is plotted for the simulated case in Figure 4-10. The exchange velocity is greatest for the cases where the canyon is perpendicular to the atmospheric wind. We expect the normalized exchange velocity to be greater for most urban situations because intersections and building height variability will lead to greater exchange between the urban canopy layer and the urban boundary layer. These topics will be addressed in Chapter 5.

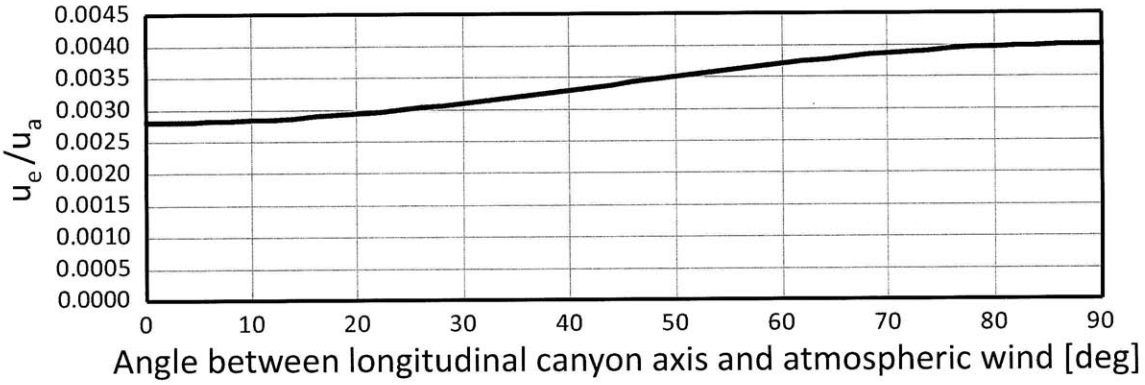

Figure 4-10: u_e/u_a vs. Angle between longitudinal canyon axis and atmospheric wind [deg]

Combining Equations 3.17 and 4.5, we can plot the exchange coefficients against the spatially averaged, normalized longitudinal bulk velocity for a particular roughness and street canyon ratio. This is done in Figure 4-11 for a canyon with a skin friction coefficient of 0.0133 and an aspect ratio of unity. A graphic like this could be generated for a particular canyon, and anemometer measurements could be plotted on the graph, normalized to the atmospheric velocity to find the exchange coefficient. In an experiment like this, care would have to be taken for anemometer placement within the canyon. Ideally the setup would involve an array of anemometers in the cross section of street canyon, as far from a street intersection as possible. In Sec-

tion 5.2, we address the idea of deriving canyon longitudinal bulk velocity from a single horizontal line of velocity measurements across the canyon, however the height of the measurements required to accurately calculate the longitudinal bulk velocity seems to vary between $H/3$ and $H/2$ of the heights of the flanking buildings. Using this data, we could populate the graph in Figure 4-11 with points based on the orientation of the canyon to the wind and u_{cl}/u_a. This data would tell us the local exchange coefficient for the canyon. Based on our simulations, we expect that the exchange coefficient will remain constant as the atmospheric wind changes in magnitude and direction, so the data would fall on a horizontal line in Figure 4-11. This type of experiment would be useful to evaluate our model. A plan for future work to gather wind data in a neighborhood in Singapore is presented in Chapter 7.

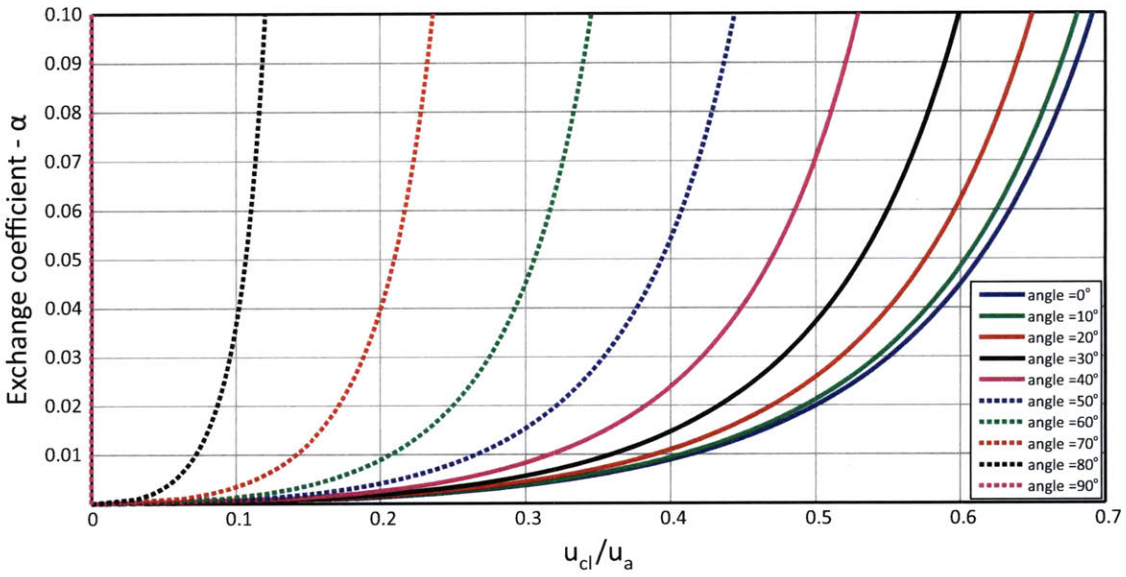

Figure 4-11: Exchange coefficient, α vs. u_{cl}/u_a: based on a street canyon with a skin friction coefficient of 0.0133 and an aspect ratio of unity for various angles

4.4 Comparison with experimental results, simulated results and other models

We can relate our exchange coefficient to the semi-empirical model developed by MacDonald et al and the analytical model developed by Bentham and Britter. [4, 35] These models focused on predicting u_e based on neighborhood parameters and the roughness height, z_0, defined in Section 2.1. The results of these models can be rearranged to find both u_{cl}/u_a and α based on a single spatially averaged neighborhood parameter that is independent of the flow, λ_f, defined in Equation 4.4. The results from rearranging these models are plotted in Figures 4-12 and 4-13. Figure 4-12 suggests that there is less turbulent exchange between the urban canopy layer and the urban boundary layer in sparsely developed neighborhoods. As the neighborhood becomes more built-up, turbulent exchange between the urban canopy layer and the urban boundary layer increases until the flow structure over the buildings becomes more like skimming flow, and then turbulent exchange between these layers decreases. Figure 4-13 suggests that as a neighborhood becomes more built-up, the average bulk longitudinal velocity in the urban canopy layer decreases. We can combine the information in Figures 4-12 and 4-13 to eliminate the independent neighborhood parameter, λ_f, from the models for an idealized, single street canyon. This will give us a first guess at predicting α independently of our model for an experimentally measured longitudinal bulk velocity, which will allow us to compare the result to our model.

The recent work of Hang et al is particularly useful to consider for the evaluation of our single canyon results. [24, 25] They built smooth-walled street canyons of various aspect ratios with a width of 30 mm that were 47.4 and 79 times longer than they were wide. These street canyons were tested in a wind tunnel, and were compared to results simulated in Fluent. The Reynolds number for the flows in these canyons is approximately 22,500, calculated with the free stream velocity of 11 m/s and the width of the canyon as the hydraulic diameter. Using Equation 4.3 and the Moody diagram in Figure 4-3, we find the skin friction coefficient for these

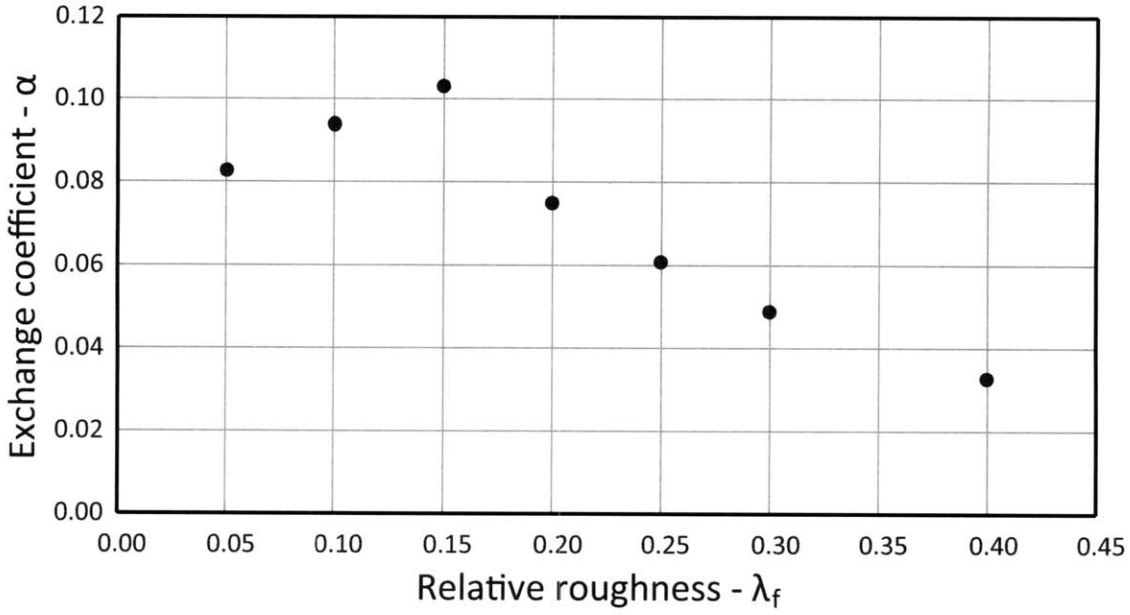

Figure 4-12: Exchange coefficient, α vs. Roughness concentration, λ_f: based on data that was spatially averaged over a neighborhood [4, 35]

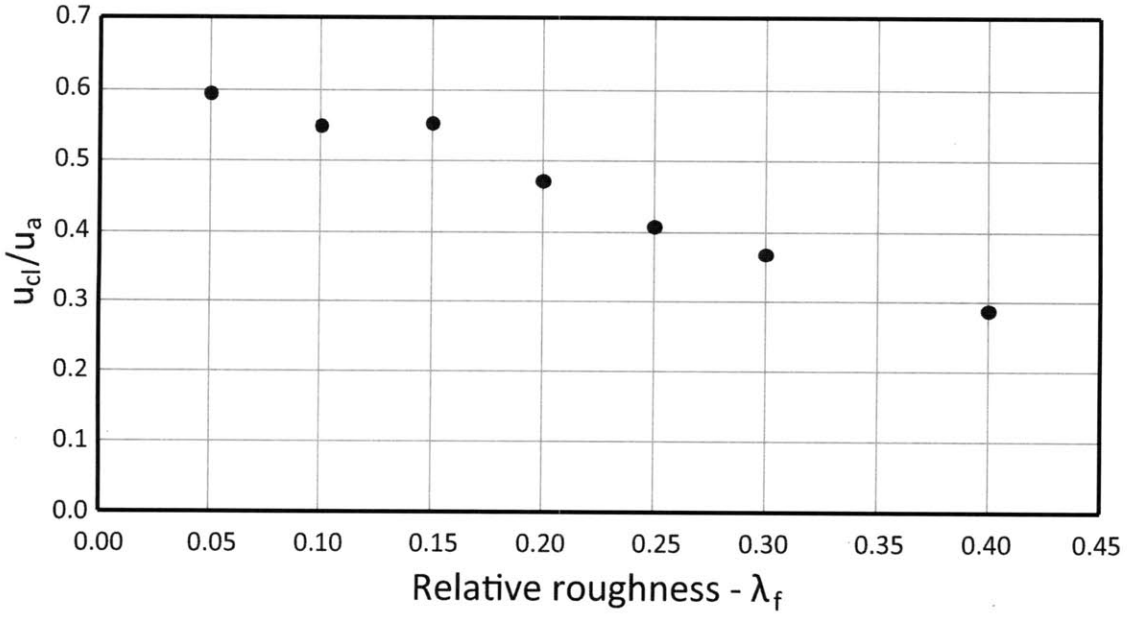

Figure 4-13: u_{cl}/u_a vs. Roughness concentration, λ_f: based on data that was spatially averaged over a neighborhood [4, 35]

simulations is approximately 0.06. This is higher than we would expect for a street canyon because of the small canyon size and therefore the low Reynolds number. The aspect ratios, normalized mass flow rates and exchange coefficients calculated by our model and the model in Figures 4-12 and 4-13 are displayed in Table 4.1. The longitudinal bulk velocities normalized to atmospheric flow, u_{cl}/u_a, calculated in these simulations are for the case where the street canyon is aligned with the flow. To compare these to the Bentham and Britter model based on the MacDonald model, we must approximate u_{cl}/u_a averaged over a canyon of any orientation. We do this by integrating Equation 4.5 over the relevant angles. First we move the cosine to the right hand side of the equation, and then integrate both sides from 0 to $\pi/2$ as

$$\int_0^{\frac{\pi}{2}} \left(\frac{u_{cl}}{u_a}\right)_{avg} d\theta = \int_0^{\frac{\pi}{2}} \beta \cos\theta \, d\theta. \tag{4.9}$$

Integrating, we find:

$$\left(\frac{u_{cl}}{u_a}\right)_{avg} \theta \Big|_0^{\frac{\pi}{2}} = \beta \sin\theta \Big|_0^{\frac{\pi}{2}}, \tag{4.10}$$

and this can be simplified to

$$\left(\frac{u_{cl}}{u_a}\right)_{avg} = \frac{\beta}{\frac{\pi}{2}} \tag{4.11}$$

where β is the longitudinal bulk velocity normalized to the atmospheric wind flow when the canyon orientation is parallel to the wind direction. Therefore the fully developed velocities in the experimental street canyons must be divided by $\pi/2$ to compare them to the normalized velocities in Figures 4-12 and 4-13. Because Hang et al calculated the flow in the fully developed region of the street canyons in terms of normalized volumetric flow rate, we display their results in the column labeled Q_{norm} in Table 4.1. [24, 25] Their definition of normalized volumetric flow rate is equivalent to u_{cl}/u_a for a given street canyon aspect ratio. Using the relationship in Equation 4.11, we calculated Q_{avg}, a normalized volumetric flow rate that is equivalent to the expected flow rate averaged over all street canyon orientations. We fit the five decaying points in Figure 4-12 with a least squares power-law fit, and all of the points in Figure 4-13 with a least squares line fit. We predicted the exchange coefficient

based on the models from the literature, α_{lit}, using these fits and Q_{avg}. This is compared to the exchange coefficient predicted by Equation 3.17, α_{calc} in Table 4.1. α_{calc} was calculated using Q_{norm} because Equation 3.17 is based on the longitudinal bulk velocity for the case where the street canyon is parallel to the atmospheric flow, which is the case studied by Hang et al.

H/W	Q_{norm}	Q_{avg}	α_{lit}	α_{calc}
2.0	0.43	0.27	0.032	0.021
2.5	0.38	0.24	0.029	0.018
3.0	0.33	0.21	0.027	0.015
4.0	0.27	0.17	0.024	0.012

Table 4.1: Comparison of calculated exchange coefficients with wind tunnel results

The results for our exchange coefficient are smaller than those based on Figure 4-12. Because the model based on the work of MacDonald's model and Bentham and Britter's model is averaged over a neighborhood, we expect the exchange coefficients to be higher than those for a single canyon because much of the exchange in the neighborhood is due to the variation in building heights and street canyon intersections. Despite the fact that we did not have to calculate λ_f for the calculation of α_{lit}, it is the independent geometric parameter that is needed determine the exchange coefficient when the normalized bulk velocity is not available. Because the single street canyon lacks intersections and variation in building heights, λ_f is not an appropriate parameter for a single canyon model because there is no frontal area after the inlet to obstruct the flow. In contrast, the hydraulic diameter is a parameter that characterizes the geometry of a single canyon. In Figure 4-14, we plotted α_{calc} against the hydraulic diameter based on the arguments for D_h of a three-sided channel in Section 3.1 .

This strong linear relationship provides more practical insight as to how the aspect ratio of a single canyon affects the exchange coefficient between the street canyon and the air above. The relationship of aspect ratio to the exchange coefficient of a neighborhood will be addressed in Section 5.3.

We also compared our simulated results for the infinitely long canyon in Section 3.1

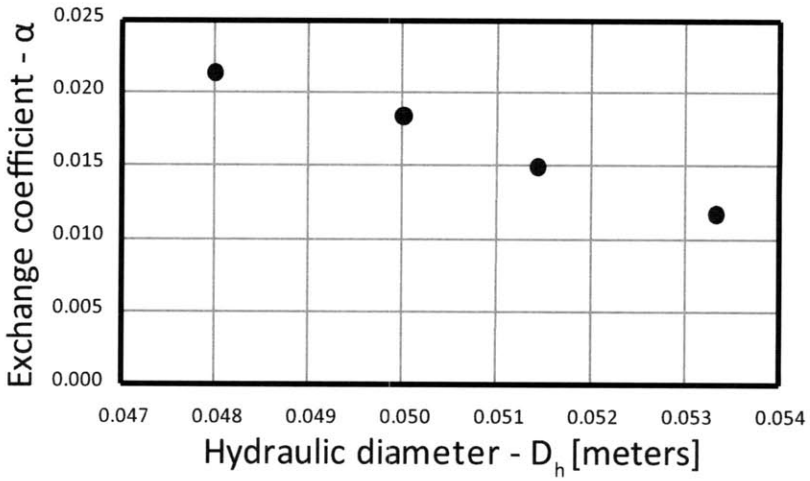

Figure 4-14: Exchange coefficient, α vs. Hydraulic diameter, D_h [meters]

to our model. The results are plotted in Figure 4-15 for the computational domain in Figure 3-7 with slip boundary conditions on the building roofs, and the case where the building roofs are modelled as rough walls. Recall that these simulations have a single street canyon with an aspect ratio of unity. Again the exchange coefficients are lower than expected, but the trends are encouraging. Because the simulated street canyon has a constant geometry, we expect the exchange coefficient to be constant for the range of roughnesses.

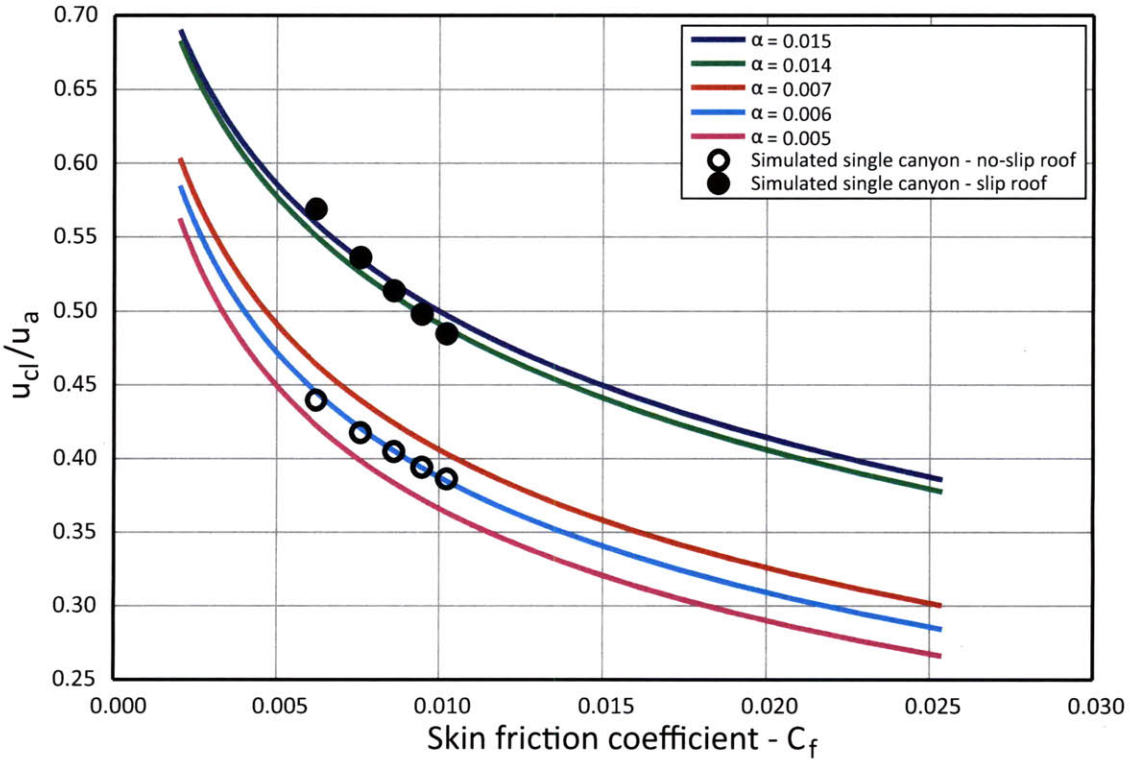

Figure 4-15: u_{cl}/u_a vs. Skin friction coefficient, C_f: comparison of model with Fluent simulations

4.5 Mesh sensitivity analysis for a single street canyon

A high quality and appropriately refined computational grid is essential to ensure the accuracy of CFD results for a particular computational domain. [21] We have found interesting and unexpected results that come from changing the coarseness of the mesh, the length of a periodic domain, and the growth rate of the mesh away from a wall boundary. Periodic boundary conditions were chosen at the inlet and outlet of many of our single canyon domains to allow for velocity profiles in the idealized street canyon to approximate an infinitely long street. These domains have few surfaces and obstructions and are very large, and we have found that they are particularly susceptible to error. We believe that this is because they lack many of the phenomena that typically shape velocity and turbulence contours in a neighborhood, such as flow separation from a building surface, or the mechanical mixing associated with an intersection.

We have attempted to investigate the most appropriate mesh for this difficult situation by carefully studying the effects of varying important Fluent settings. Table 4.2 shows turbulent kinetic energy contours and longitudinal velocity contours for the domain in Figure 3-7 where the roof boundary is set to a slip boundary condition. The Nikuradse sand grain roughness for all of the street canyon walls is set to 0.5 meters.

The results in the bottom three rows of Table 4.2 are for the case where a uniform velocity inlet of 10 m/s is set as the inlet boundary condition. Because the inlet velocity is in the range of atmospheric wind speeds, and the dimensions of the street canyon in the domain is 20 x 20 meters, the Reynolds number of these simulations is similar to those found in real streets. The flow is allowed to develop towards a pressure outlet. The pressure outlet boundary condition requires the specification of a static pressure at the outlet boundary, however all other quantities are calculated from the interior. [20] The results with these boundary conditions are considered the control of the mesh sensitivity experiment, because they are not confounded by the periodic boundary condition. The 1000 meter long canyon with a uniform velocity at the inlet

has the same velocity contours at the outlet, regardless of the initialization of the turbulence parameters or the coarseness of the mesh. When increasing the coarseness of the mesh does not yield a different output, this means that the result is insensitive to the mesh, and that the coarser mesh is appropriate for simulating the problem. The outlet of the 2000 meter long canyon with uniform inlet is essentially the fully developed solution. It has been run for the 2 meter uniform mesh, as the 1 meter uniform mesh had a significantly longer computational time. Because the result was not sensitive to mesh or turbulence initialization parameters for the 1000 meter long canyon, we assert that a single 2000 meter long simulation is appropriate to compare against the periodic simulations, so we consider the outlet of this simulation to be the basis of comparison for this experiment.

The 1 meter uniformly meshed periodic simulations have very different outlet contours than our control. The longitudinal velocity profiles appears to still be developing - the fully developed state has not been reached. The outlet contours are mostly insensitive to the length of the canyon or the turbulence initialization parameters. The 2 meter uniformly meshed periodic simulations are much more promising. While the 500 meter case seems to show fundamental differences in the turbulence structure based on the turbulence initialization parameters, the 1000 meter cases are insensitive to it. Both 1000 meter periodic cases behave similarly to the control, and while the contours don't match the control exactly, they are almost exactly the same in the area near the canyon, which is our area of interest. For this reason, our simulations to produce the graph in Figure 3-8 were run with a 1000 meter long periodic canyon.

Another important parameter to consider when meshing is the number of finite volumes in the domain, as this is directly related to the simulation computation time. The number of volumes can be reduced or distributed more effectively by allowing the size of the volumes to grow in areas where the velocity derivatives are expected to be small, and by concentrating more volumes near walls and obstacles. We tested various meshes that all have a 2 meter uniform mesh in the street canyon. The expansive volume above the street canyon was meshed with hexahedral elements

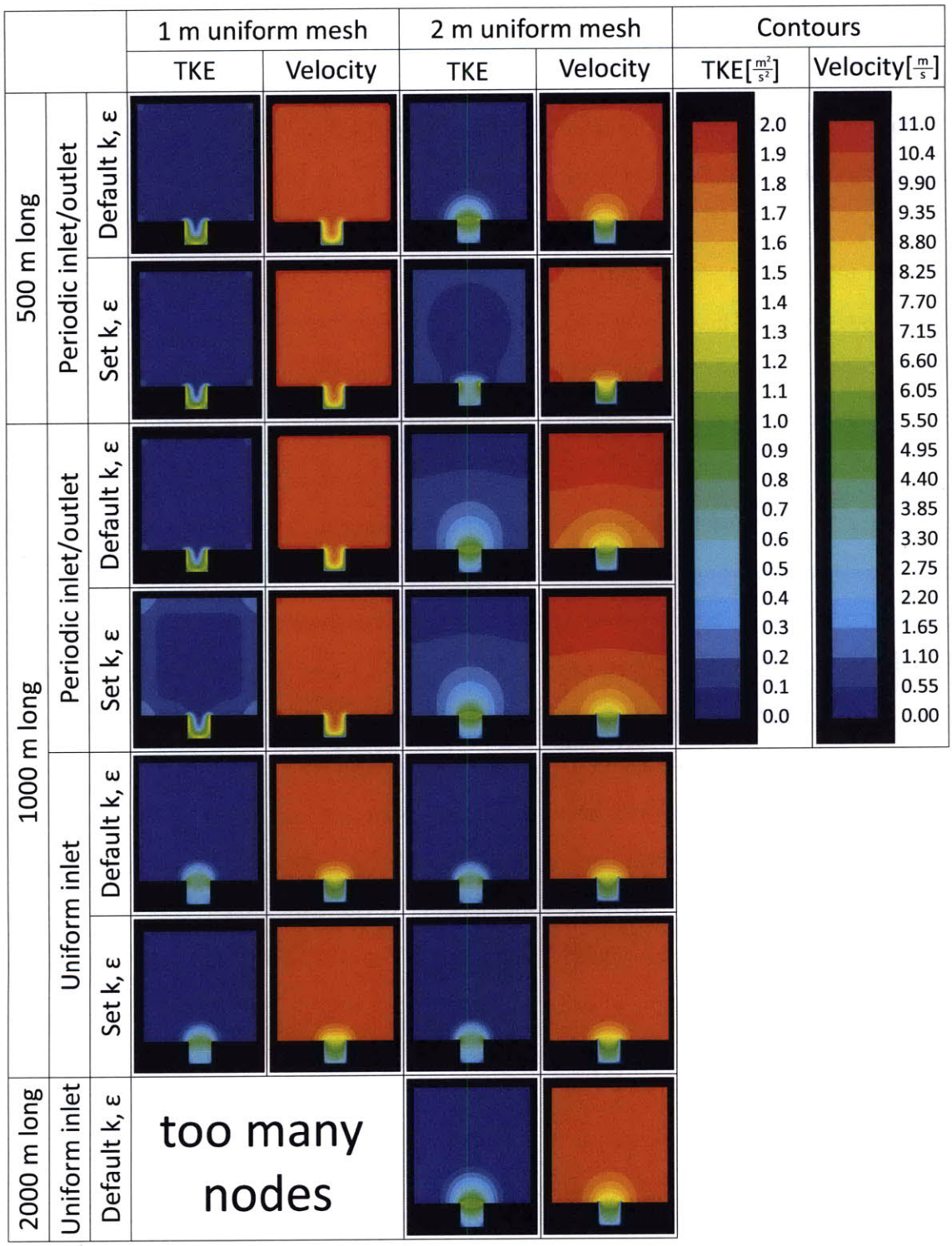

Table 4.2: Comparison of simulated turbulent kinetic energy and velocity contours for idealized street canyon with various lengths, inlet conditions, initialization parameters and mesh sizes

that were allowed to grow at a rate of 1.01 and 1.07 in the vertical direction away from the canyon, starting at 2 meters with the layer of finite volumes closest to the street canyon. This idea is displayed schematically in Figure 4-16. The expansive volumes with growth rates were compared with a 2 meter uniformly meshed canyon. They were all run for a 2000 meter long canyon with a velocity inlet and pressure outlet condition, and for a 500 meter long canyon with periodic boundary conditions. Tests were conducted for the scenario where the building roofs are modelled as slip boundary conditions, as well as the the scenario where the roofs are modelled as rough walls. The walls of the three-sided channel, and the rough roofs were modelled with a Nikuradse sand grain roughness of 0.5 meters. The results for these simulations are displayed in Table 4.3.

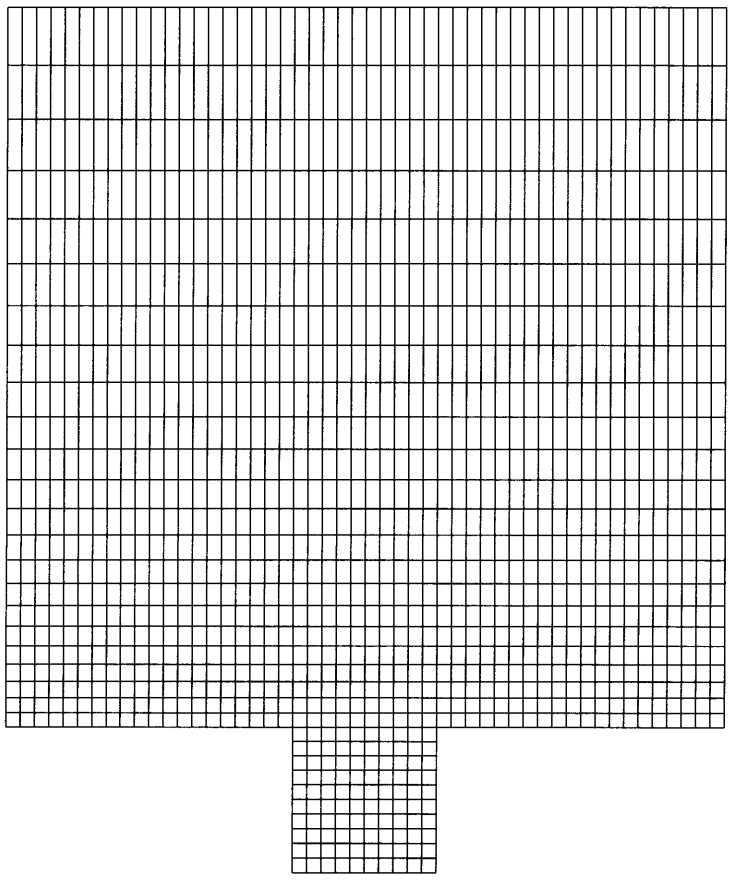

Figure 4-16: Schematic of mesh gradient

First, we will consider the upper two rows of Table 4.3 – the cases where the

building roof surfaces have slip boundary conditions. The simulations with velocity inlet and pressure outlet boundary conditions yield the same velocity and turbulence contours at the outlet, while the periodic boundary condition results vary with the mesh growth rate. Because the simulations with the velocity inlet and pressure outlet conditions are insensitive to the meshing, we will use these as a comparison to assess the appropriate mesh growth rate for the periodic simulation. The contours of the uniformly meshed periodic case seem to be more similar to the velocity inlet cases in the area above the canyon, however the contours in and near the street canyon are similar for all three periodic cases. Upon close inspection the uniformly meshed, periodic case best matches the non-periodic cases because we notice that the mesh growth rate seems to slow the velocity just above the canyon, causing slightly slower velocities in the canyon.

Next, we consider the lower two rows of Table 4.3, where the building roofs have rough wall, no-slip boundary conditions. The non-periodic cases are insensitive to the mesh growth rate, so they can be used as a basis for comparing the periodic cases. While the contours in the expansive volume of the uniformly meshed, periodic case are the best match to the non-periodic cases, the velocity and turbulent kinetic energy contours in and around the street canyon are most similar to the periodic cases with mesh growth rates. The uniformly meshed periodic case fails to capture the high turbulence just above the canyon. Additionally, the periodic cases with mesh growth rates have in canyon velocity contours that are more similar to the non-periodic cases. We conclude that if we are to use periodic boundary conditions to simulate buildings with rough wall conditions on the roofs, a mesh with a vertical growth rate is most appropriate, however it would be best to avoid the periodic condition altogether, as it seems to be much more sensitive to meshing than the velocity inlet and pressure outlet conditions. In the cases of neighborhoods in Chapter 5, we expect the flows to develop in a shorter length than in the infinitely long canyon because there will be mixing induced by intersections, cross-sections and buildings of various heights. Thus, for these cases and future work with idealized geometries we will not use periodic boundary conditions.

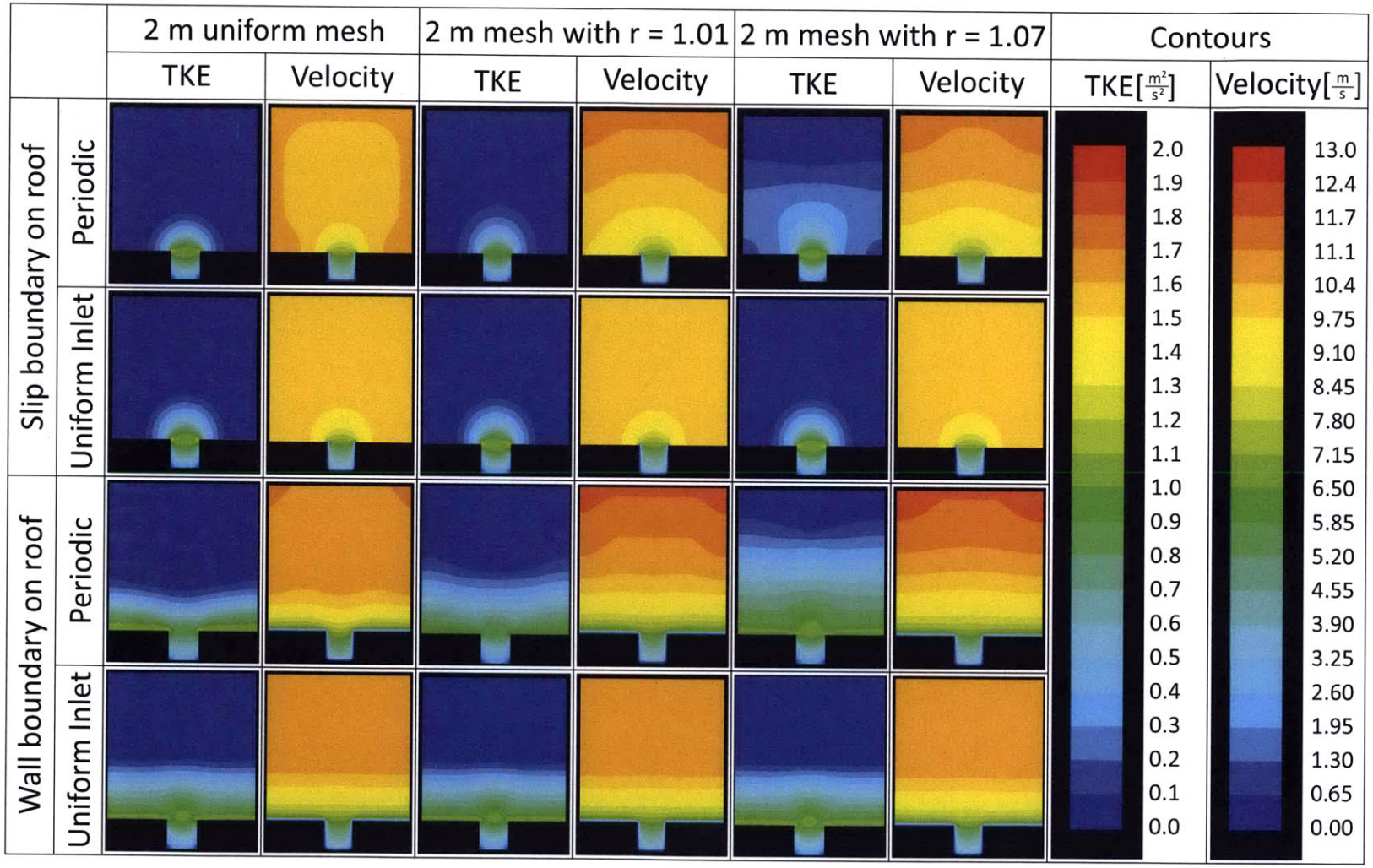

Table 4.3: Comparison of simulated turbulent kinetic energy and velocity contours for idealized street canyon with various mesh growth rates and boundary conditions

Chapter 5

Repeating neighborhoods

Fluid flow through neighborhoods is more complex than the flow in a single street canyon. There will be more exchange between the urban canopy layer and the urban boundary layer because of non-uniformities in the urban form. This includes intersections and sharp changes in street canyon angle, variability in building heights, changes in roughness, and varying aspect ratios. In this chapter we focus specifically on neighborhoods with intersections, as this element is completely absent from the single street canyon analyses in Chapters 3 and 4. In Section 5.1 we introduce four idealized neighborhoods, and discuss their similarities and differences. In Section 5.2, we discuss the development of flow through these neighborhoods, and calculate the longitudinal bulk velocity for the fully developed section of these neighborhoods. We calculate the exchange coefficients for these neighborhoods and compare them to a model in the literature in Section 5.3. [4, 35] Finally, in Section 5.4, we address the need for a geometry-based parameter to determine the expected exchange between the urban canopy layer and the urban boundary layer for a particular neighborhood.

5.1 Four idealized neighborhoods

We chose four idealized neighborhoods that were inspired by the work of Steemers et al, 1997. [48] These neighborhoods built on the previous work of Leslie Martin and Lionel March, 1973. [38] The Martin and March studies focused on different types of neighborhoods that are based on grids, and attempt to quantify the benefits of various layouts that are equal in density of people per unit area. Martin and March primarily studied the land use efficiency of various layouts, and how the form of each neighborhood contributes to or undermines the creation of open space for parks and courtyards. They also discussed how the different building geometries influence the efficiency of the floor layout. For example, they found which geometries minimize the floor space needed for circulation. They also discussed how neighborhood geometry affects the exposure of building façades to direct sunlight. [38] Steemers et al expanded on this study of sunlight and buildings. They found the view factors for each layout and calculated incident solar radiation on all building and ground surfaces of the idealized neighborhoods. They used this work to assess which neighborhoods would be suitable for extreme climates, and extended this work to determine which idealized neighborhoods use the most energy. They released polystyrene beads in physical models to qualitatively assess areas that are prone to pollutant retention and low wind speeds. Additionally, they began to look at pollutant retention quantitatively by performing a smoke dispersion test in a wind tunnel, and analyzing the percent of smoke still visible in the models at fixed time intervals. They asserted that areas with high air movement are preferable for outdoor comfort for some climates and seasons, while high air movement is always preferable with regards to pollutant dispersal. [48] With this in mind, we have focused our study of neighborhood form on which neighborhoods have the greatest exchange coefficient, and what geometrical parameters contribute to this exchange coefficient.

Like the work of Steemers et al, we chose geometrical parameters to hold constant across the idealized neighborhoods to limit the variables that may affect to our parameter of interest, the exchange coefficient. The first parameter we chose was

the surface area of the buildings per unit plan area, because the heat transfer across these surfaces will determine the energy consumption required to condition the air buildings. In the calculation of this area, we only considered the vertical façades, we assume that building roofs are adiabatic. This is a justified assumption because roofs are generally more insulated than building façades, and in many cases the top floors are used for heating, ventilation and cooling equipment storage, so the air in these spaces is minimally conditioned. The second parameter we chose is the floor area per unit plan area. Because these neighborhoods are being built to be tested in Fluent, we allowed this parameter to vary slightly among the neighborhoods as a tradeoff for ease and consistency in our meshes. These parameters, along with the aspect ratio of the canyons in the y,z-plane are presented for the four neighborhoods in Table 5.1. The areas are defined per unit hectare (ha) of plan area, that is per 10,000 meters^2. The building floor area per hectare is within 5% of 20,000 m^2 for all neighborhoods.

	H/W	Façade surface area per ha [m^2]	Floor area per ha [m^2]
Grid	1.60	15360	19200
Slab	1.05	15360	20160
Pavilion Court	1.07	15360	19200
Terrace Court	2.4	15360	20400

Table 5.1: Idealized neighborhood statistics

The first, and tallest neighborhood we consider is a Grid-style neighborhood, similar to Grid City from Chapter 2. The Grid neighborhood is displayed in Figure 5-1. Because a building storey is approximately 4 meters high, we consider the high-rise buildings in the Grid neighborhood to be 12 storeys tall, the tallest buildings in any of our idealized neighborhoods. A hectare holds four of these discrete high-rise buildings. The dimensions of the simulated Grid neighborhood domain were 2000 x 250 x 288 meters in the x,y,z-directions, respectively. This is equivalent to 40 x 5 high-rise buildings in a domain with a vertical dimension that extended five building heights above the rooftops as per the COST 732 guidelines. [21] This guideline was used in all neighborhood domains. The urban canopy layer, that is the volume below the height of the building roofs, was meshed with 2 meter uniform

hexahedral elements. As in Chapter 4, above the buildings, the vertical dimension of the hexahedral elements were allowed to grow to reduce computational time. The growth rate was approximately 1.030.

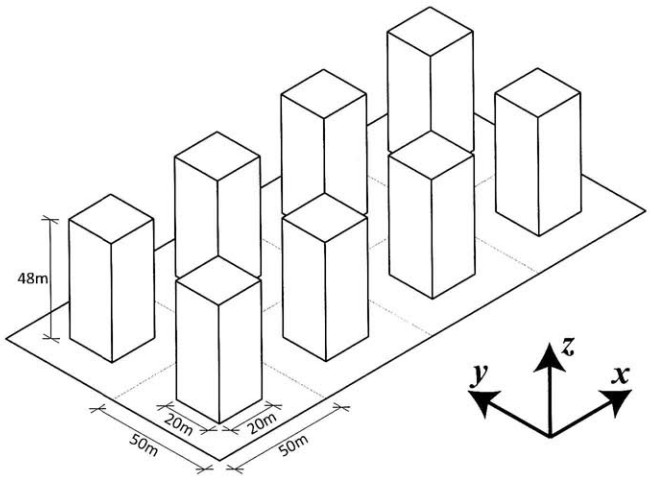

Figure 5-1: Schematic of Grid neighborhood geometry

The next neighborhood considered is a Slab-style neighborhood, depicted in Figure 5-2. This domain measured 2000 x 200 x 240 meters in the x,y,z-directions, respectively, which is equivalent to 20 x 4 Slab buildings. The buildings in the Slab neighborhood are 10 storeys tall. Again the urban canopy layer was meshed with 2 meter hexahedral elements, and the volume above the building roofs were meshed as in the Grid neighborhood, but with a vertical growth rate of 1.027. A major difference between the Slab neighborhood and the Grid neighborhood is that in the Slab neighborhood, the canyons with longitudinal axes along the y-axis are less than half as wide as the canyons along the x-axis.

The Pavilion Court neighborhood is shown in Figure 5-3. A single unit of the Pavilion Court neighborhood sits alone on a hectare of lot area. The simulated domain measured 2000 x 400 x 182 meters in the x,y,z-directions, respectively. This is equivalent to 20 x 4 Pavilion Court buildings. The vertical mesh growth rate was set to 1.021 in the volume above the buildings. The canyons along the x-axis have the same aspect ratio as the canyons along the y-axis, and the buildings are 8 storeys tall.

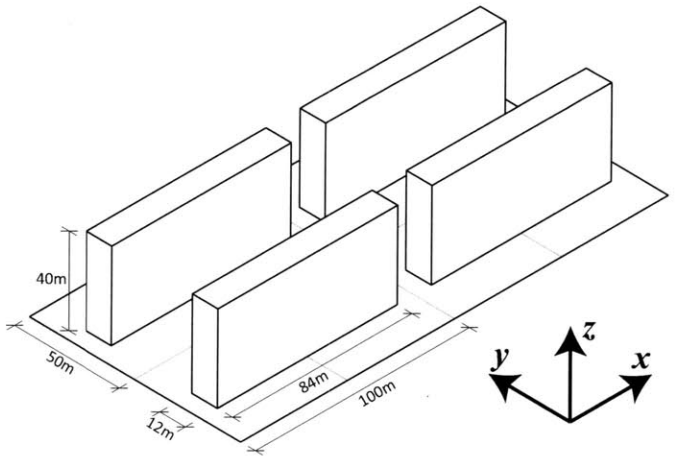

Figure 5-2: Schematic of Slab neighborhood geometry

The Terrace Court neighborhood is displayed in Figure 5-4. Like the Pavilion Court neighborhood, this neighborhood has courtyards, however the Terrace Court neighborhood does not have intersections, that is there are no canyons with longitudinal axes in the y-direction in this domain. It can be likened to infinitely long canyons with additional courtyard geometry that will cause some separation in the flow and may slightly increase the exchange between the urban canopy layer and the urban boundary layer. This domain measured 2000 x 300 x 144 meters in the x,y,z-directions, respectively, this is equivalent to three long Terrace Court units. The vertical mesh growth rate above the buildings was set to 1.014. The buildings are 6 storeys tall.

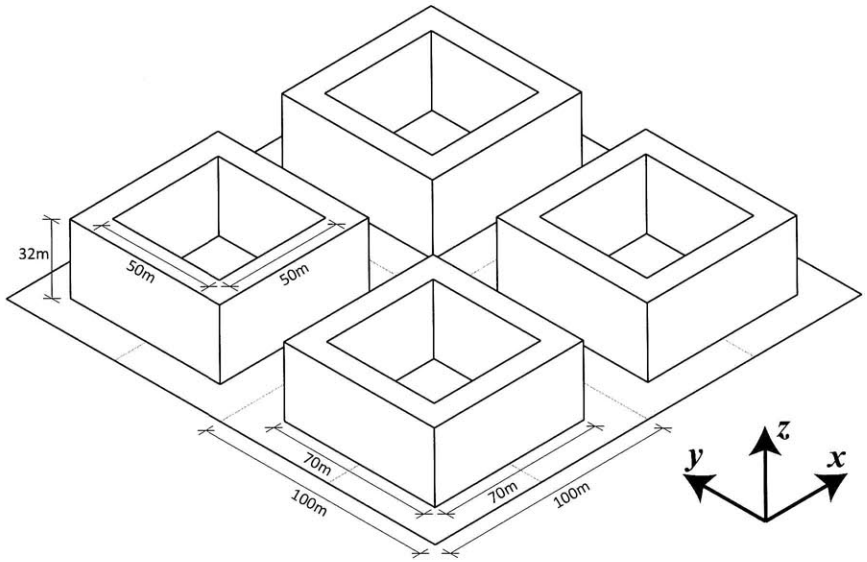

Figure 5-3: Schematic of Pavilion Court neighborhood geometry

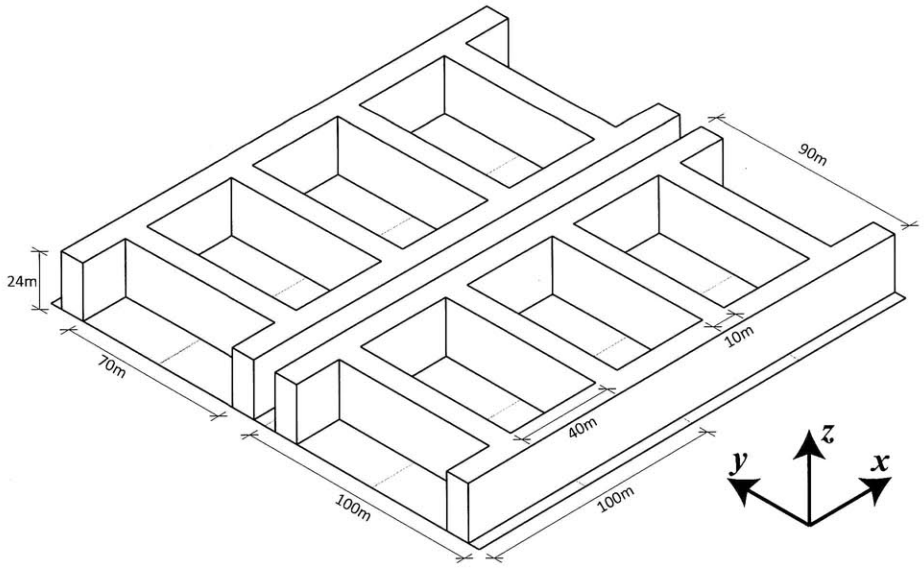

Figure 5-4: Schematic of Terrace Court neighborhood geometry

5.2 Longitudinal bulk velocities in idealized neighborhoods

These neighborhoods were simulated in Fluent 6.3. Instead of using periodic boundary conditions, the inlets were prescribed a uniform velocity profile of 10 m/s in the x-direction, and the outlets were set to pressure outlet boundary conditions. The lateral and top boundaries were assigned slip boundary conditions. All ground and building surfaces were set to no-slip wall boundary conditions with a Nikuradse sand grain roughness of 0.8 meters. Because we expect these neighborhoods to have a higher exchange coefficient than the isolated canyons in Chapters 3 and 4, it follows that the velocities will be fully developed early in the 2000 meter long domains. To test this assumption we studied the longitudinal bulk velocity down the length of the centermost canyon in each neighborhood domain.

Spatially averaging over each y,z-plane along the street canyon to find the bulk velocity profile along the canyon requires the manipulation of a great amount of data. These street canyon volumes encompass between 10^5 and 10^6 nodes. Each node is averaged with its neighbors to find a cell-centered value, and these are each averaged with other values in the same y,z-plane. To avoid these calculations in present and future work, we compare calculation methods for approximating the longitudinal bulk velocity down the Pavilion Court street canyon. The results of this comparison are displayed in Figure 5-5. The alternative methods are assessed on their ability to predict the development length of the flow, as well as the ability to calculate the correct fully developed longitudinal bulk velocity. The bulk velocities associated with the black line were calculated as in Equation 2.2 for each y,z-plane along the street canyon. This line will be the baseline for comparison of other techniques, as it is the most computationally expensive, but also the most true to our definition of longitudinal bulk velocity. The red line in Figure 5-5 is the raw data along the line at a height of $z = H/2$, down the center of the canyon. This line was chosen because it is common to measure velocities in this way in wind tunnel studies, as a dense mesh of vertical and horizontal data is not practical. This is how the experimental

data used in Section 4.4 was gathered. [24, 25] This single plane correctly predicts the distance along the canyon where the flow becomes fully developed, approximately 600 meters, however it fails to accurately predict the fully developed longitudinal bulk velocity relative to the atmospheric velocity. It over predicts the velocity by more than 30%. This is an unacceptable margin of error. For each of the ideal neighborhoods, the fully developed longitudinal bulk velocity was calculated near the exit of the domain, halfway along the length of one of the buildings. This calculation involves the manipulation of less than 10^3 nodes to solve Equation 2.2. These results were normalized to u_a and are displayed in Table 5.2.

	u_{cl}/u_a
Grid	0.44
Slab	0.76
Pavilion Court	0.64
Terrace Court	0.32

Table 5.2: Idealized neighborhood longitudinal bulk velocities

Using these nodes, we calculated the average velocity at the height of each mesh element in the Pavilion Court neighborhood. Next, we compared these values to the fully developed longitudinal bulk velocity in the Pavilion Court neighborhood, and found that the longitudinal bulk velocity most closely matched the average velocity at $z = 10$ meters. Finally, we calculated the average velocity at $z = 10$ meters at each node along the street canyon. The results of this calculation are plotted with a grey line in Figure 5-5. This line matches the black line well, the development lengths and the fully developed velocities are almost exactly the same. Additionally, this plane captures some of the variations in velocity that are due to the intersections.

This method of calculation was used to approximate the longitudinal bulk velocity down a typical canyon for the four neighborhoods. The results are displayed in Figure 5-6. The planes used to approximate the bulk velocities for these cases were $z = 24$, 12, and 12 meters for the Grid, Slab, and Terrace Court neighborhoods respectively. The comparison of the neighborhoods in Figure 5-6 increases our understanding of which geometric parameters influence the flow through the neighborhood.

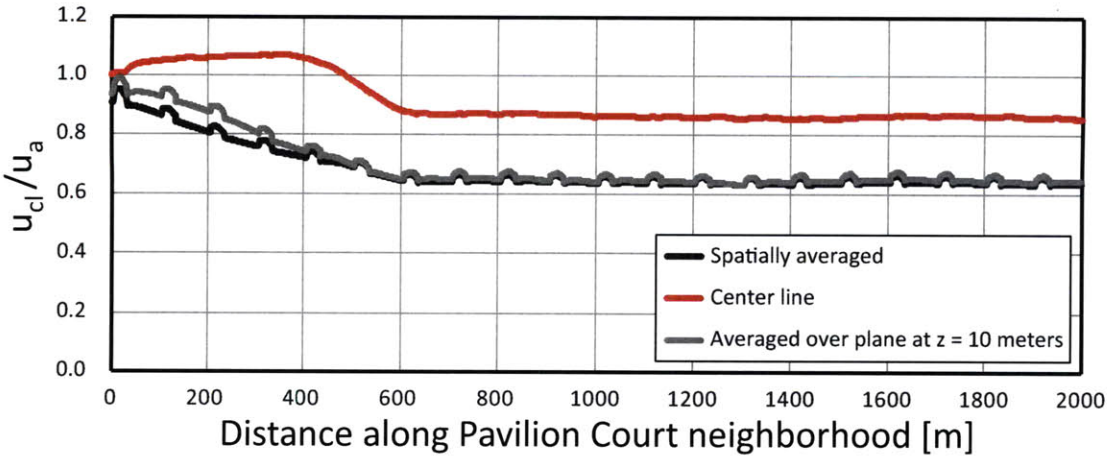

Figure 5-5: u_{cl}/u_a vs. Distance along Pavilion Court neighborhood [meters]

For example, though the Slab and Pavilion Court neighborhoods have street canyons of nearly the same aspect ratio and are lined with walls of the same Nikuradse sand grain roughness, the fully developed velocities for these cases are noticeably different. This difference can be attributed to different values of the exchange coefficient, as per Equation 3.17, and this exchange coefficient must be determined by some other neighborhood scale geometric parameter.

The small variations in the fully developed section of the neighborhoods can be attributed to the intersections. Numerically, this is obvious – in sections of the street canyon that are flanked by buildings, the no-slip wall boundary condition enforces velocities of zero at the extreme nodes. Despite averaging these values to approximate cell-centered velocities, these zero values still contribute to the spatial averaging of velocities. At the intersections, there is no boundary at these nodes, so the velocity is allowed to have a non-zero value and we expect the average velocity to be higher. Fluid mechanically, because there is momentum in the center of the canyon, and the shear stress from the wall is no longer present, the velocity of the air near the lateral extents of the street canyon will be greater. The air in the longitudinal street canyon interacts with the air in the street canyons that are perpendicular to the flow at the intersection in a way that is similar to the exchange at rooftop. Flow separation and reattachment on these bluff body flows, and the vortices associated with the flow

increase the exchange coefficient and turbulence throughout neighborhood domain. These effects are even more pronounced in areas where there is likely to be flow separation, such as the off the roof and building façades that are parallel to the flow at the windward side of an intersection. This explains why these variations can be seen in the grey and black lines in Figure 5-5, but not in the red line. The red line is the furthest spot in the width of the canyon from the no slip boundary conditions and the separation near the windward façades.

The green line in Figure 5-6 has no intersections, so the longitudinal bulk velocity curve does not vary along the section of the canyon where the flow is fully developed. This is because there are no areas of increased flow separation from windward walls in intersecting canyons. When separation occurs in the canyon, vortices are created and there is an increase turbulent mixing with the air above, as well as an increase in street canyon velocities. Considering only the neighborhoods with intersections, the development length of the flow seems to be inversely related to the ratio of longitudinal bulk velocity to atmospheric velocity. This could mean that geometries that have higher exchange coefficients tend to reach fully developed flow in a shorter length. This reinforces our assumption in Chapter 3, i.e. that flow in a neighborhood can be considered fully developed. The inlet to an isolated real neighborhood would not be uniform, but rather like flow over a flat plate, so the development lengths would be less than those in Figure 5-6. Additionally, neighborhoods rarely exist in isolation, so flow in a neighborhood that is surrounded by a larger city of similar geometry can be modelled using the Equations derived in Chapters 3.

To gain more insight to the flow through neighborhoods, we consider the Slab neighborhood in greater detail because the canyons along the y-axis are very different in geometry than those along the x-axis. Not only are the aspect ratios different, the y-axis canyon has an aspect ratio of 2.5 compared to 1.05 for the street canyon along the x-axis, but the length of the street canyon that is flanked by buildings is much less than the length of the street canyon that is involved in an intersection. While this situation is not practical for realistic neighborhoods, this comparison should provide insight as to how neighborhood geometry influences flow through the street canyons.

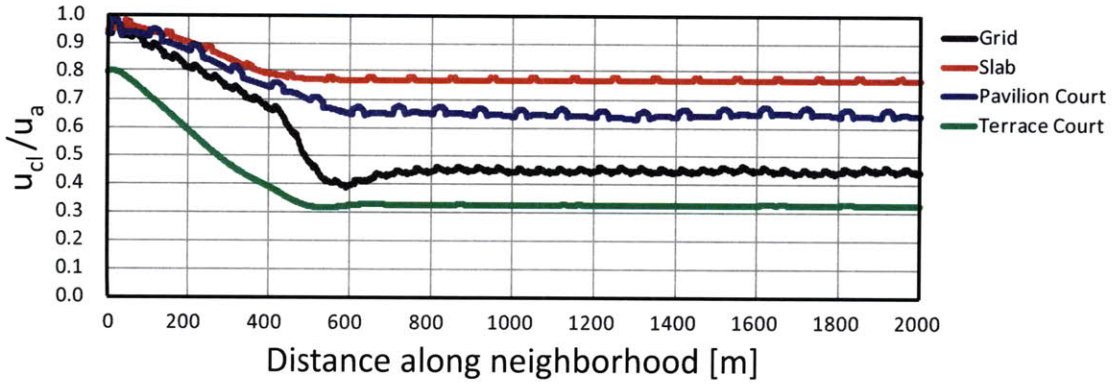

Figure 5-6: u_{cl}/u_a vs. Distance along neighborhood [meters]: comparison of four idealized neighborhoods

The Rotated Slab neighborhood domain was sized to be 300 x 2000 x 240 meters in the x,y,z-directions, respectively, and the inlet was set to a uniform velocity of 10 m/s in the y-direction. The results of this simulation are plotted in Figure 5-7, with the data for the Slab neighborhood from Figure 5-6. Though the longitudinal bulk velocity of the Rotated Slab neighborhood is definitely approaching a fully developed value, it is not fully developed like the other four neighborhoods. The large velocity variations are due to the wide intersections from the street canyons along the x-axis. Though these intersections lead to greater mixing than the mixing in an infinitely long canyon of similar aspect ratio, the fact that the flow is not fully developed means that the exchange coefficient for this case is probably lower than the other neighborhoods.

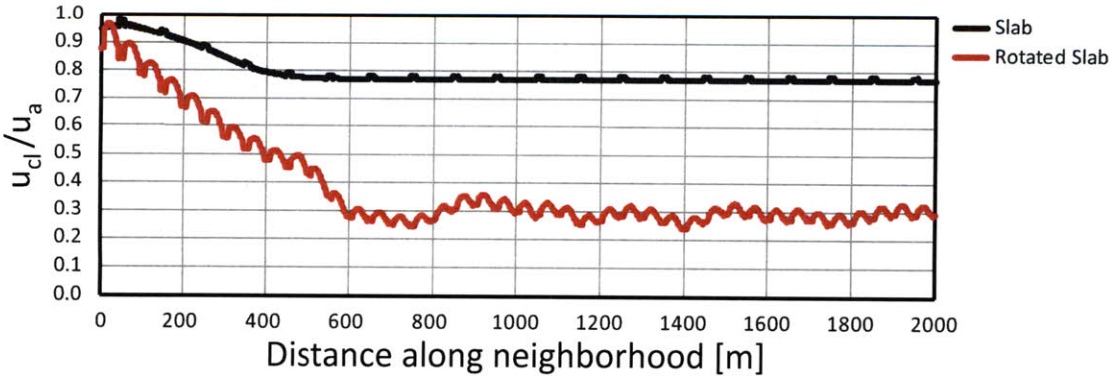

Figure 5-7: u_{cl}/u_a vs. Distance along neighborhood [meters]: comparison of two orientations of the Slab neighborhood

5.3 Exchange coefficients for the idealized neighborhoods

As described in Section 4.4, the longitudinal bulk velocities calculated with the Bentham and Britter model based on the MacDonald model are averaged over a canyon of any orientation. [4, 35] Using Equation 4.11 and the spatially averaged longitudinal bulk velocities for the fully or nearly fully developed areas of the street canyons in the neighborhoods, we find orientation averaged longitudinal street canyon velocities normalized to atmospheric wind speed for each neighborhood. These values are plotted against the frontal area index, as defined in Section 4.1, in Figure 5-8. The Pavilion Court and Terrace Court neighborhoods are plotted for two different values of the frontal area index. For the Pavilion Court neighborhood, the filled-in point, depicted as Pavilion Court 1 in Figure 5-8, only considers the frontal area associated with the outside of the building, whereas the empty point, depicted as Pavilion Court 2 in Figure 5-8, considers the frontal area to be the outside of the building and the leeward wall of the courtyard. For the Terrace court neighborhood, the filled-in point considers the frontal area to be the width of the building, 90 meters, times the height of the building, whereas the empty point considers the frontal area to be only the leeward wall of the courtyard. The frontal area index parameter is somewhat ambiguous for these two ideal neighborhoods. If we consider the parameter as it was intended, for measures of roughness concentration as in Figure 4-2, we can argue that as the size of the courtyards shrink, the flow above and between the Pavilion Court buildings will be the same as the case where there are no courtyards, so the correct calculation for Pavilion Court neighborhood frontal area index would be the filled-in point. However, if we consider how the geometry affects the exchange with the air above, it is unknown how the increased surface area affects the flow. Similar arguments can be made for the Terrace Court neighborhood – as the courtyard shrinks, the neighborhood approaches infinitely long canyons, which have no meaningful value for the frontal area index. Additionally, the frontal area index should be a measure of obstructions to the street canyon flow, and a façade inside a courtyard does not

obstruct flow in a street canyon. Despite these ambiguities, the trend of the simulated data is similar to the Bentham and Britter model based on the MacDonald model. [4, 35] That is, as the frontal area index of the neighborhood increases, the average longitudinal bulk velocity averaged over all canyon orientations and normalized to the atmospheric wind decreases.

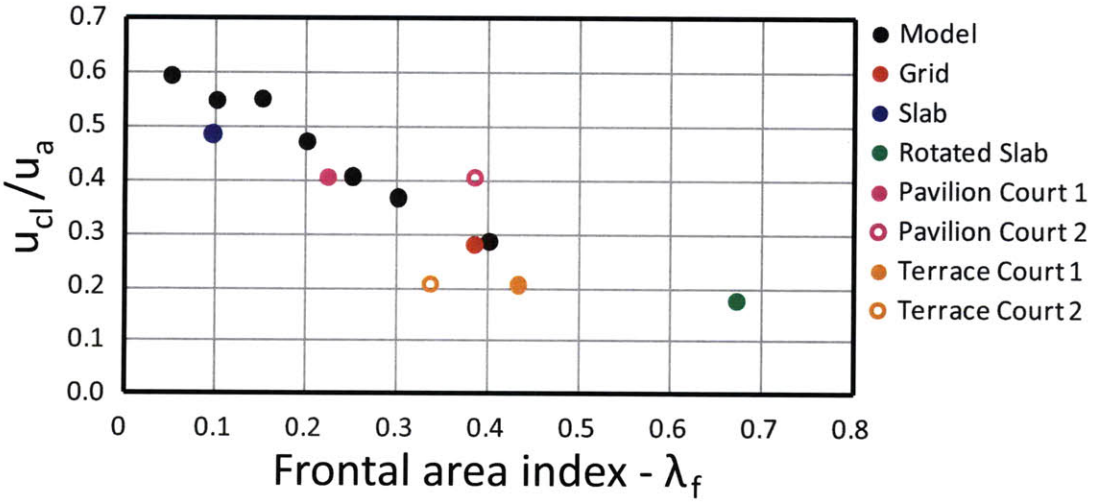

Figure 5-8: u_{cl}/u_a vs. Frontal area index, λ_f: comparison of model to idealized neighborhoods [4, 35]

Using the longitudinal bulk velocity calculated for the case where the wind is aligned with the canyon, we can solve for the exchange coefficient for each neighborhood with Equations 3.6 and 3.17. These results are plotted with the Bentham and Britter model in Figure 5-9. These results are less promising than those in Figure 5-8. The exchange coefficient for the Slab neighborhood is extremely high. Likely, this is because the frontal area index for this case is very low. Because the bluff bodies obstructing the flow are small in comparison to the plan area, and they are all perfectly aligned with each other, the flow in this neighborhood does not behave like a flow in a series of street canyons. The mixing is not driven primarily by mechanical mixing at intersections, rather the flow behaves like the three-sided channel enclosed by a large idealized volume in Figure 3-7. One major difference is that this street canyon is very close to other street canyons, so the these flows interact across the narrow intersections, and by exchange with the urban boundary layer just above the street

canyon. Because the area above each street canyon is so close to the area above the neighboring street canyons, these areas of high turbulence interact with each other, and this increased mixing contributes to the large exchange coefficient, which is not practical for a realistic neighborhood. The other neighborhoods seem to follow the general trend of the model from the literature, however even the Rotated Slab neighborhood appears to have a very low exchange coefficient. This may be due to the very different aspect ratios between the longitudinal canyon and the recirculating canyons in this neighborhood. This effect may contribute to the exchange coefficient of the Slab neighborhood as well. These results lead us to believe that the frontal area index alone is not a robust enough parameter to fully describe urban geometry.

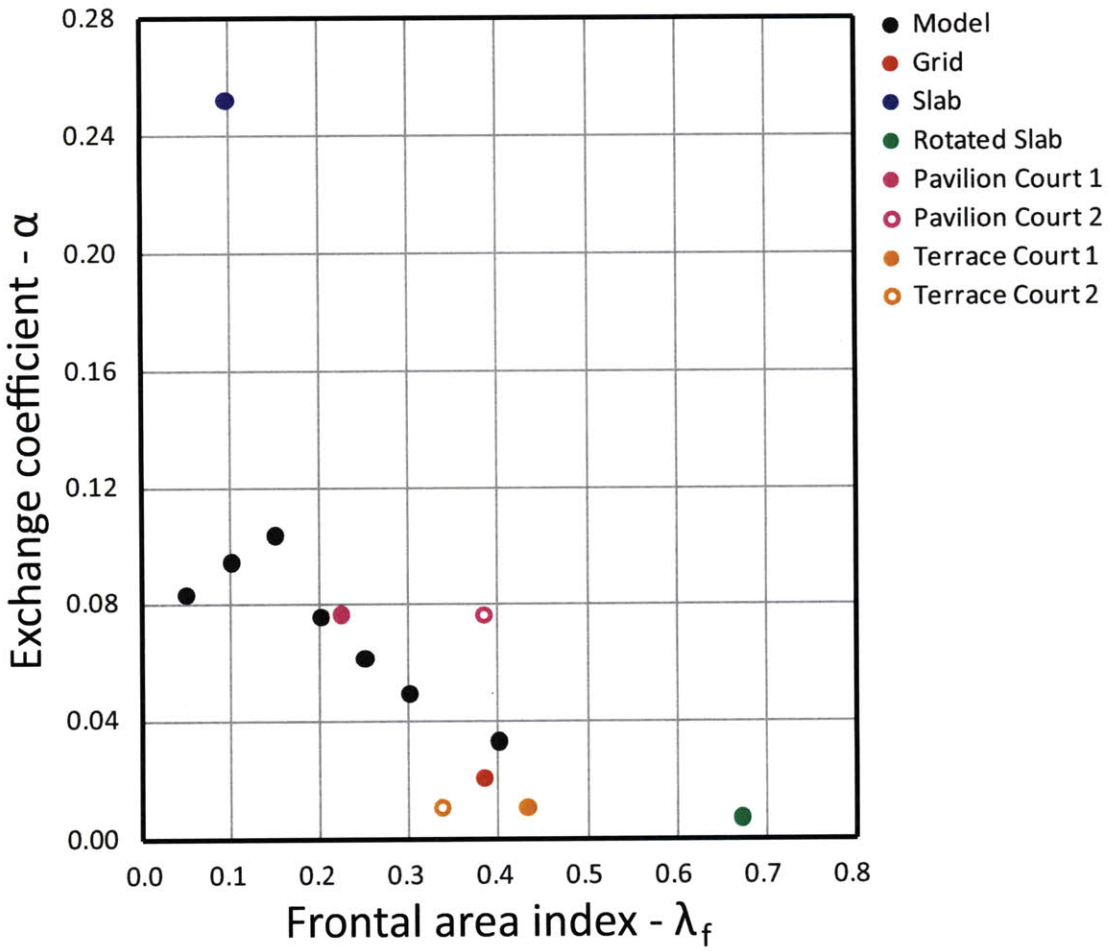

Figure 5-9: Exchange coefficient, α vs. Frontal area index, λ_f: comparison of model to idealized neighborhoods [4, 35]

We eliminate the frontal area index by plotting the averaged longitudinal bulk canyon velocity normalized to the atmospheric wind speed against the exchange coefficient for the simulated neighborhoods and the model from the literature in Figure 5-10. The Slab neighborhood is not considered in this graph so that we may focus on the trends of the neighborhoods with exchange coefficients that are similar to the model. These neighborhoods match the model well, however it is surprising that the Terrace Court neighborhood follows a trend so similar to the neighborhoods with intersections because this neighborhood has no intersections, and therefore has less flow separation and turbulence in and near the street canyons. While this trend is interesting, we would rather find a trend between a geometric parameter and the exchange coefficient so that the exchange coefficient for a neighborhood can be determined without simulation.

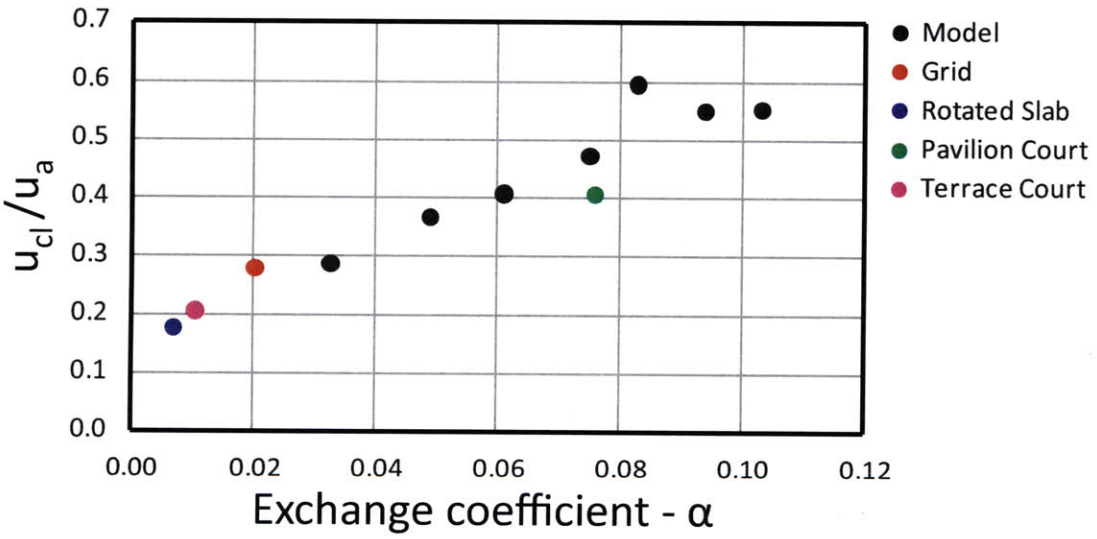

Figure 5-10: u_{cl}/u_a vs. Exchange coefficient, α: comparison of model to idealized neighborhoods [4, 35]

5.4 A geometry-based parameter for determining the exchange coefficient of a neighborhood

One geometric parameter worth considering is the average aspect ratio in the neighborhood. If the average aspect ratio defined the exchange coefficient of the neighborhood, then Equation 3.17 could be solved using that exchange coefficient for a particular canyon in the neighborhood with a specific aspect ratio. The average aspect ratio is calculated as a weighted average based on the length of street canyons with a particular aspect ratio. For the Slab and Rotated Slab neighborhoods, the average aspect ratio is calculated as:

$$\left(\frac{H}{W}\right)_{avg} = \frac{2.5 \cdot 12\,\text{m} + 1.05 \cdot 84\,\text{m}}{12\,\text{m} + 84\,\text{m}} = 1.23. \tag{5.1}$$

This data is plotted in Figure 5-11 for all neighborhoods except the Slab neighborhood. There no strong trend among the Grid, Rotated Slab and Pavilion Court neighborhoods, however it seems like in general as the average aspect ratio increases, the exchange coefficient decreases. The average aspect ratio is not the appropriate geometric parameter to assign an exchange coefficient to a neighborhood, because there is no strong trend among these three neighborhoods. We expect that the appropriate geometric parameter will have a strong trend among the the Grid, Rotated Slab and Pavilion Court neighborhoods, and that the Terrace Court neighborhood will not follow the trend. This is because the Terrace Court neighborhood will behave more like the infinitely long canyons in Chapter 4, which exhibited much lower exchange coefficients than those in Figure 5-11 due to less turbulent mixing in the flow. Again, there is less mixing in the Terrace Court neighborhood and in the infinitely long canyon because there are no intersections to induce flow separation.

Consider the Pavilion Court neighborhood, as the courtyard shrinks we expect the exchange coefficient to decrease. The two relevant geometric parameters that measure this change are the perimeter of the building and the footprint of the building. If these parameters are to be used to characterize the neighborhood, they must be

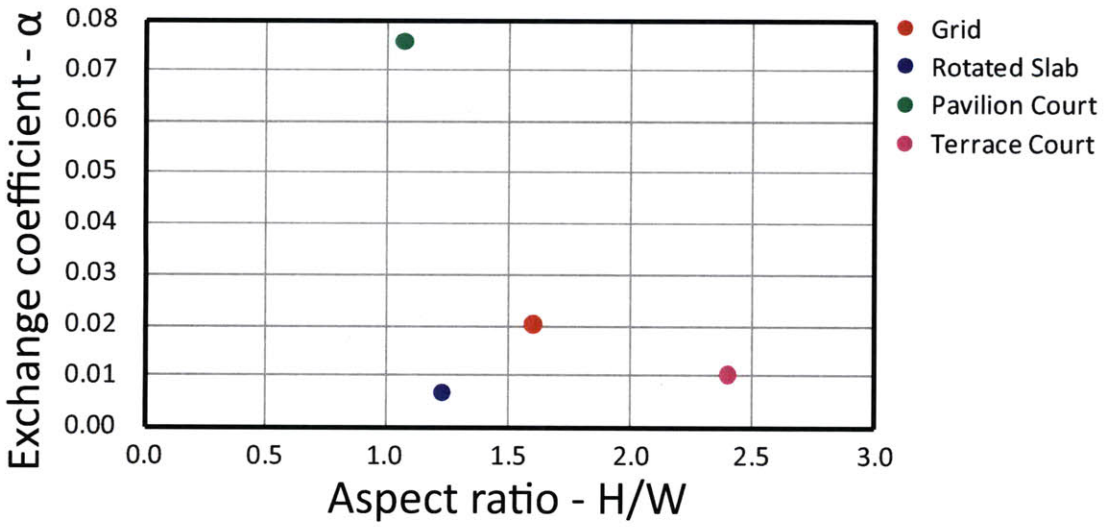

Figure 5-11: Exchange coefficient, α vs. Average neighborhood aspect ratio, $(H/W)_{avg}$: comparison of four idealized neighborhoods

non-dimensionalized. We define the non-dimensional building perimeters in a neighborhood as

$$P = \frac{perimeter\ of\ buildings}{specific\ perimeter}, \tag{5.2}$$

where *perimeter of buildings* is the sum of the perimeters of all of the buildings in some unit of plan area of the neighborhood, and the $specificperimeter$ is the perimeter of the unit of area of the neighborhood. Of course, when comparing neighborhoods with this parameter, the size and shape of the unit area considered should remain constant for each neighborhood. For example, in the case of the ideal neighborhoods, it is convenient to consider a square unit area of one hectare.

The non-dimensional footprint of the buildings in a neighborhood is

$$\lambda_p = \frac{plan\ area\ of\ buildings}{specific\ area}, \tag{5.3}$$

where the *plan area of buildings* is the sum of the plan areas of all of the buildings in some unit area of a neighborhood, and the $specific\,area$ is the area of the unit of area considered.

Neither of these parameters consider the heights of the building geometry in the

neighborhood. Figure 5-9 suggests that height does affect the exchange coefficient, as the height is in the numerator of λ_f. We can combine λ_f with the parameters in Equations 5.2 and 5.3 to create a parameter that we expect to vary directly with the exchange coefficient. The exchange velocity is graphed against the ratio of P to λ_f in Figure 5-12 for the four neighborhoods with exchange coefficients of less than 0.1. The empty point associated with Pavilion Court 2 is based on the calculation of λ_f with the inner courtyard façade, which is inappropriate if we consider the frontal area index as a measure of the façades that obstruct street canyon flow, because the courtyard façade is not in a street canyon. The three filled-in points that represent neighborhoods with intersections behave as expected – as the combined parameter, P/λ_f, increases, the exchange coefficient increases. Even more promising is the fact that neither Terrace Court points follow this trend, but rather they exhibit a lower than expected exchange coefficient, which makes sense because this neighborhood does not have intersections. In fact, with our earlier assumption about λ_f, the combined parameter value for the Terrace Court neighborhood should be zero. The value of the combined parameter in Figure 5-12 has a value of 10 for the Slab neighborhood, a value which would also follow this trend.

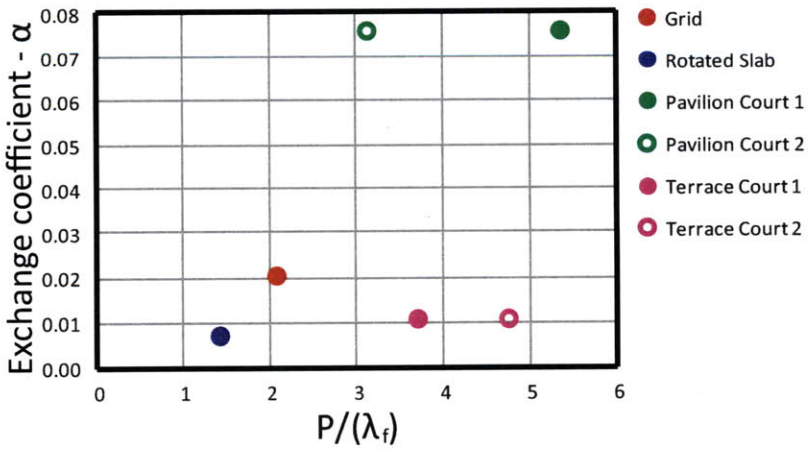

Figure 5-12: Exchange coefficient, α vs. P/λ_f: comparison of four idealized neighborhoods

We expect that decreasing λ_p in the Grid neighborhood would probably lead to an

increase in exchange coefficient, as per the general trend in Figure 5-11. Specifically, decreasing λ_p leads to a decrease in the aspect ratio for the Grid neighborhood. We expect that decreasing λ_p in the Pavilion Court neighborhood by increasing the courtyard size would also lead to an increase in the neighborhood exchange coefficient. The reason for this increase, however, is different than for the Grid neighborhood. In the Pavilion Court neighborhood, decreasing λ_p by increasing the size of the courtyard would result in increased turbulence above the courtyard that will now be closer to the area above the neighboring street canyons, and will increase the exchange between the street canyons and the urban boundary layer. For this reason, we divide the combined parameter from Figure 5-12 by λ_p to create another parameter, $P/\left(\lambda_p\,\lambda_f\right)$. We expect the exchange coefficient to vary directly with this parameter, and this expectation is met. The results of this study are plotted in Figure 5-13. Again, the filled-in point is more relevant for the Pavilion Court neighborhood. The value of this parameter for the Slab neighborhood is 49.6, which also follows the trend in Figure 5-13, however it is not shown because it is a physically unrealistic neighborhood.

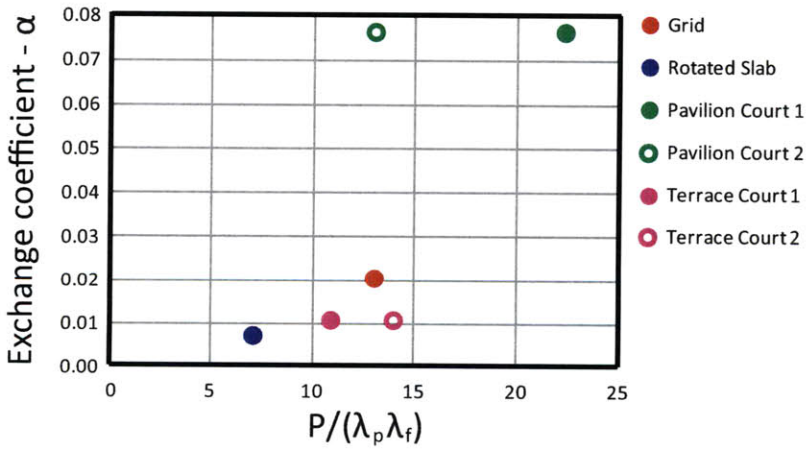

Figure 5-13: Exchange coefficient, α vs. $P/\left(\lambda_p\,\lambda_f\right)$: comparison of four idealized neighborhoods

This study does not provide a definitive geometric parameter to define the neighborhood exchange coefficient, however the trends suggested in the above figures are interesting, and will lead to insight about the appropriate parameter in future work.

Future work also includes studying neighborhoods with buildings of different heights. Like intersections, we expect variability of building heights to contribute to the local exchange coefficient for a given neighborhood. This would be partially captured in the calculation of λ_f, however as the extents of the unit area considered when calculating these parameters is increased, the influence of local variation in building heights would be less captured by λ_f. Therefore, future work also includes studying the appropriate extents of the unit area to consider when calculating the local neighborhood exchange coefficient.

Chapter 6

Limitations

The work in Chapters 3, 4 and 5 is an attempt to understand the fluid mechanics responsible for air flow through a neighborhood. Beginning with an ideal street canyon and ending with four simple neighborhoods, we found methods to predict street canyon velocities and the exchange between the urban boundary layer and the urban canopy layer based on only atmospheric wind conditions, building geometry and surface roughness. One gap that we have not addressed in this work is buoyancy driven flow. The CFD work in this study and the experimental comparisons to this work have all occurred in isolated situations where there are no heated surfaces or temperature differences between the fluid and the surfaces. In real neighborhoods shortwave radiation from the sun heats building surfaces, heat is rejected from building conditioning units and other anthropogenic heat sources, such as cars, fill the street canyons. These heat sources cause temperature differences in the neighborhood that may influence the street canyon flow. [43]

We address this question with a version of the Richardson number, a non-dimensional constant which represents the relative importance of natural convection to forced convection in some flow. [32, 33, 39] This concept is introduced in Section 6.1. We apply this idea to street canyon geometry based on methods from the literature in Section 6.2.

6.1 Buoyancy and the Richardson number

To begin, we consider the Grashof number, a ratio of buoyancy forces to viscous forces. The Grashof number. Gr, is defined as:

$$Gr = \frac{g\,\beta\,(T_s - T_\infty)\,L^3}{\nu^2}, \tag{6.1}$$

where g is the acceleration due to gravity, β is the volumetric thermal expansion coefficient, T_s is the temperature of some heated surface, T_∞ is the temperature of the free stream flow over the surface, L is a characteristic length to be discussed in Section 6.2 and ν is the dynamic viscosity of the fluid. [28] The volumetric thermal expansion coefficient, β, is defined as

$$\beta = \frac{1}{V}\left(\frac{\partial V}{\partial T}\right)_P, \tag{6.2}$$

where V is the volume of the fluid, T is the temperature of the fluid, and the subscript P signifies that the expansion is occurring at a constant pressure. This expression can be rewritten in terms of density by discretizing the derivative in Equation 6.2 for small changes in volume:

$$\beta \approx \frac{1}{V}\left(\frac{V_2 - V_1}{T_2 - T_1}\right)_P = \frac{\rho}{m}\left(\frac{\frac{m_2}{\rho_2} - \frac{m_1}{\rho_1}}{T_2 - T_1}\right) = \frac{1}{\rho}\left(\frac{\rho_1 - \rho_2}{T_2 - T_1}\right)_P \approx -\frac{1}{\rho}\left(\frac{\partial \rho}{\partial T}\right)_P. \tag{6.3}$$

For an ideal gas, Equation 6.3 can be simplified as

$$\beta = -\frac{1}{\rho}\left(\frac{\partial \rho}{\partial T}\right)_P = \frac{1}{\rho}\frac{P}{R\,T^2} = \frac{1}{T}, \tag{6.4}$$

where R is the ideal gas constant, P is the pressure and $\rho = P/(R\,T)$ for an ideal gas. [39] The temperature in Equation 6.4 is that of the fluid. Combining Equations 6.1 and 6.4, we express the Grashof number for an ideal gas as:

$$Gr = \frac{g\ (T_s - T_\infty)\ L^3}{T_\infty\,\nu^2}. \tag{6.5}$$

The Grashof number in Equation 6.5 characterizes flow driven by temperature differences, that is flow due to natural convection. To compare the importance of forced convection to natural convection in a particular flow, we derive a dimensionless group that characterizes forced convective flow. The Reynolds number, as defined in Equation 3.2, does just this, however we wish to derive a form of the Reynolds number in terms of the Grashof number so that we may compare these dimensionless groups directly to ascertain what type of flow is dominant. Consider a fluid element traveling in a buoyancy driven flow. The work done on the element by the buoyancy force must be equal to the gain in kinetic energy of the fluid as

$$\rho\, u^2 \;\sim\; g\, \Delta\rho\, L, \tag{6.6}$$

where u is the velocity of the fluid due to natural convection in the buoyancy driven flow. [39] This equation can be rewritten in terms of this natural convection velocity as:

$$u \;\sim\; \sqrt{\frac{\Delta\rho}{\rho}\, g\, L}. \tag{6.7}$$

Substituting Equation 6.7 into the expression for the Reynolds number, Equation 3.2, for some characteristic length we find

$$Re = \sqrt{\frac{g\, \Delta\rho\, L^3}{\rho\, \nu^2}}, \tag{6.8}$$

which is like a Reynolds number for natural convection flow. [39] The Reynolds number has the form of the square root of the Grashof number for an ideal gas as defined in Equation 6.5. We may therefore consider the relative importance of natural convection to forced convection in the flow by considering the Richardson number, Ri, which for our purposes is defined as

$$Ri = \frac{Gr}{Re^2}. \tag{6.9}$$

If the Richardson number is much greater than one, natural convection dominates

the flow, whereas if it is much less than one, forced convection dominates the flow. The relationships derived in Chapters 3, 4 and 5 are based on the assumption that the flow in the neighborhood is driven by forced convection.

6.2 Application of the Richardson number to a street canyon geometry

There has been some simulation work to apply the Richardson number to street canyon flows. Li et al use large-eddy simulation techniques to study the effect of the Richardson number on the recirculating flow street canyons with aspect ratios of 0.5, 1 and 2. [32, 33] They study each case for a Richardson number of zero, where there are no temperature differences in the flow or between the fluid and the canyon surfaces, Richardson numbers of 0.5-0.9 which they consider weak heating and Richardson numbers of 2.0-2.9 which they consider strong heating. They also perform a more detailed study considering the recirculating flow in street canyons with an aspect ratio of unity for Richardson numbers of 0.6, 1.2 and 2.4. Their work is based on a temperature difference between the ground surface of the street canyon and the free stream flow above the street canyon. They find that increasing the Richardson number increases the magnitude of the vertical velocities in the flow near both the windward and leeward walls for the street canyon with an aspect ratio of unity. This in turn increases the exchange between the flow in the urban boundary layer and the flow in the street canyon. The flow structure in the case of unity aspect ratio, however, is nearly the same for the strong, weak and no heating cases. The other aspect ratios studied by Li et al were found to have different flow structures with different Richardson numbers, and in all cases an increase in Richardson number led to an increase in the vertical velocities in the street canyons and an increase in exchange with the air above.

As mentioned in Section 6.1, external flows are dominated by forced convection when the Richardson number is much less than unity. [39] Assuming that the characteristic length is the height of the canyon, which makes sense for heating the ground surface, and the free stream temperature of the air is 303 Kelvin, typical of Singapore, we may plot the required fluid velocities to maintain a Richardson number of unity for various aspect ratios and temperature differences. This plot is displayed for a 10 meter wide canyon for typical temperature differences in Figure 6-1. [10]

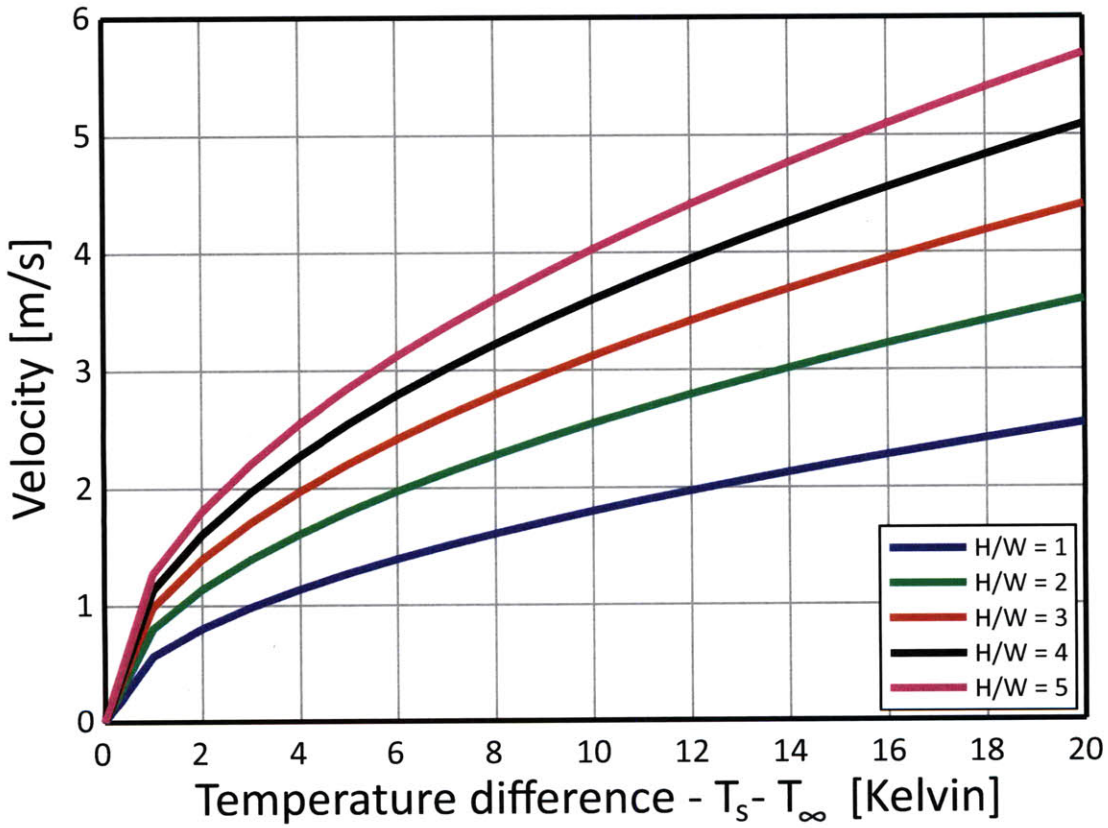

Figure 6-1: Velocity [m/s] vs. Temperature difference, $T_s - T_\infty$ [Kelvin]: based on a 10 meter wide street canyons of various aspect ratios with free stream temperature of 303 Kelvin and ground surface heating equivalent to a Richardson number of unity

In Figure 6-1, we consider the velocity to be that of the atmospheric wind speed to match the assumptions of Li et al. For a given aspect ratio, if the velocity of the flow falls above the curve in Figure 6-1 we consider the flow to be primarily driven by forced convection, and therefore our work is directly applicable. At night, and in temperate climates, this case is probably the norm. The work of Li et al was only done for the recirculating case, which should be the scenario where buoyancy flow is most likely to dominate because the vertical velocities in the canyon are of similar magnitude to the horizontal velocities in the canyon. We assert that the limit for forced convection dominating the flow may be greater than unity for cases more similar to longitudinal flow. We re-plot Figure 6-1 for a Richardson number of three in Figure 6-2, which Li et al considered to be a Richardson number that represents strong heating.

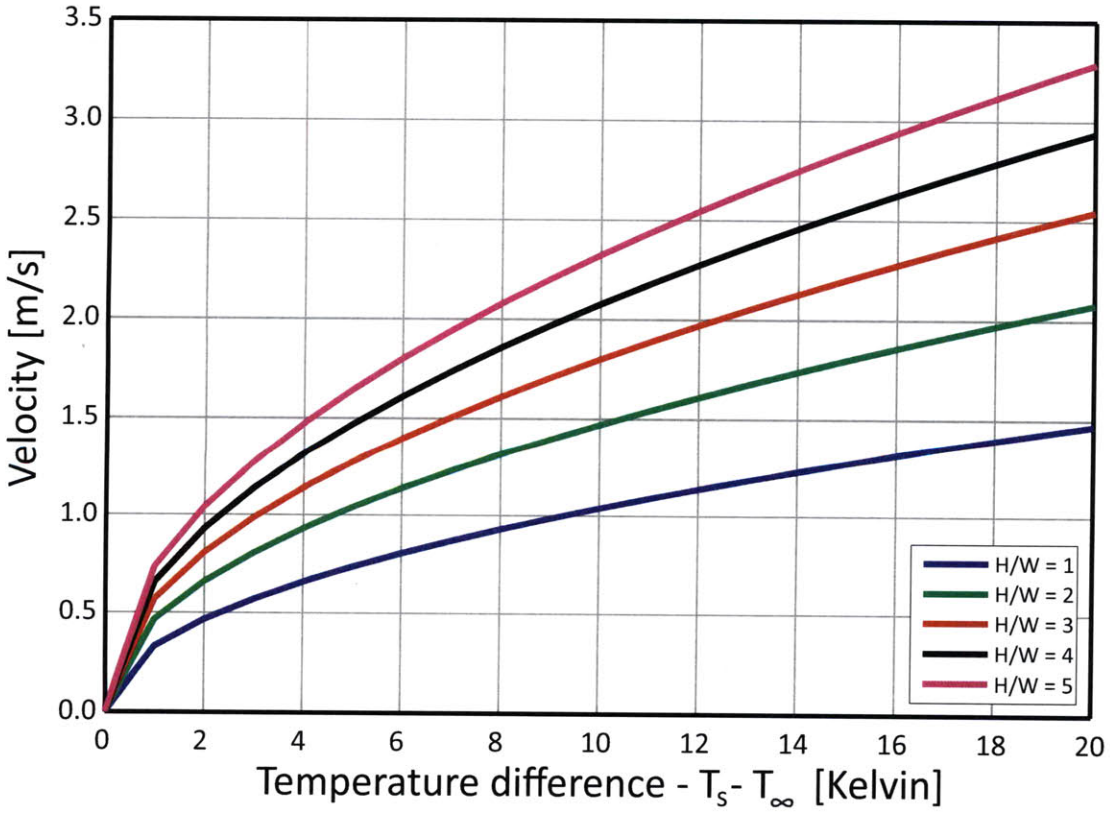

Figure 6-2: Velocity [m/s] vs. Temperature difference, $T_s - T_\infty$ [Kelvin]: based on a 10 meter wide street canyons of various aspect ratios with free stream temperature of 303 Kelvin and ground surface heating equivalent to a Richardson number of three

As expected, the velocities required to meet the threshold curves in Figure 6-2 are lower than those in Figure 6-1. The idea that buoyancy is less important than expected in street canyon flows is supported by the experimental work of Louka et al. [34] They consider the Nantes'99 field experiment which was conducted during a time of low wind speeds and high solar intensities, so as to consider the thermal effects on the air flow. The street canyon they considered had an aspect ratio of 1.4, and the flow was oriented as recirculating flow as in the work of Li et al. Parts of the windward canyon wall were found to have surface temperatures that were more than 15 Kelvin warmer than the air temperature. The wind speed above the street canyon was approximately 1 m/s. Even with this low atmospheric wind speed, the wall temperatures remained at values less than 10 Kelvin hotter than the air temperatures for much of the day. They found that the temperature gradient extended only 20 cm from the walls for much of the study period. They suggest that this could be important for models meant to study air quality issues in street canyons. They note that changes in the flow structure interfere with only 20% of the cross-sectional area of the street canyon, and that the numerical simulation tended to overestimate the influence of wall heating as these effects were not seen in the flow measurements.

Though higher wind speeds are required for forced convection flow to dominate in street canyons with greater aspect ratios, we assert that for most canyon orientations façades in street canyons with greater aspect ratios receive less solar radiation. Therefore, the wall surface temperatures are expected to be lower than those façades in street canyons with an aspect ratio of unity. Considering this argument, the fact that shortwave radiation only occurs during the day, the fact that many climates do not have large differences between surface and air temperatures and the work of Li et al and Louka et al, we assert that our work is relevant in a majority of neighborhoods. Limiting cases may require the addition of a thermal model to accurately predict the exchange between the urban canopy layer and the urban boundary layer. This future work will be discussed in Chapter 7.

Chapter 7

Conclusions and future work

In this thesis, we provided background information that supports the need for a simple model to be used by urban planners for the assessment of early design phase iterations. We devised a method to predict velocities in idealized street canyons, in realistic street canyons and through idealized, repeating neighborhoods. We also introduced an exchange coefficient to predict the turbulent exchange between the urban canopy layer and the urban boundary layer above. We developed a methodology to parameterize large roughness elements typical of building façades for our model. We also used these parameterizations in CFD modelling as a simplification to explicitly meshing façades. This significantly reduced mesh size and computational time. We evaluated our work with a CFD package, Fluent, with experimental work and with models from the literature, and we are encouraged by the results. We related our findings about neighborhood scale flow to the underlying fluid mechanics associated with flow over sparsely-packed and densely-packed bluff bodies. We found that intersections and courtyards significantly affect the magnitude of the exchange between the urban canopy layer and the urban boundary layer. We studied various geometry-based neighborhood parameters, and their relationship to the exchange coefficient. Finally, we discussed cases where the flow may be influenced by buoyancy effects, and found that these cases are less common than the momentum driven flow case that our work is based on.

In the future, we intend to apply these methods to a real Singaporean neighbor-

hood. To this end, our group is collaborating with Dr. Matthias Roth, Associate Professor in the Department of Geography at the National University of Singapore. Dr. Roth is working with a post doctoral student to set up a dense sensor network in recently developed neighborhoods in Punggol and Sengkang, Singapore. [3] The network includes temperature and humidity sensors, and we hope to include 2D airflow sensors in the coming months. We intend to use the data gathered to further assess the methods of our work. We would also like to compare these measurements to CFD simulations. These comparisons will allow us to address how well the model predicts flow in situations with realistic building geometry with heat (i.e. experimental data), and without heat (i.e. CFD simulations without the energy equation). We would also like to study experimental work in non-Singaporean neighborhoods to compare the performance of our model in various climates.

We would also like to assess the roughness parameterizations described in Chapter 4 with CFD. If the equivalent Nikuradse sand grain roughness applied to a simulated street canyon yields a similar solution to the case with explicitly modelled building façades, then these parameterizations would be useful to engineers interested in accurately simulating neighborhood scale flow. Because we can also calculate an equivalent skin friction coefficient for a canyon, this parameterization would also be worthwhile to assess as it pertains to shear stress wall boundary conditions in CFD.

Future work also includes extending the simple model to include a methodology for predicting buoyancy effects and temperature in street canyons and neighborhoods. Our goal is that this approach will be able to study many of the important heat transfer processes that occur in the street canyon and at neighborhood scales, including the interaction between the environment and buildings. We would also like to include a model for the transport of anthropogenic heat sources through the neighborhood. We would like to find simple methods to parameterize the effect that these heat sources on street canyon temperature. This work is already being addressed by Bruno Bueno, a graduate student in the Building Technology Group at MIT, in a more computationally intensive way by coupling an urban canopy model with a building energy simulation software package. [10, 11] We are also collaborating with Dr. Xianxiang

Li, who is conducting large-eddy simulations to study the detailed flow processes of a heated street canyon oriented at ninety degrees to the atmospheric flow. [32, 33] Mr. Bueno's work, Dr. Li's work and the experimental data gathered by Dr. Roth would be useful for assessing heat transfer parameterizations.

We intend to extend the meaning of our exchange coefficient to study the transport of pollutants along, into and out of neighborhoods. Pollutant retention times should be related to the exchange velocity and flow in a particular canyon. Finding relationships for these parameters will allow us to predict areas in a neighborhood that are prone to high pollutant concentrations. This work will require extensive literature review on dispersion, as well as CFD modelling and comparison with neighborhood scale experiments. We are collaborating with Dr. Rex Britter, Emeritus Professor of Environmental Fluid Dynamics in the Department of Engineering at the University of Cambridge and currently Visiting Scientist in the Senseable City Laboratory in the Urban Studies and Planning Department and the Building Technology Group at MIT. Dr. Britter has worked extensively on topics of air quality and modelling, including work on the DAPPLE project, which developed a computationally inexpensive pollutant dispersion model intended to be used by first responders in London, and work on the COST Action 732 guidelines, which provided guidance for the quality assurance and improvement of micro-scale meteorological models. [2, 6, 21] Dr. Britter's expertise in simple models and pollutant dispersion will provide us with valuable guidance for extending our work to these topics.

Finally, we intend to start working with local and Singaporean urban planners to learn about the planning process. We will determine what geometry and building information is available for buildings in the early design phase, and we will incorporate this information into our model to enhance ease of use by, and its applicability to urban planners. We will also use our interactions with urban planners to provide us with the insight to develop spatial and spatially averaged outputs that urban planners deem useful for assessing the impact of a designed neighborhood on the microclimate.

References

[1] Ali-Toudert, F. *Dependence of outdoor thermal comfort on the street design in hot and dry climate.* PhD thesis, Berichte des Meteorologischen Institutes der Universität Freiburg, 2005.

[2] Arnold, S.J. Introduction to the dapple air pollution project. *Science of the Total Environment 332* (2004), 139–153.

[3] Balazs, B., Hall, T., Roth, M. and L.K. Norford. Microclimate in a high-rise residential development in Singapore. In *The seventh International Conference on Urban Climate* (Yokohama, Japan, 2009).

[4] Bentham, T. and R.E. Britter. Spatially averaged flow within obstacle arrays. *Atmospheric Environment 37* (2003), 2037–2043.

[5] Blocken, B., Stathopoulos, T. and J. Carmeliet. CFD simulation of atmospheric boundary layer: wall function problems. *Atmospheric Environment 41* (2007), 238–252.

[6] Britter, R.E. and M. Schatzmann. COST Action 732 quality assurance and improvement of micro-scale meteorological models. Tech. rep., COST Office, 2007.

[7] Britter, R.E. and S.R. Hanna. Flow and dispersion in urban areas. *Annual Review of Fluid Mechanics 35* (2003), 469–496.

[8] Bruse, M. et al. ENVI-met 3.0: Updated model overview. Tech. rep., http://www.envi-met.com/documents/papers/overview30.pdf (accessed May, 2010), March 2004.

[9] Bruse, M. et al. ENVI-met 3, January 2010. www.envi-met.com, (accessed May, 2010).

[10] Bueno, B. An Urban Weather Generator: coupling a building simulation program with an urban canopy model. Master's thesis, Massachusetts Institute of Technology, 2010.

[11] Bueno, B. et al. Integrating building energy and urban climate studies through a coupling scheme between EnergyPlus and the Town Energy Balance TEB model. *Boundary-Layer Meteorology* (Submitted 2010).

[12] CHAPRA, S.C. AND R.P. CANALE. *Numerical Methods for Engineers*, sixth edition ed. McGraw Hill, 2010.

[13] CHENG, H. AND I.P. CASTRO. Near wall flow over urban-like roughness. *Boundary-Layer Meteorology 104* (2002), 229–259.

[14] CHEONG, S.M. ET AL. Public housing in singapore: Residents' profile, housing satisfaction and preferences: Hdb sample household survey 2008. Tech. rep., Research and Planning Department - Housing & Development Board, 2010.

[15] CHOW, W.T.L. AND M. ROTH. Temporal dynamics of the urban heat island of Singapore. *International Journal of Climatology 26* (2006), 2243–2260.

[16] CHOW, W.T.L., POPE, R.L., MARTIN, C.A. AND A.J. BRAZEL. Observing and modeling the nocturnal park cool island of an arid city: horizontal and vertical impacts. *Theoretical and Applied Climatology* (Submitted and accepted, 2010).

[17] DOBRE, A. ET AL. Flow field measurements in the proximity of an urban intersection in London, UK. *Atmospheric Environment 39* (2005), 4647–4657.

[18] ELIASSON, I., OFFERLE, B., GRIMMOND, C.S.B. AND S. LINDQVIST. Wind fields and turbulence statistics in an urban street canyon. *Atmospheric Environment 40* (2006), 1–16.

[19] EMMANUEL, R., ROSENLUND, H. AND E. JOHANSSON. Urban shading - a design option for the tropics? a study in colombo, sri lanka. *International Journal of Climatology 27* (2007), 1995–2004.

[20] FLUENT INC. *Fluent 6.3 User's Guide.* Lebanon, NH, 2006.

[21] FRANKE, J., HELLSTEN, A., SCHLUNZEN, H. AND B. CARISSIMO, Ed. *Best practice guideline for the CFD simulation of flows in the urban environment* (Hamburg, Germany, 2007), vol. COST Action 732, COST Office, University of Hamburg, Meteorological Institute, Centre for Marine and Atmospheric Sciences.

[22] GRIMMOND, C.S.B. AND T.R. OKE. Aerodynamic properties of urban areas derived from analysis of surface form. *Journal of Applied Meteorology 38* (1999), 1262–1292.

[23] HAMLYN, D., HILDERMAN, T. AND R.E. BRITTER. A simple network approach to modelling dispersion among large groups of obstacles. *Atmospheric Environment 41* (2007), 5848–5862.

[24] HANG, J., LI, Y., SANDBERG, M. AND L. CLAESSON. Wind conditions and ventilation in high-rise long street models. *Building and Environment 45* (2010), 1353–1365.

[25] HANG, J., SANDBERG, M., LI, Y. AND L. CLAESSON. Flow mechanisms and flow capacity in idealized long-street city models. *Building and Environment 45* (2010), 1042–1053.

[26] HEDQUIST, B.C., BRAZEL, A.J., DI SABATINO, S., CARTER, W. AND H.J.S. FERNANDO. Phoenix urban heat island experiment: micrometeorological aspects. In *Eighth Symposium on the Urban Environment, Timothy R. Oke Symposium* (2009), American Meteorological Society.

[27] HOSKER, R.P. Flow around islolated structures and building clusters: a review. *ASHRAE Transactions 91-2B* (1985), 1671–1692.

[28] INCROPERA, F.P. AND D.P. DEWITT. *Fundamentals of Heat and Mass Transfer*, fifth edition ed. John Wiley & Sons, Inc., 2002.

[29] KOH GUI QING. Singapore woos immigrants to boost population. *Reuters* (March 2007). http://www.reuters.com/article/idUSSIN163320070326, (accessed, May 2010).

[30] KOLOSEUS, H.J. AND J. DAVIDIAN. Free surface instability correlations and roughness-concentration effects on flow over hydrodynamically-rough surfaces. Tech. rep., USGS Water-Supply Paper 1592-C, D, 1966.

[31] KUNDU, P.K. AND I.M. COHEN. *Fluid Mechanics*, 4th edition ed. Elsevier Inc., 2008.

[32] LI, X.X. ET AL. Flow and pollutant transport in urban street canyons if different aspect ratios with ground heating. *Atmospheric Environment* (Submitted April, 2010).

[33] LI, X.X. ET AL. Large-eddy simulation of flow and pollutant transport in urban street canyons with ground heating. *Atmospheric Environment* (Submitted December, 2009).

[34] LOUKA, P. ET AL. Thermal effects on the airflow in a street canyon – Nantes'99 experimental results and model simulations. *Water, Air, and Soil Pollution: Focus 2* (2002), 351–364.

[35] MACDONALD, R.W., GRIFFITHS, R.F. AND D.J. HALL. An improved method for the estimation of surface roughness of obstacle arrays. *Atmospheric Environment 32* (1998), 1857–1864.

[36] MAH BOW TAN. Speech by Minister for National Development, at URA corporate plan seminar 2007 at Orchard Hotel. http://www.mnd.gov.sg/, (accessed May, 2010), February 2007.

[37] MAH BOW TAN. Speech by Minister for National Development, on planning for growth and a quality environment during committee of supply debate. http://www.mnd.gov.sg/, (accessed May, 2010), March 2007.

[38] MARTIN, L. AND L. MARCH, Ed. *Urban Space and Structures.* Cambridge University Press, London, 1972.

[39] MILLS, A.F. *Heat Transfer*, 2nd ed. Prentice Hall, 1998.

[40] MINISTRIY OF COMMUNITY DEVELOPMENT, YOUTH AND SPORTS - FAMILY SERVICES DIVISION. Children Development Co-Savings (Baby Bonus) Scheme. http://www.babybonus.gov.sg/bbss/html/English2008.pdf, (accessed May, 2010), January 2010.

[41] MORTON, B.R., TAYLOR, G. AND J.S. TURNER. Turbulent gravitational convection from maintained and instantaneous sources. *Proceedings of the Royal Society of London. Series A, Mathematical and Phyiscal Sciences 234* (1956), 1–23.

[42] NIKURADSE, J. Laws of flow in rough pipes. Tech. rep., National Advisory Committee for Aeronautics, Technical Memorandum, 1950.

[43] OKE, T.R. *Boundary Layer Climates,* 2^{nd} *edition.* Methuen, London, 1987.

[44] OLIVARI, D. AND C. BENOCCI, Ed. *Flow around Bluff Bodies: Numerical and Experimental Approaches.* von Karman Institute for Fluid Dynamics, May 1984.

[45] SCHLICHTING, H. AND K. GERSTEN. *Boundary Layer Theory*, 8th edition ed. Springer, 2000.

[46] SKOTE, M. ET AL. Numerical and experimental studies of wind environment in an urban morphology. *Atmospheric Environment 39* (2005), 6147–6158.

[47] SOULHAC, L., PERKINS, R.J. AND P. SALLIZZONI. Flow in a street canyon for any external wind direction. *Boundary-Layer Meteorology 126* (2008), 365–388.

[48] STEEMERS, K. ET AL. City texture and microclimate. *Urban Design Studies 3* (1997), 25–50.

[49] STULL, R.B. *An Introduction to Boundary Layer Meteorology.* Kluwer Academic Publishers, Norwell, MA, 1988.

[50] WHITE, F.M. *Fluid Mechanics*, 5th edition ed. McGraw Hill, 2002.

[51] WOODING, R.A., BRADLEY, E.F. AND J.K. MARSALL. Drag due to regular arrays of roughness elements of varying geometry. *Boundary-Layer Meteorology 5* (1973), 285–308.

[52] YEOH, B.S.A. Bifurcated labour: the unequal incorporation of transmigrants in Singapore. *Tijdschrift voor Economische en Sociale Geografie 97* (2006), 26–37.